Primary Propulsion for Piloted Deep Space Exploration

NIAC Phase I Final Report

Michael R. LaPointe
Horizon Technologies
Development Group
Cleveland, OH

Prepared for:

NASA Institute for Advanced Concepts
NIAC Grant 07600-022

December 1999

CONTENTS

LIST OF TABLES

LIST OF FIGURES

LIST OF FIGURES, CONTINUED:

1.0 INTRODUCTION

Chemical rockets and low-thrust electric propulsion systems are well suited for Earth orbit applications and long-duration robotic space flight, but advanced propulsion technologies must be developed to enable more complex missions and promote the human exploration and development of space. To maximize the payloads for such missions, the propellant exhaust velocity, V_e, must be comparable to or greater than the required mission velocity, ΔV[1]

$$\frac{M_f}{M_0} = e^{-\Delta V / V_e} \tag{1}$$

where M_f is the rocket mass after the propellant is expended and M_0 is the initial rocket mass, including propellant. For an exhaust velocity much smaller than the required mission velocity, most of the rocket mass will be in the form of propellant and less payload will be carried by the engine. Mission velocities required by the piloted deep space exploration scenarios envisioned by the National Aeronautics and Space Administration (NASA) Human Exploration and Development of Space (HEDS) initiative generally fall in the range of 10^4 m/s < V_e < 10^5 m/s, which correspond to optimum thruster specific impulse (I_{sp}) values of 1,000 to 10,000 seconds.[2,3] The highest specific impulse provided by chemical combustion is around 500 seconds, hence a significant amount of chemical propellant would have to be expended to perform piloted deep space exploration missions. Electric propulsion systems, although capable of achieving the required I_{sp} values, are low thrust devices better suited for use as primary propulsion systems on small robotic spacecraft[4,5] or for auxiliary propulsion in satellite stationkeeping and orbit maneuvering applications.[6,7]

A number of advanced concepts have been proposed and investigated over the past several decades in an effort to meet the propulsion requirements for piloted deep space exploration. Recent concepts include high energy density chemical propellants, nuclear thermal and nuclear electric thrusters, fusion vehicles, and antimatter annihilation engines. While each concept has merit, each also suffers from apparent performance or feasibility issues. High energy density chemical fuels can potentially provide an increase of 10 to 100 seconds in specific impulse over current chemical propulsion systems, which would significantly improve launch vehicle performance but is still too low to meet future deep space exploration requirements.[8,9] Advanced nuclear thermal engines can provide specific impulse values approaching 1000 s, an improvement over chemical systems but still not optimum for deep space exploration.[10-12] Nuclear electric propulsion, in which a nuclear reactor is used to supply power for an electric propulsion system, can provide the required high specific impulse values and represents a promising avenue for further research and development.[13-15] However, electric propulsion engines are typically low thrust devices that require continuous operation over a long period of time to achieve a required mission velocity. This is generally not an issue for orbit maneuvering and robotic exploration missions, where nuclear electric propulsion typically outperforms chemical and nuclear thermal engines in mission design

studies.[16,17] However, the performance of high power electrostatic and electromagnetic engines under consideration for piloted deep space exploration missions is presently limited by electrode erosion and associated thruster lifetime issues.[18-20] Electrodeless plasma thruster concepts, in which radio and microwave frequencies are used to generate and heat a plasma propellant, have been investigated to alleviate the problems associated with electrode erosion,[21-25] but to date the plasma densities and temperatures produced by these devices are insufficient to meet the thrust and specific impulse requirements for deep space exploration.

Fusion-based engines, in which a hot, dense plasma is ignited and sustained by controlled thermonuclear fusion reactions, appear to provide near-optimum performance values for fast interplanetary and deep space missions of interest.[26] The primary reactor designs investigated for spacecraft propulsion include the plasma torus,[27] magnetic mirror,[28] laser and particle beam inertial confinement fusion,[29,30] and dense plasma focus systems.[31-33] However, even though fusion reactors have been under continuous development for several decades, an enormous amount of research and development remains before sustained fusion will be achieved.

Perhaps even more exotic than fusion thrusters are engine designs based on antimatter annihilation, in which energetic antiproton annihilation byproducts are either directly exhausted for thrust or are confined and used to heat a propellant. Antiproton-based engines have received considerable attention over the past few years, and although a number of potentially useful thruster designs have emerged, they are constrained by the tremendous difficulty and expense associated with the production and storage of significant amounts of antiprotons.[34-38]

In summary, the broad range of mission characteristics and propulsion concepts outlined above highlight a number of requirements that must be satisfied by propulsion systems used on future piloted deep space missions. Moderate to high specific impulse values are required to maximize the payload mass fraction, which effectively eliminates chemical engines as primary deep space propulsion systems. High-power electric propulsion engines can provide the necessary specific impulse values, but electrode erosion limits thruster lifetimes, which may place unwarranted constraints on future mission options. This suggests that electrodeless plasma thrusters would be good candidates for deep space missions, but current electrodeless systems cannot produce the proper combination of plasma density and temperature for piloted HEDS missions. Electrodeless fusion-based systems offer high plasma densities and high temperatures, but controlled fusion for either power or propulsion is still decades away. The mission requirements call for a robust electrodeless thruster that can generate, heat, and expel a high-density plasma with a specific impulse that optimizes the spacecraft mass ratio for a given mission ΔV. The pinched plasma thruster concept introduced during this NIAC Phase I research project may bridge the gap between current high power electric propulsion systems and the more exotic fusion and antimatter-based thrusters of the future, enabling new and revolutionary capabilities both for on-orbit maneuvering and for piloted deep space exploration.

1.1. Theta-Pinch Thruster Concept.

The theta-pinch thruster concept is derived from the experimental theta-pinch devices investigated during the early years of controlled fusion research.[39-42] The early theta-pinch systems consisted of an insulating, cylindrical discharge chamber, open at each end, surrounded by a single-turn coil, as shown in Figure 1.

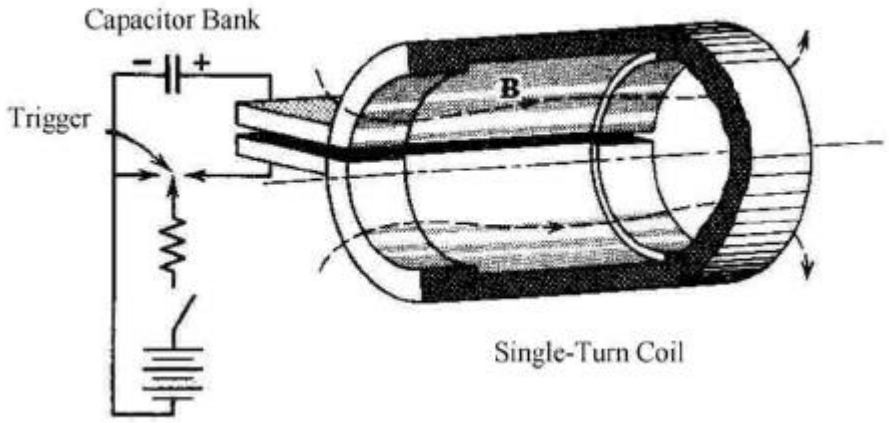

Figure 1. Theta-Pinch Schematic.

The single-turn coil is attached to a high-energy capacitor bank and high voltage switch. Neutral gas (typically deuterium) is injected into the chamber, and the outer gas layers are partially ionized by either a brief current pulse sent through the discharge coil or through radio-frequency heating by antennas located outside of the discharge chamber. The main capacitor bank is then discharged to provide a large transient current in the single-turn coil surrounding the discharge chamber. The rapidly rising current in the coil creates a time-varying longitudinal magnetic field within the chamber, which in turn induces an azimuthal current in the preionized plasma sheath via Faraday's law of induction. The sheath current interacts with the axial magnetic field produced by the coil to generate a radially inward Lorentz force on the plasma ions and electrons. These particles move inward toward the axis of the chamber, and through collisions sweep the other gas particles along in a "snowplow" effect. The partially ionized gas is radially compressed at a speed greater than the local speed of sound, creating a radial shock wave characteristic of irreversible heating processes. Compression continues until the kinetic pressure of the shock-heated plasma balances the magnetic pressure of the axial magnetic field. Radial pressure balance is generally achieved within a fraction of a microsecond, at which point the shock heating is complete. The pulsed current sent through the coil has a rise time much longer than a microsecond, however, and as the current in the coil continues to increase so does the axial magnetic field strength. The increasing magnetic pressure produced by the increasing field continues to compress and heat the plasma until the peak current is reached, typically within a few microseconds. The axial magnetic field that heats the plasma also serves to provide radial confinement, which prevents the plasma from contacting the walls of the discharge chamber. The plasma is free to flow

along axial magnetic field lines, however, and it quickly escapes from both ends of the discharge chamber.

1.2. Phase I Research Program.

Because the plasma escapes equally from both ends of the discharge chamber, a simple open-ended theta-pinch cannot provide net thrust. The thruster concept investigated during this Phase I research program retains the basic simplicity of the theta-pinch discharge, but abrogates the symmetry of the standard theta-pinch geometry by placing a superconducting magnetic field coil at the upstream end of the chamber. The superconducting magnet acts as a charged particle mirror, reflecting the axial plasma flow from the upstream end of the chamber, back along the axial magnetic field lines and out of the open downstream end of the chamber to produce thrust.

As might be expected, several issues must be resolved to determine whether a pulsed, asymmetric theta-pinch can be made into an effective plasma thruster. Key technical program elements undertaken during this 6-month research period include the modeling of plasma temperatures and densities needed to produce useful combinations of thrust and specific impulse; an analysis of the magnetic field strengths and discharge bank energies required for adiabatic plasma compression and heating; a preliminary look at potential plasma instabilities that may occur during compression; and realistic estimates of the total efficiency of a mirrored theta-pinch system operated as a high-power pulsed plasma rocket. The encouraging results of the Phase I program suggest that a scaled theta-pinch thruster operated with an upstream magnetic mirror can be an enabling propulsion technology for piloted deep space exploration, providing high average thrust at specific impulse values comparable to current electric propulsion engines.

The following chapter (*Thruster Scaling Analysis*) presents the results of a simple scaling analysis that was used to predict the plasma properties and potential performance that might be expected of an ideal theta-pinch thruster. The scaling analysis established the general feasibility of the thruster concept, and led to the development of a more advanced analytic model that is described in Chapter 3 (*Analytic Theta-Pinch Model*). The analytic theta-pinch simulation incorporates time-dependent equations for plasma compression, heating, and exhaust that are based on previously published theta-pinch models, and the numerical predictions compare well with experimental data reported for the Scylla-IC collisional theta-pinch machine. Chapter 4 (*Thruster Performance Scaling*) uses the analytic model developed in Chapter 3 to evaluate the potential performance of various theta-pinch thrusters under a variety of discharge conditions, leading to the identification of optimum thruster operating regimes and a preliminary design for a scaled theta-pinch thruster experiment. Chapter 5 (*Preliminary 2-D Simulation*) outlines the development of a 2-D numerical simulation that was initiated during the latter stages of the Phase I research program in an effort to better predict theta-pinch plasma properties. Preliminary results for the 2-D simulation are presented, and a list of required code modifications is presented as a guide to future research. The report concludes with a brief summary of the Phase I program results and a list of recommendations for high power theta-pinch thruster development.

2.0 THRUSTER SCALING ANALYSIS

A simple scaling analysis was undertaken at the beginning of the Phase I effort to estimate the potential performance of a theta-pinch thruster and to provide some guidance for subsequent MHD numerical simulations. As described in the previous chapter, the theta-pinch thruster employs strong, time-varying magnetic fields to radially compress and heat a plasma propellant which then expands axially from one end of the chamber to provide thrust. The ideal exhaust velocity of the ionized propellant is a function of the temperature, which can be approximated using the equation:[44]

$$V_e = \sqrt{\frac{2g}{(g-1)}\frac{RT}{M}h_i} \tag{2}$$

where V_e is the propellant exhaust velocity (m/s), T is the propellant temperature (K), M is the propellant molecular weight (expressed in amu), R is the universal gas constant (8.3144 J/K-mol), γ is the adiabatic index for the propellant gas, and η_i is ideal cycle efficiency. The adiabatic index is given by:

$$g = \frac{N+2}{N} \tag{3}$$

where N is equal to the number of degrees of freedom of the gas. An ionized gas propellant has 3 degrees of freedom, yielding a value of γ = 5/3 for the adiabatic index. The ideal cycle efficiency is given by:

$$h_i = 1 - \left(\frac{P_{ex}}{P_{ch}}\right)^{\frac{(g-1)}{g}} \tag{4}$$

where P_{ex} is the exhaust pressure and P_{ch} is the chamber pressure. During operation P_{ch} greatly exceeds P_{ex}, hence the value of η_i is generally close to unity and is taken as such for this preliminary analysis. It is a common practice in plasma physics research to express particle temperatures in units of electron-Volts (eV), where 1 eV = 11,605 K, and that convention will be adopted here. Converting the plasma temperature in Equation 2 from degrees-K to eV and substituting the value of γ = 5/3 yields the following expression for the ideal exhaust velocity, expressed in m/s:

$$V_e = 2.2\times10^4\sqrt{\frac{T(eV)}{M}} \tag{5}$$

The specific impulse (Isp) of the rocket is related to the exhaust velocity by the equation:

$$I_{sp} = \frac{V_e}{g} \tag{6}$$

where g is the acceleration of gravity, 9.8 m/s^2, and the specific impulse is expressed in seconds. Equations 5 and 6 can be combined to find the propellant temperature needed to provide a given specific impulse for a given propellant species. In Figure 2, the required plasma temperature is presented as a function of ideal specific impulse for an ionized hydrogen propellant.

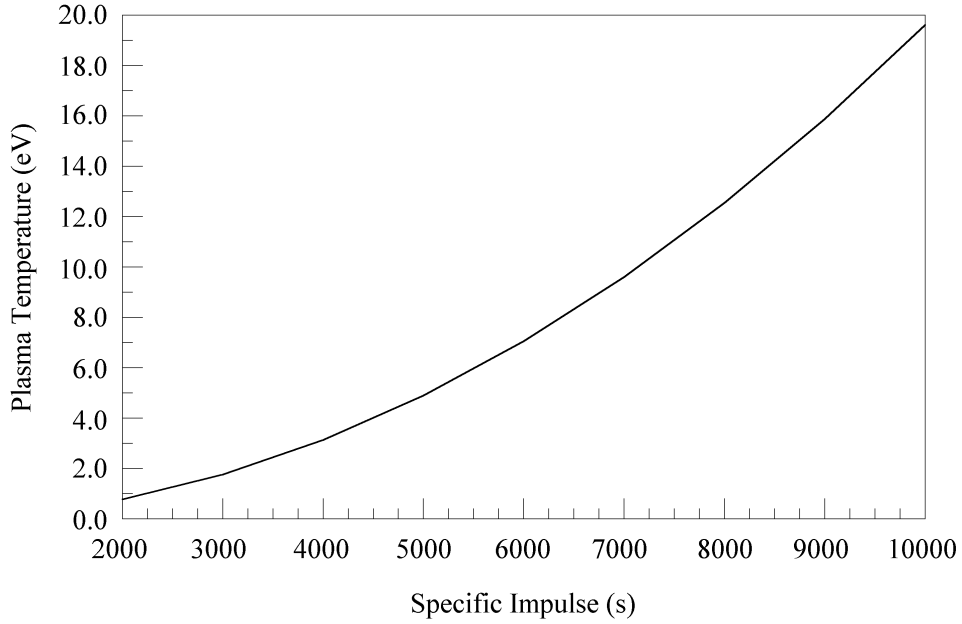

Figure 2. Hydrogen plasma temperature vs. specific impulse.

For a given specific impulse, the required plasma temperature can be used to determine the amount of compression that must be provided by the theta-pinch coil. Because the required plasma temperatures are significantly lower than the keV temperatures investigated with fusion theta-pinch devices, the thruster does not require shock heating of the plasma during compression. Consequently, the compression is assumed to be adiabatic, *i.e.* slow enough that shock waves do not develop. In this case the final plasma temperature is simply related to the initial plasma temperature through the ratio of initial to final plasma radius:[45]

$$\frac{T_f}{T_0} = \left(\frac{r_0}{r_f} \right)^{4/3} \tag{7}$$

where T_0 and T_f are the initial and final plasma temperatures, respectively, and r_0 and r_f are the initial and final plasma radius, respectively. The value (r_0/r_f) is the compression ratio, the amount of compression that must be supplied by the axial magnetic field during the pulsed discharge. The compression ratio required to provide a given specific impulse can be determined using Equations 5 through 7 and an assumed initial plasma temperature. Figure 3 shows the resulting compression ratio as a function of ideal specific impulse for a hydrogen propellant preionized to an initial temperature of 0.1-eV.

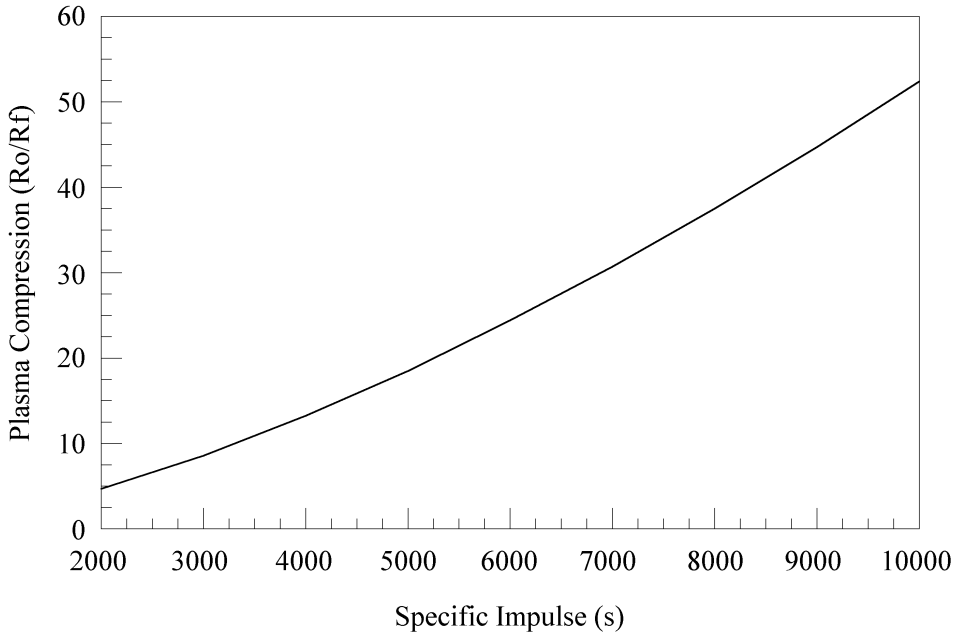

Figure 3. Hydrogen plasma compression ratio vs. specific impulse.

To provide a final temperature commensurate with an ideal specific impulse of 5,000 s, a hydrogen plasma with an initial temperature of 0.1-eV would have to be compressed by a factor of around 20. To provide sufficient temperature to reach 10,000 seconds in specific impulse, the same plasma would have to be compressed by roughly a factor of 54.

The pressure of the compressed plasma column, P_f, is related to the initial gas fill pressure, P_0, by the adiabatic pressure law:[45]

$$\frac{P_f}{P_0} = \left(\frac{r_f}{r_0}\right)^{5/3} = \left(\frac{n_f}{n_0}\right)^{\frac{5}{3}} \tag{8}$$

which can be expressed in terms of either the initial and final plasma mass densities, ρ_0 and ρ_f, or the initial and final plasma number densities, n_0 and n_f. Plasma pressures, densities, and temperatures are assumed to be related by the ideal gas law:

$$\begin{aligned} P_0 &= r_0 R T_0 = \sum n_0 k T_0 \\ P_f &= r_f R T_f = \sum n_f k T_f \end{aligned} \tag{9}$$

where the summation is taken over all species present in the plasma. Equations 7, 8, and 9 can be combined to find the following expression for the ratio of final to initial pressure in terms of the plasma compression ratio:

$$\frac{P_f}{P_0} = \left(\frac{r_0}{r_f}\right)^{\frac{10}{3}} \tag{10}$$

The radial plasma pressure is balanced by the pressure of the axial magnetic field created by the time-varying current in the discharge coil. As the current in the coil increases, the magnetic field continues to compress the plasma column. The axial magnetic field strength, B_0, required for compression is given by:[46]

$$P = \frac{B_0^2}{2m_0} = \sum nkT + \frac{B_i^2}{2m_0} \tag{11}$$

where B_i represents internal magnetic fields that may be induced within the plasma column during compression, and μ_0 is the permeability of free space ($4\pi\times10^{-7}$ H/m). For this initial analysis, it is assumed that no internal magnetic fields are induced within the plasma column.

Although the axial magnetic field provides radial compression, the plasma is still free to move along field lines and exit the discharge chamber. To provide directed thrust, a magnetic mirror field is provided at the upstream end of the discharge chamber. The mirror field does not provide perfect reflection of the ionized plasma, however, and some fraction of the particles will be lost. The probability, P_{lost}, that a particle will be lost through the mirror is given by:[47]

$$P_{lost} = 1 - \left(\frac{R_M - 1}{R_M} \right)^{1/2} \tag{12}$$

where R_M is the ratio of the mirror magnetic field strength, B_M, to the strength of the axial magnetic field in the chamber, B_0:

$$R_M = \frac{B_M}{B_0} \tag{13}$$

A small loss probability is required to ensure that most of the plasma is directed axially downstream and out of the engine. A mirror ratio of $R_M = 2$ yields a loss probability of around 30%, while a mirror ratio of $R_M = 5$ yields a loss probability of around 10%. The limit on the achievable mirror ratio is governed by the strength of the axial magnetic field along the discharge chamber and the technology constraints placed on generating a constant magnetic mirror field at the upstream end of the chamber. A reasonable upper limit for the magnetic mirror field is 10 T, which can be achieved using current superconducting magnet technology. It will be assumed in the analysis to follow that the mirror field is limited to 10 T, and that a mirror ratio $R_M > 5$ is required to minimize particle losses from the upstream end of the chamber.

Assuming plasma losses through the mirror field can be neglected, the impulse bit, I_{bit}, produced by the pulsed theta-pinch engine is approximately given by:

$$I_{bit} \approx \Delta m \times V_e \tag{14}$$

where Δm is the amount of propellant mass expelled during the pulsed discharge and V_e is the average propellant exhaust velocity. The average thrust of the engine, F, is related to the impulse bit by:

$$F = I_{bit} \times f\,(Hz) \tag{15}$$

where f is the engine repetition rate, measured in Hertz. The average propellant mass flow rate, $\dot{m}$, is equal to the propellant mass injected during each pulse, Δm, multiplied by the pulse repetition frequency:

$$\dot{m} = \Delta m \times f\,(Hz) \tag{16}$$

The average engine thrust can thus be written in terms of the average mass flow rate multiplied by the propellant exhaust velocity:

$$F = \dot{m} \times V_e \tag{17}$$

in agreement with more standard expressions for steady-state rocket thrust.

The amount of mass injected during each pulse is the product of the initial propellant gas density, ρ_0, and the volume of the discharge chamber initially filled by the gas, $\pi r_0^2 L$:

$$\Delta m = r_0 p r_0^2 L \tag{18}$$

The pulse repetition frequency, f, will be limited by how quickly the plasma evacuates the discharge chamber. The time to evacuate the chamber can be approximated as the time it takes a particle moving along an axial field line at velocity V_e to travel the full length of the discharge chamber. The corresponding pulse time, τ_p, is thus L/V_e, yielding a maximum pulse repetition frequency f_{max} of:

$$f_{\max} = \frac{1}{t_p} = \frac{V_e}{L} \tag{19}$$

The frequency f_{max} corresponds to the maximum pulse repetition frequency at 100% engine duty cycle. Substituting Equations 16, 18 and 19 into Equation 17 yields the following expression for the average thrust at 100% duty cycle:

$$F = \dot{m} V_e = r_0 p r_0^2 L \times \left(\frac{V_e}{L} \right) \times V_e = r_0 p r_0^2 V_e^2 \tag{20}$$

The length of the discharge chamber does not enter the thrust calculation due to the approximation made in Equation 19 for the pulse repetition frequency.

2.1 Results for Hydrogen Propellant.

Based on the above set of equations, a short computer program (SCALING.F) was written to calculate the potential performance of a pulsed theta-pinch engine operated at 100% duty cycle. Input parameters include the desired engine specific impulse, the initial (uncompressed) plasma number density, and the internal radius of the discharge chamber; code output includes the plasma compression ratio, compressed plasma temperature, plasma column pressure, required axial magnetic field strength, and maximum average engine thrust. An initial plasma temperature of 0.1-eV was assumed for all cases, corresponding to partial plasma preionization prior to compression. The code listing for SCALING.F is presented in Appendix A.

The scaling program was initially used to evaluate the potential performance of a theta-pinch thruster operated with hydrogen propellant. The predicted plasma temperature required to achieve a given ideal specific impulse using hydrogen was previously presented in Figure 2. As shown in that figure, modest plasma temperatures are able to provide significant specific impulse values due to the low molecular weight of hydrogen. For example, to achieve a specific impulse of 5,000 s requires a hydrogen plasma temperature of approximately 4.9 eV, while a specific impulse of 10,000 s can be achieved for a plasma temperature of around 19.6 eV. The predicted compression ratios needed to achieve a given specific impulse were also previously shown, in Figure 3. In viewing that figure, it is interesting to note that relatively small plasma columns will be generated during the pulsed discharge. This has some very beneficial implications for the design of the upstream magnetic mirror coil. The plasma does not expand significantly along the axial direction during the initial compression phase, so only the fully compressed plasma column will interact with the magnetic mirror field. The small radius of the compressed column allows the use of a small radius magnetic mirror field coil, which alleviates the fabrication and material mass constraints imposed by the construction and use of large-diameter field coils. From Figure 3, an engine specific impulse of 5,000 s requires a compression ratio of approximately 18.5; assuming an initial plasma (chamber) radius of 1 m, the compressed plasma radius will be around 5.4 cm. The magnetic mirror coil radius can thus be on the order of 6 cm rather than the full 1-m radius of the discharge chamber and still effectively mirror the compressed plasma column. For a specific impulse of 10,000 s the compression ratio is increased to around 52.4, a result of the higher plasma temperature needed to achieve higher specific impulse. Again assuming an initial plasma radius of 1-m, the compressed radius will be around 1.9 cm, which again allows the use of a small diameter mirror coil at the upstream end of the chamber.

In terms of compression field strength, Figure 4 shows the central (axial) magnetic field values required to provide a specific impulse of 5,000 s as a function of the initial hydrogen plasma number density. Combined with an estimate of the magnetic mirror field strength, this graph can be used to determine the maximum initial hydrogen number density that can be injected into the engine. For example, suppose the mirror field has a

strength of 10 T, and it is desired that the particle loss fraction through the mirror not exceed 10%. Using Equation 12, the mirror ratio must be equal to or greater than 5, which limits the central magnetic field strength to around 2 T. Using Figure 4 and assuming a maximum magnetic field strength of 2-T, the maximum initial hydrogen number density that can be injected into the engine during each pulse is approximately 7.5×10^{21} m^{-3}.

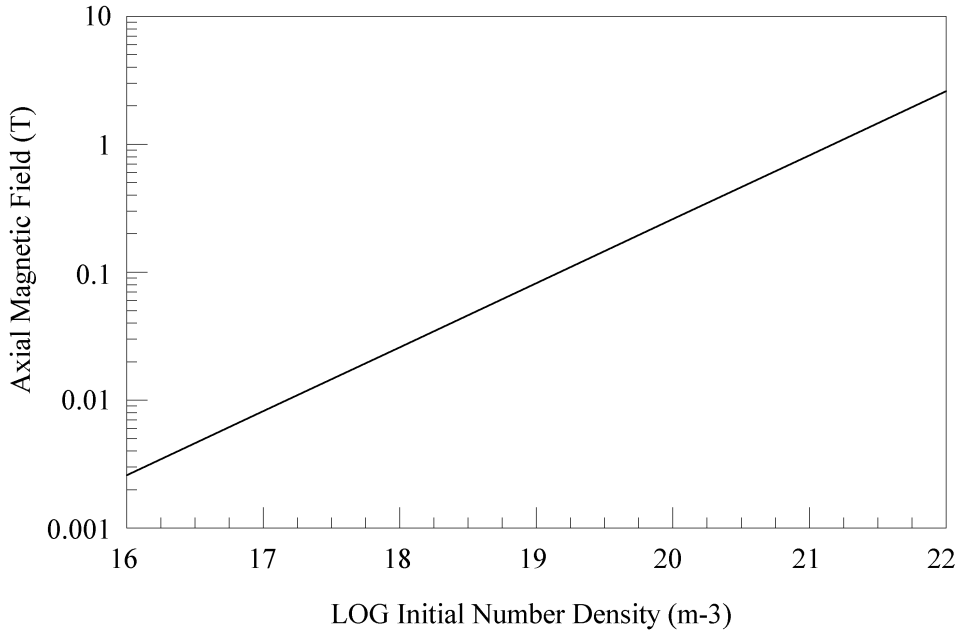

Figure 4. Magnetic field strength vs. initial hydrogen number density, Isp = 5,000 s.

Figure 5 on the next page shows the average thrust of an ideal theta-pinch engine operating at 5,000 seconds specific impulse and 100% duty cycle as a function of the initial hydrogen number density and engine chamber radius. Not surprisingly, a larger chamber radius provides a higher thrust at a given number density because more propellant mass can be injected, heated and expelled during each pulse. The maximum hydrogen number density that can be injected into the engine at the beginning of each pulse is approximately 7.5×10^{21} m^{-3}. Using Figure 5, the maximum average thrust achieved by operating the engine with this propellant number density is around 6,500 N for a 0.5-m chamber radius, and 35,000 N for a 1-m chamber radius. Although ideal approximations, these values are orders of magnitude higher than the thrust produced by current high power electric propulsion systems with similar specific impulse, indicating that the theta-pinch thruster may indeed be an enabling technology for a new set of mission applications.

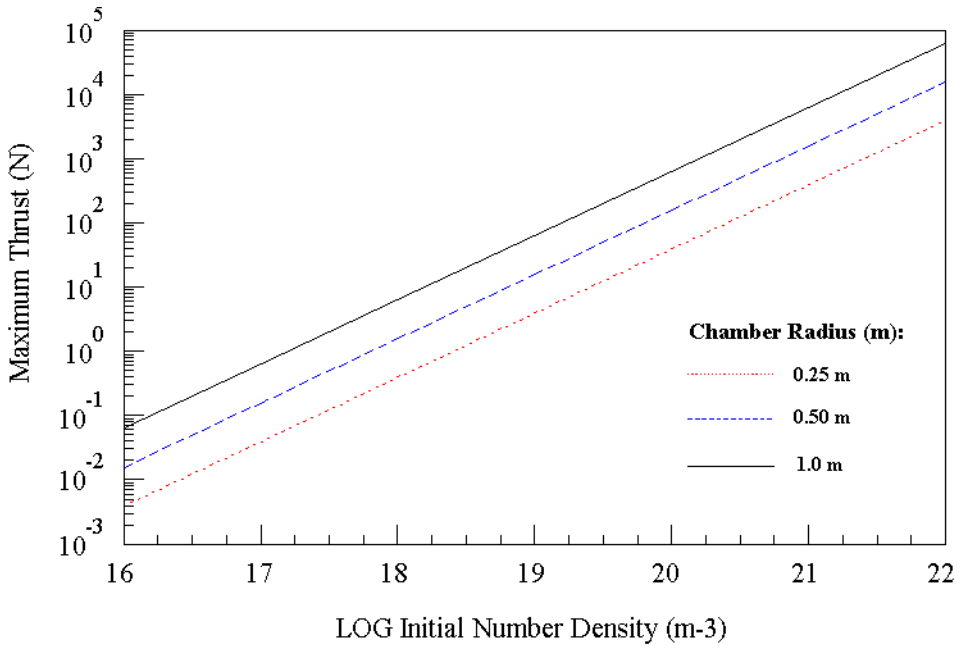

Figure 5. Thrust at 100% duty cycle vs. initial hydrogen number density, Isp = 5,000 s.

To evaluate performance at even higher values of specific impulse, suppose the thruster is operated with hydrogen at an ideal specific impulse of 10,000 s. Using Figure 2, the required plasma temperature is 19.6 eV, which can be achieved using a plasma compression ratio of 52.4 (Fig 3). The axial magnetic field strength required to achieve this temperature is shown in Figure 6 as a function of the initial hydrogen propellant number density. As previously discussed, a maximum magnetic mirror field strength of 10 T and a mirror ratio is 5 limits the maximum axial magnetic field strength to 2 T. Using this value in Figure 6, the maximum initial hydrogen plasma number density that can be injected into the engine during each pulse is 2.5×10^{20} m^{-3}, roughly 30 times lower than the plasma density used in the 5,000-s specific impulse engine discussed above. The lower number density is a result of the limited axial magnetic field strength and the higher plasma temperatures needed to provide higher specific impulse values. The magnetic field pressure has to balance the compressed plasma pressure, which is proportional to the plasma number density and temperature. For a given magnetic field strength (in this case 2-T), the higher plasma temperature required to provide a high specific impulse requires a lower initial plasma density be used to keep the compressed plasma pressure equal to or less than the radially confining magnetic field pressure.

Figure 7 shows the predicted thrust of the 10,000-s specific impulse engine operating at a 100% duty cycle for various initial hydrogen number densities and chamber radius values. For an initial number density of 2.5×10^{20} m^{-3} and a chamber radius of 1 m, the achievable thrust is approximately 4,000 N. The reduced thrust at higher specific impulse is a result of the higher compressed plasma temperature and lower initial number density that can be supported by the axial magnetic field. Still, the predicted thrust is substantially higher than the Newton-class thrust values achieved by current high power electric propulsion systems operating at high specific impulse.

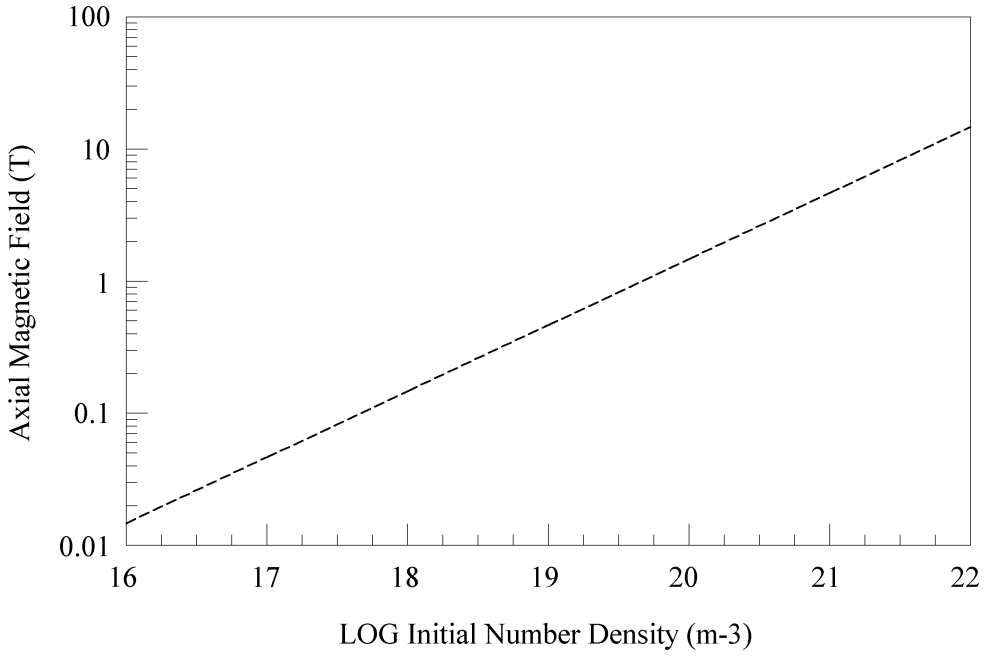

Figure 6. Magnetic field strength vs. initial hydrogen number density, Isp = 10,000 s.

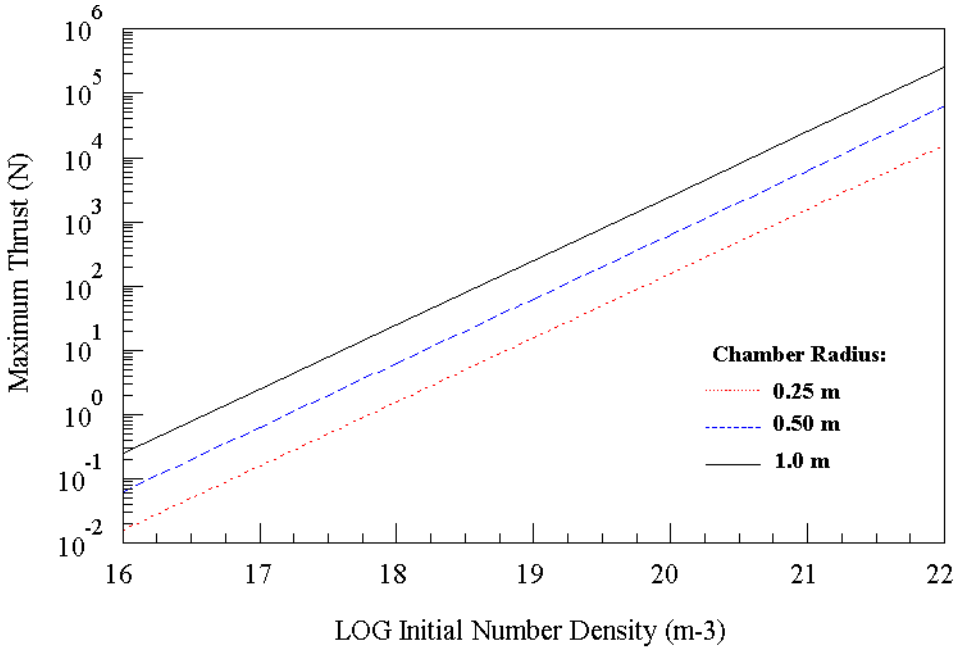

Figure 7. Thrust at 100% duty cycle vs. initial hydrogen number density, Isp = 10,000 s.

2.2 Results for Xenon Propellant.

High power Hall thrusters and electrostatic ion propulsion systems use xenon propellant, and the scaling model presented in Section 2.0 was used to determine if there might be an advantage in operating the theta-pinch thruster with xenon. A propellant atomic mass of M = 131 was used in place of M = 1 for ionized hydrogen in the model, and an initial preionization temperature of 0.1 eV was again assumed.

The xenon plasma temperature as a function of ideal engine specific impulse is shown in Figure 8. Comparing this figure with Figure 2 for hydrogen, it is apparent that significantly higher plasma temperatures are required for xenon to achieve the same specific impulse as hydrogen. To achieve an engine specific impulse of 5,000 s, a plasma temperature of 640 eV would be required for xenon compared to 4.9 eV for hydrogen. This result could have been anticipated by examining Equation 2, in which the exhaust velocity is shown to be proportional to the square root of the temperature and inversely proportional to the square root of the propellant ion mass.

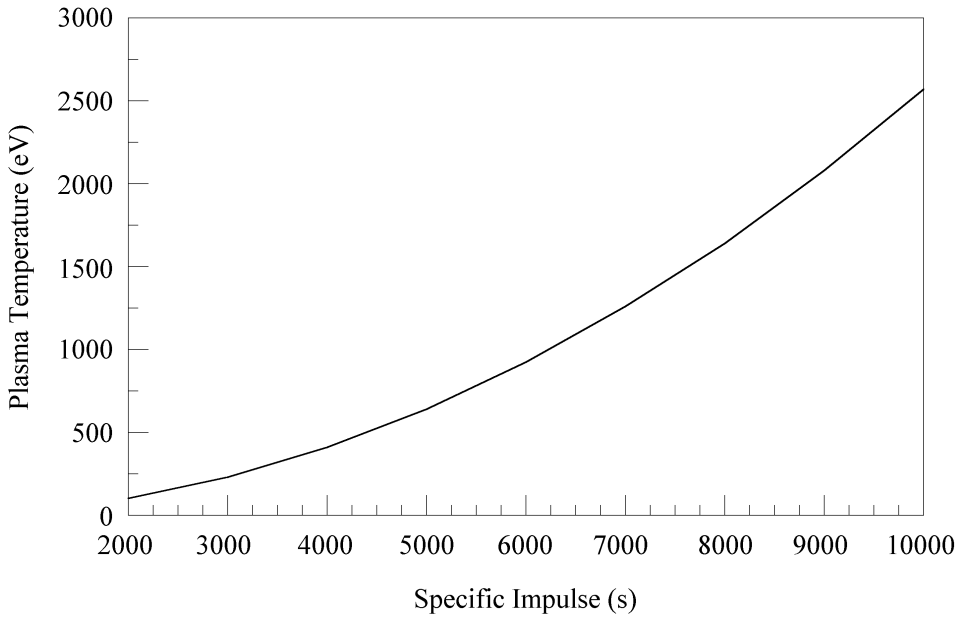

Figure 8. Xenon plasma temperature vs. specific impulse.

Using Equation 7, the plasma compression ratio needed to achieve a temperature of 640 eV is about 717 for an initial xenon plasma temperature of 0.1-eV. Assuming an axial magnetic field strength of 2-T, Equation 9 predicts a xenon plasma pressure of around 1.6×10^{6} Pa at maximum compression. Using Equation 10 and assuming a preionization temperature of 0.1-eV, the maximum initial xenon number density that can be injected into the engine is around 3×10^{16} m^{-3}, significantly lower than the number densities allowed with hydrogen propellant. For a 1-m radius thruster with an initial xenon number density of 3×10^{16} m^{-3} operating a specific impulse of 5,000 s, Equation 20 predicts a maximum average thrust of approximately 25 N. The lower thrust is a consequence of the lower initial xenon number density and higher compressed plasma temperatures that must

be supported by the axial magnetic field during compression. While this issue has not been explored in detail, there is no apparent advantage to running the theta-pinch thruster with propellants significantly heavier than hydrogen or deuterium.

2.3 Pulsed Power Requirements.

As described in Chapter 1, the axial magnetic field that compresses and heats the plasma is produced by the discharge of a time-varying current through a single turn coil that runs the length of the thrust chamber. The current, I, required to generate an axial magnetic field strength of B_0 along a discharge chamber of length L is given by:

$$B_0 = \frac{\mu_0 I}{L} \tag{21}$$

where μ_0 is the permeability of free space. To generate a central field strength of 2-T over a 10-m long discharge chamber would thus require a discharge current of around 1.6×10^7 A. This is the peak current that must be generated in the single-turn coil at the time of maximum compression; as the plasma escapes from the discharge chamber, the required magnetic field pressure and corresponding discharge current can be reduced. Over the pulse period, the current waveform should rapidly increase to radially compress and heat the plasma, reach and hold a peak compression value as the plasma begins to exit the discharge chamber, and then decrease as the plasma density within the chamber begins to fall. The optimum waveform will therefore depend on the time history of the plasma within the discharge chamber, and this in turn requires an accurate 2-D time-dependent model of the plasma dynamics, which is not yet available. A detailed analysis of the desired current waveform, and experimental techniques to optimize the discharge coil current during the pulse period, remain to be evaluated as part of a more extensive research program.

Although specific models have not been developed to predict total discharge voltages and coil currents, an estimate of the power required to compress and heat the plasma can be obtained using a formula derived by Kolb.[48] The inductance of the discharge coil is taken to be L_c, and the combined inductance of the coil and cylindrical plasma column, L_{tot}, is given by:

$$L_{tot} = L_c\left[1-\left(r_p/r_c\right)^2\right] \tag{22}$$

where r_p is the plasma column radius and r_c is the radius of the discharge coil. The corresponding circuit equation for the discharge coil and cylindrical plasma is:

$$V_L = V_0 - \frac{1}{C}\int_{t_0}^{t} I dt = L_c \frac{d}{dt}\left[\left(1-\frac{r_p^2}{r_c^2}\right)I\right] \tag{23}$$

where V_L is the voltage at the coil, V_o is the initial voltage, and C is the total system capacitance. Assuming adiabatic compression such that $T/T_0 = (n/n_0)^{\gamma-1}$ and $n/n_0 = (r_0/r_p)^2$,

equal magnetic and kinetic pressures such that $(B_0^2/2\mu_0) = nkT$, and using Equation 21 to define the current required to produce a magnetic field strength of B_0 over a coil length L, yields the following equation for the current, I:

$$I = \left(2L^2 n_0 kT_0 / m_0\right)^{1/2} \left(r_0 / r_p\right)^g \tag{24}$$

where r_0, T_0 and n_0 are the initial plasma radius, temperature, and number density prior to compression, and r_p is the plasma radius following compression. Substituting Equation 24 into Equation 23 yields an equation for the plasma radius as a function of time, which Kolb uses to find the maximum temperature T_{max} achieved at the peak of the compression cycle:[48]

$$T_{\max} \approx T_0 \left(\frac{r_c}{r_0}\right)\left(\frac{E_{bank}}{E_0}\right)^{1/2} \tag{25}$$

where E_{bank} is the total bank energy used to drive the compression, and E_0 is the initial energy contained in the uncompressed, preionized plasma. Equation 25 can be inverted to provide an expression for the total bank energy as a function of the desired plasma compression temperature:

$$E_{bank} = E_0 \left(\frac{r_0}{r_c}\right)^2 \left(\frac{T_{\max}}{T_0}\right)^2 \tag{26}$$

Section 2.1 discussed a 1-m radius, 10-m long theta-pinch engine, operated with hydrogen propellant at a specific impulse of 5,000 s, that required a compressed plasma temperature of 4.9 eV. The plasma number density used in that example was 7.5×10^{21} m^{-3}, the magnetic mirror ratio was 5, and the initial plasma preionization temperature was 0.1-eV. For these values, the initial plasma energy is 3.77×10^3 J, and the required bank energy is approximately 9×10^6 J for a chamber to coil ratio (r_0/r_c) near unity. If the preionization temperature was increased from 0.1-eV to 1-eV, the initial plasma energy would be 3.77×10^4 J and the bank energy would be reduced to around 9.1×10^5 J. While these numbers are only approximate, they demonstrate that to operate a theta-pinch thruster at high repetition rates will require large in-space energy storage and delivery systems to achieve reasonable pulse repetition rates and correspondingly high average thrust values.

In addition to on-board power limitations, the pulse repetition rate will also be constrained by the amount of time it takes the plasma to completely clear the discharge chamber. Rearranging Equation 19 and solving for the pulse repetition rate as a function of specific impulse and chamber length, L, gives:

$$f = \frac{V_e}{L} = \frac{gI_{sp}}{L} \tag{27}$$

where g is the acceleration of gravity (9.8 m/s^2). Based on Equation 27, the maximum pulse repetition rate is presented in Table 1 as a function of chamber length and specific impulse.

Table 1. Maximum Pulse Repetition Rate (Hz) vs. Isp and Chamber Length.

Isp (s)	L = 1 m	L = 10 m	L = 20 m	L = 50 m
2,000	9,800	980	490	196
5,000	2.45×10^4	2,450	1,225	490
7,000	3.45×10^4	3,450	1,725	690
10,000	4.90×10^4	4,900	2,450	980

The maximum pulse repetition rate sets a limit on the pulse rate that can be provided by the pulsed power circuit. From Table 1, a 10-m long engine operating at 5,000 s specific impulse and 100% duty cycle requires a pulse repetition rate of 2,450 Hz. The energy bank, which presumably consists of high voltage capacitors, would have to charge and discharge 2,450 times each second for the duration of the engine burn; the total engine burn time thus becomes a function of the rated life of the capacitors. Although capacitor technology is continually improving, state-of-the-art capacitors are typically rated for around 10^9 shots. Assuming a repetition rate of 2,450 Hz, the engine would be able to operate for around 4.1×10^5 s, or roughly 110 hours, before the capacitors begin to fail. Detailed mission analyses are required to determine whether this component lifetime is sufficient for missions of interest, or whether improved power systems must be developed. While it is probable that improved capacitor technologies will be available in the 20-40 year time frame considered under the NIAC program, alternative approaches such as high energy solid state drivers and direct-drive nuclear systems should also be investigated as a means to provide longer life for the pulsed power system.

Depending on future mission requirements and available power systems, the pulse repetition frequency can be reduced and the engine operated at less than 100% duty cycle, with a corresponding decrease in the average thrust. Alternatively, the chamber radius or length can be increased to maintain the average thrust and reduce the pulse repetition rate, at the expense of increasing the discharge current required to provide the axial magnetic field. The optimum design of the discharge chamber and pulsed power system will ultimately depend on the required engine thrust and total burn time for a given mission, an issue that must be addressed once the plasma dynamics of the theta-pinch thruster have been more fully examined.

2.4 Summary.

The scaling analysis presented in this chapter indicates that the pulsed theta-pinch thruster may be a viable propulsion concept for the bold, high power space exploration missions of the future. Operated with hydrogen propellant, the thruster appears capable of providing up to several thousand Newtons of average thrust with specific impulse values exceeding 5,000 seconds. These potential capabilities make it unique among plasma propulsion systems, and reasonable advances in space nuclear power may enable system development, testing, and deployment within the 40-year time frame envisioned by the NASA Institute for Advanced Concepts.

3.0 ANALYTIC THRUSTER MODEL

The scaling analysis presented in the previous chapter indicates that a pulsed theta-pinch thruster may be a viable propulsion system for future deep space exploration missions. As part of the Phase I effort, a time-dependent analytic model was developed to more accurately simulate plasma compression and exhaust physics. The equations and assumptions used in the simulation are discussed in Section 3.1, and the source code for the analytic model is reproduced in Appendix B. Section 3.2 compares the numerical simulation with experimental data reported for the Scylla-IC theta-pinch, and Section 3.3 describes the potential performance of the Scylla-IC as a hypothetical thruster, assuming perfect particle reflection from the upstream end of the chamber. The chapter concludes with a brief summary of the analytic model and it's implications for the successful development of a high power theta-pinch thruster.

3.1 Theta-Pinch Simulation.

Theta-pinch experiments typically consist of two phases: rapid radial plasma compression by a driving magnetic field, followed by the loss of the radially confined plasma along axial magnetic field lines. Radial plasma diffusion is orders of magnitude less than axial plasma flow losses in theta-pinch machines, allowing radial plasma diffusion to be neglected in the analytic model. In the absence of shocks, the initial radial compression is a reversible process and the adiabatic relations for pressure and temperature can be employed to describe the compression phase. In addition, radial compression of the plasma is accomplished on a time scale much smaller than the total plasma confinement time, and the total particle inventory (ions and electrons) can safely be assumed to remain constant during compression.

Compression. Based on these approximations, the change in plasma pressure due to compression by an external, time-varying magnetic field, B_0, is:

$$\overline{P}(t) = \frac{B_0^2(t)}{2\mu_0} \tag{28}$$

where μ_0 is the permeability of free space, $\overline{P}$ is the radially averaged plasma pressure, and induced magnetic fields within the plasma have been neglected. During adiabatic compression, the radius, r, of the plasma changes according to the relation:

$$\frac{\overline{P}(t)}{P_0} = \left(\frac{r_0}{r(t)}\right)^{10/3} \tag{29}$$

where r_0 is the initial plasma radius and P_0 is the initial plasma pressure. Given the initial plasma radius, initial pressure, and average pressure, Equation 29 can be inverted to find the time-dependent plasma radius during compression. The average plasma number

density, expressed as particle number per unit volume, is just the initial number of plasma particles, N_0, divided by the time-varying volume of the compressing plasma column:

$$\bar{n}(t) = \frac{N_0}{pr^2(t)L} \tag{30}$$

where $\bar{n}$ is the average plasma number density and L is the length of the plasma column. The initial particle inventory, N_0, can be determined from the initial plasma conditions:

$$N_0 = \frac{P_0}{kT_0}\left(pr_0^2 L\right) \tag{31}$$

where k is Boltzmann's constant and T_0 is the initial plasma density in degrees-K. The column-averaged temperature of the plasma during compression, $\bar{T}$, is determined from the ideal gas equation:

$$\bar{T}(t) = \frac{\bar{P}(t)}{k\bar{n}(t)} \tag{32}$$

Given the discharge chamber length, initial plasma radius, initial pressure, initial temperature, and applied magnetic field history, the corresponding plasma pressure, radius, number density, and temperature during compression can be determined from the above set of self-consistent equations.

Post Compression. The plasma stops its radial compression once the applied magnetic field has reached its maximum value. In most theta-pinch experiments, the driving magnetic field is crow-barred at this point to sustain the axial field and keep the plasma radially confined for as long as possible. The post-compression part of this numerical theta-pinch simulation follows the analysis of Stover et al.,[49,50] who derive a simple end-loss model for plasma flow from open-ended theta-pinch devices. The post-compression plasma pressure is given by:

$$\bar{P} = \frac{B_0^2}{2m_0} - \frac{B_i^2}{2m_0} \approx \frac{B_0^2}{2m_0} \tag{33}$$

where again B_i represents internal magnetic fields induced within the plasma column as a result of compression, and B_0 represents the time-dependent axial magnetic field. The effect of an internal magnetic field is to decrease the net pressure applied by the external axial magnetic field, resulting in less plasma compression. For the collisional, relatively low temperature plasmas of interest in this study, the induced magnetic fields are typically much smaller (<10%) than the driving magnetic fields, hence internally generated magnetic fields are neglected in this analysis.

The internal energy of the plasma ions, E_i, is:

$$E_i = \frac{3}{2}\bar{n}k\bar{T}\left(pr^2 L\right) \tag{34}$$

and the time rate of change of the ion internal energy is given by:

$$\frac{\P E_i}{\P t} = -e\frac{\P N}{\P t} - \bar{P}\frac{\P A}{\P t} - \frac{E_i}{t_{th}} \tag{35}$$

where A is the plasma column cross sectional area, τ_{th} is the ion thermal conduction time, and ε is the average energy loss per particle due to the axial flow of particles from the plasma column, equal to $\frac{5}{2}T$ for a collisional plasma. The first term on the right hand side thus represents the loss of energy due to plasma particles flowing from the chamber, the second term represents the work done on the plasma due to the compression of the plasma cross sectional area by the driving magnetic field, and the third term represents heat transfer by ion thermal conduction across the end of the plasma column.

The time dependent loss of particles from the chamber is given by:

$$\frac{\P N}{\P t} = -\frac{N}{t_{con}} \tag{36}$$

where τ_{con} is the particle confinement time. Based on a study of theta-pinch end-loss data, Stover et al. define the particle confinement time as:

$$t_{con} = \frac{L}{2}\left(\frac{m_i}{2k\bar{T}}\right)^{\frac{1}{2}} c \tag{37}$$

where m_i is the ion mass and χ is an empirical end loss parameter, approximately equal to 2.5 for collisional theta-pinch machines. The factor of (L/2) in the above equation results from the loss of plasma from both ends of the theta-pinch device.

Note that the above equations are not appropriate for modeling hot collisionless plasmas, where separate electron and ion temperatures and additional plasma transport properties must be taken into account. However, for the lower temperature collisional plasmas of interest in the theta-pinch thruster, the equations provide a self-consistent technique for analyzing time dependent theta-pinch behavior during radial compression and subsequent end-loss.

3.2 Comparison With Experiment.

To determine the accuracy of the numerical model, comparisons were made with the Scylla I-C theta-pinch machine.[49-51] The Scylla I-C consists of a 1-m long single turn coil

that surrounds a 0.038-m diameter discharge chamber which is open at both ends. The driving magnetic field for the Scylla-IC device is shown in Figure 9 below.

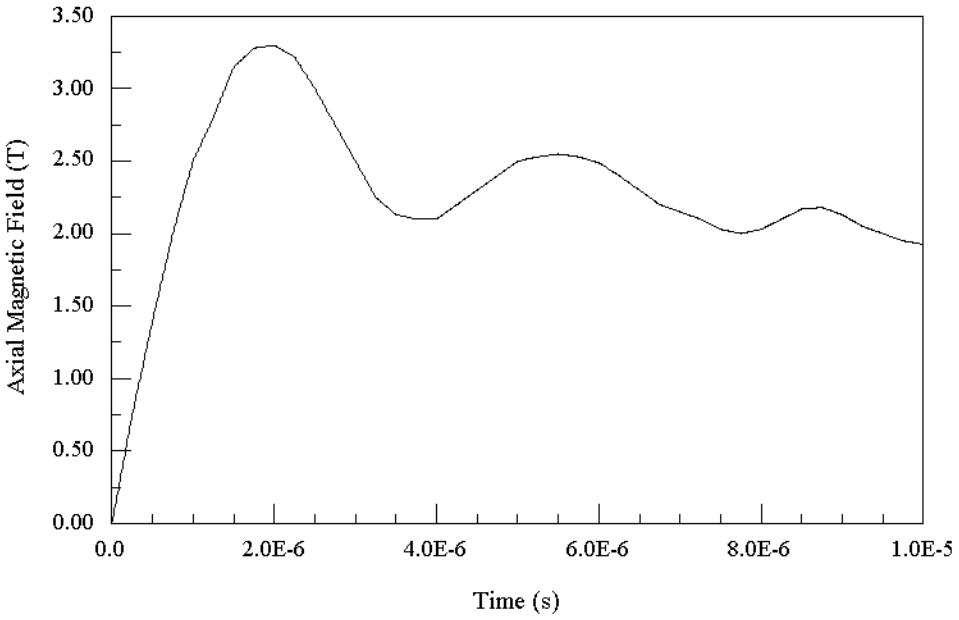

Figure 9. Driving magnetic field for Scylla-IC theta-pinch.[49]

The analytic model outlined in Section 3.1 was used to predict the plasma number density and temperature of the Scylla I-C device as a function of time. The initial chamber pressure was 100 mTorr, the gas was deuterium, and the preionization temperature was approximately 1 eV (1.16×10^4 K). The predicted column-average plasma number density is compared to the experimental centerline number density in Figure 10 below.

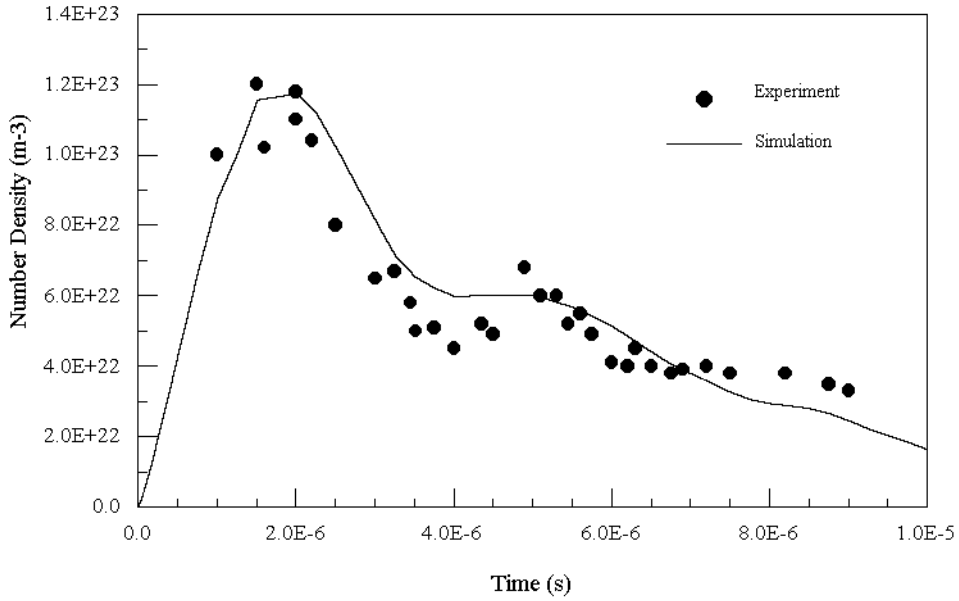

Figure 10. Scylla-IC plasma number density vs. time.

The analytic model accurately predicts the peak plasma number density as a function of time, and does a reasonable job of reproducing the experimental values at later times in the simulation. To achieve this fit, an additional assumption was made that the ratio of kinetic to magnetic field pressure is approximately 0.7 (plasma $\beta \approx 0.7$). This assumption derives from the experimental measurement of internal magnetic field lines trapped within the plasma during compression, which is not explicitly calculated in the code. Diamagnetic loop measurements made during the Scylla-IC experiments indicate that typical β values ranged from 0.7 to 0.8, and the simulation results are fairly insensitive within that range.

Figure 11 compares the predicted column-average plasma temperature with the experimentally measured centerline plasma temperature:

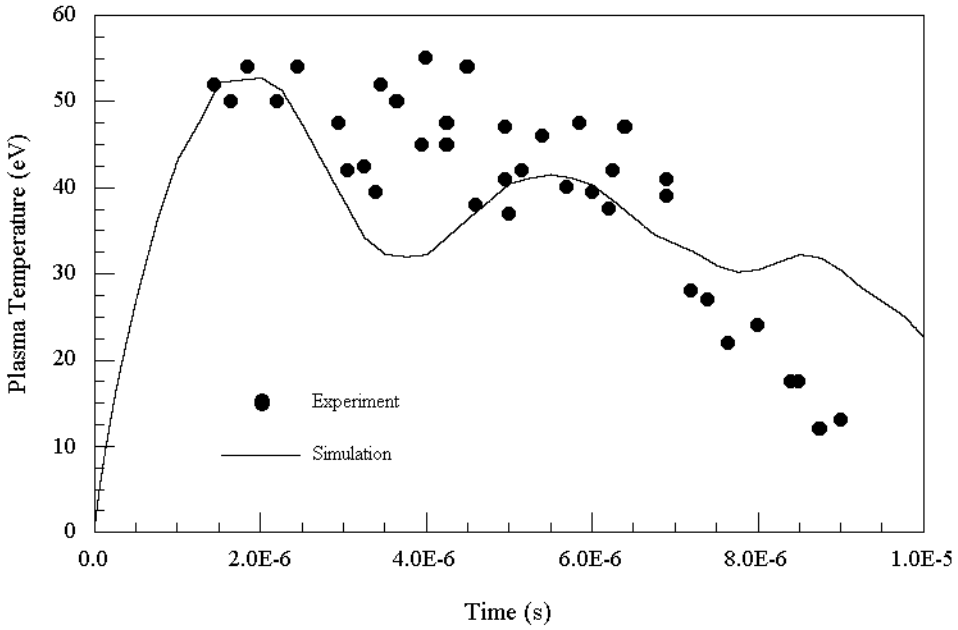

Figure 11. Scylla-IC plasma temperature vs. time.

The predicted temperature at 2 μs exactly reproduces the measured plasma temperature at peak compression, but the predicted dip in plasma temperature at approximately 4 μs is not observed in the experimental data. The predicted temperatures are also about 50% higher than the experimentally measured values at late confinement times. As discussed by Stover,[49] the latter effect may be due to the arrival of rarefaction waves from the ends of the theta-pinch, which is not modeled in this simple analysis. The simulated temperature dip at 4 μs appears to follow the driving magnetic field, and it is not apparent why the experimental data does not also show the same decrease in centerline temperature. The effect might be explained by differences between the uniform plasma model used in the above set of equations and the actual experimental plasma profile, which is more likely a Gaussian distribution around the centerline where the temperature is measured. These effects cannot be modeled using the simple set of equations above, and await a more detailed examination with a 2-D numerical simulation currently under development.

3.3 Theta-Pinch Thruster Model.

In general, the analytic model described in Section 1 reproduces the column-averaged plasma densities and temperatures experimentally measured for the Scylla-IC theta-pinch, providing some confidence that the code can be used as a predictive tool to evaluate theta-pinch thruster performance. As noted in Section 3.1 the simulation is only valid for collisional plasmas, and can't be used to model low density, high temperature plasma pinches. This is not anticipated to be a serious limitation, however, since the scaling analysis presented in Chapter 2 indicates that theta-pinch thrusters operate most effectively in the collisional plasma regime.

To predict the performance of a theta-pinch thruster, some additional equations for exhaust velocity, specific impulse, and impulse bit must be added to the simulation. The average plasma exhaust velocity, V_e, and corresponding specific impulse, I_{sp}, can be estimated using the root-mean-square formula for plasma velocity:

$$V_e(t) = \sqrt{3k\overline{T}/m_i} \tag{38}$$

$$I_{sp} = \frac{V_e}{g} \tag{39}$$

where k is Boltzmann's constant, $\overline{T}$ is the average temperature of the plasma distribution, and m_i is the ion mass. This is slightly different than the ideal velocity used in the Chapter 2 scaling analysis, and represents a more accurate average velocity for the radially confined plasma distribution. The time-dependent plasma mass flow rate, $\dot{m}$, can be calculated from the time evolution of the plasma particle number, N(t):

$$\dot{m} = \frac{dm}{dt} = m_i\left(\frac{dN}{dt}\right) \tag{40}$$

The impulse bit, I_{bit}, delivered by the plasma exhaust is given by:

$$I_{bit} = \int_{tc}^{t\,\max} \dot{m}V_e\,dt \approx \sum_{tc}^{t\,\max} \dot{m}(t)V_e(t)\Delta t \tag{41}$$

where the integration and summation times extend from the time at maximum compression (*tc)*, when the plasma begins to move axially along magnetic field lines, to the maximum plasma confinement time (*tmax)*, defined either by the axial loss of the plasma from the discharge chamber or by the loss of radial plasma confinement due to the termination of the driving magnetic field. Multiplying the impulse bit by the pulse repetition rate provides a value for the time-averaged thrust provided by the theta-pinch engine.

In addition to specific impulse and impulse bit, a parameter of interest for electric propulsion systems is the total thrust efficiency, defined as the ratio of directed propellant kinetic energy to initial stored energy. In systems with low thrust efficiency, a significant amount of the discharge power will end up deposited in the current carrying support structure, which in the case of the theta-pinch thruster is the discharge coil. An estimate can be made of the pulsed thruster efficiency,η, using the equation:

$$h = \frac{\frac{1}{2}\Delta m \overline{V}_e^{\,2}}{E_{bank}} \times 100\% \qquad (42)$$

where Δm is the total propellant mass ejected during the pulsed discharge, $\overline{V}_e$ is the average plasma exhaust velocity, and E_{bank} is the capacitor bank energy discharged during the pulse. For the same mass injection and power per pulse, the efficiency calculated using Equation 42 for a single pulse would be the same as the efficiency observed under repetitively pulsed operation.

3.4 Scylla-IC as a Thruster

Since the analytic model is known to work fairly well for the Scylla-IC theta-pinch, it was used to predict the potential performance of the Scylla-IC operated as a thruster. It is assumed that all of the deuterium plasma is reflected from the upstream end of the discharge chamber, and that plasma flow along the thruster axis does not begin until full radial compression is reached. The initial plasma pressure is assumed to be 100 mTorr and the initial preionization temperature is assumed to be 1-eV, in agreement with the experimental Scylla-IC values used in Section 3.2. The driving field used for the Scylla-IC theta-pinch, shown in Figure 9, is used for the Scylla-IC thruster simulation.

The column-averaged plasma number density and plasma temperature as a function of time for the hypothetical Scylla-IC thruster are shown in Figures 12 and 13, respectively. Experimental plasma number density and temperature values for the Scylla-IC theta-pinch are included for comparison. The rise in number density during compression is similar to the rise in plasma number density for the Scylla-IC theta-pinch (Fig. 10), with peak number densities at compression reaching identical values. However, thruster number density values remain higher than theta-pinch number density values during the exhaust phase because the plasma can only escape from one end of the thruster chamber, but can exit from both ends of the theta-pinch chamber with equal probability.

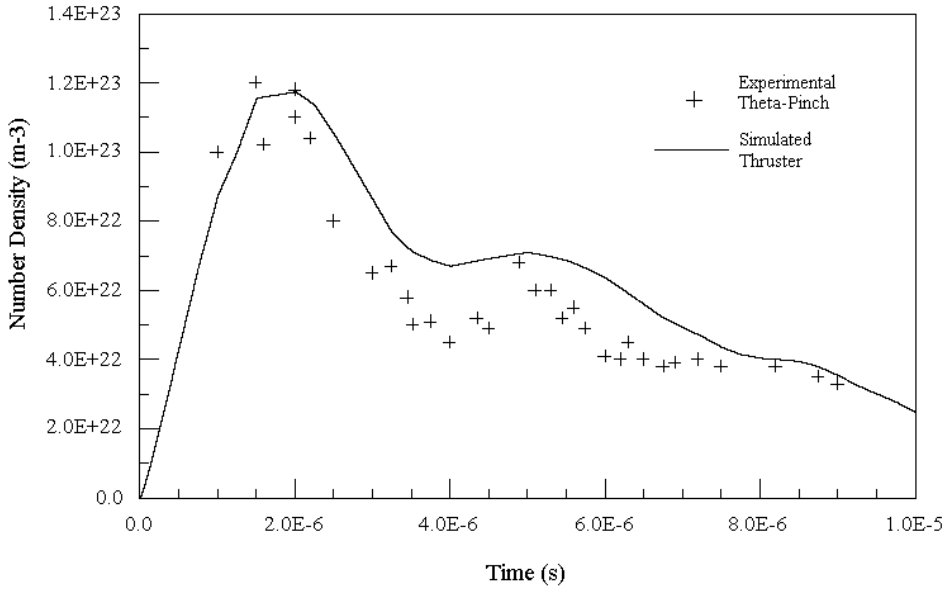

Figure 12. Scylla-IC thruster plasma number density vs. time.

As shown in Figure 13, the average plasma temperature of the hypothetical Scylla-IC thruster peaks at the same value during maximum compression as the temperature in the theta-pinch device, but subsequent temperatures remain below the average values observed in the actual theta-pinch. This results from the ideal gas approximation used to describe the relation between plasma temperature and density (Equation 32). The plasma pressure is balanced in the radial direction by the driving magnetic field (Equation 33), which is the same in the thruster and theta-pinch simulations. However, because the number density in the thruster remains higher at later times than the corresponding number density in the theta-pinch device, the plasma temperature defined by the ideal gas equation is lower in the thruster simulation than in the theta-pinch.

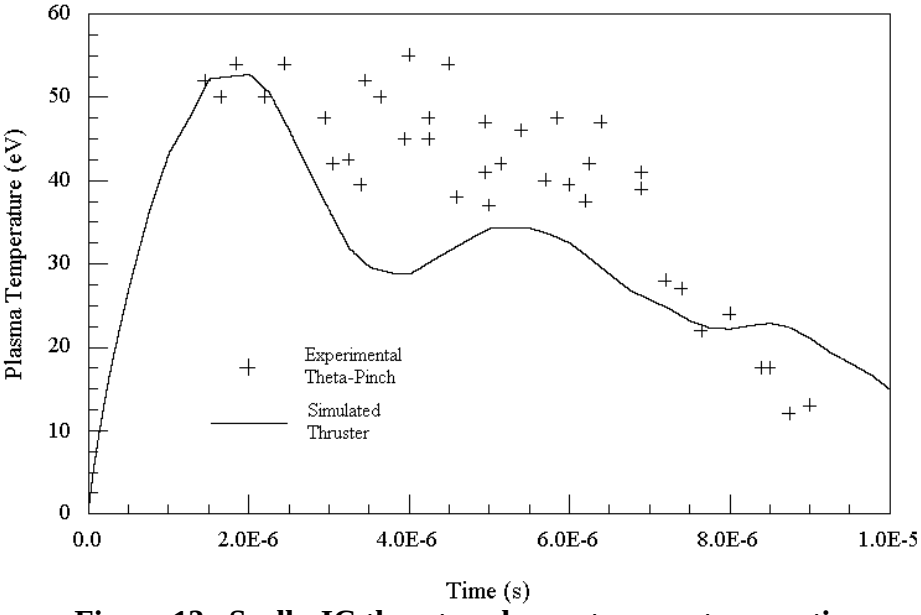

Figure 13. Scylla-IC thruster plasma temperature vs. time.

The time-dependent exhaust velocity of the deuterium plasma is shown in Figure 14. The velocity is identically zero during the compression phase of the simulation, corresponding to a rapid radial compression with no axial motion. Following maximum compression at approximately 2-μs, the plasma begins to leave the downstream end of the discharge chamber along the axial magnetic field lines. The initial plasma velocity is around 8.7×10^4 m/s, corresponding to an initial specific impulse of 8,900 s at the beginning of the exhaust phase. The average velocity decreases as the plasma temperature decreases, falling to a value of around 4.7×10^4 m/s during the later stages of the simulation. The average predicted velocity over the pulse duration is 6.4×10^4 m/s, yielding an average specific impulse of 6,500 s for the hypothetical Scylla-IC thruster operated with deuterium propellant.

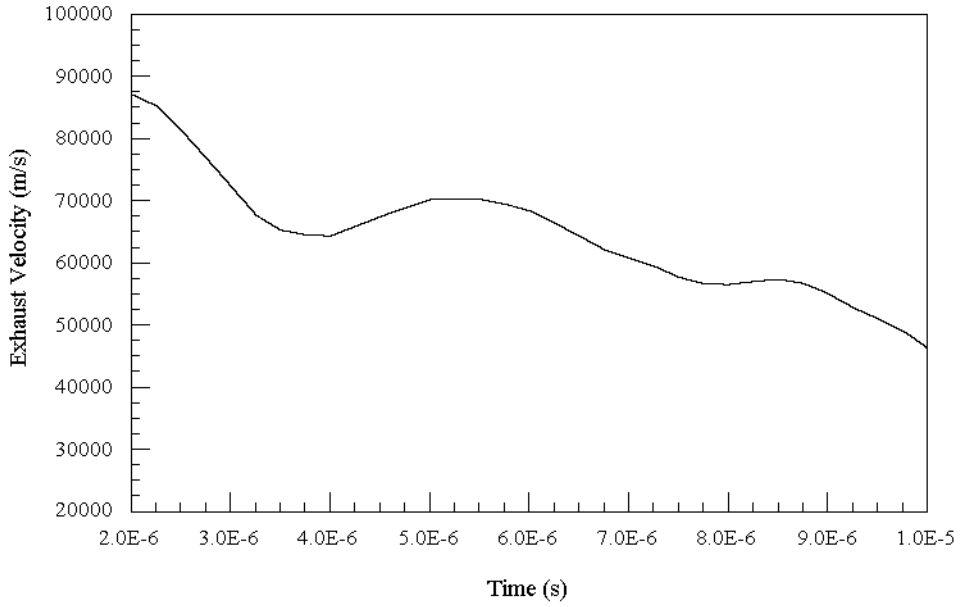

Figure 14. Scylla-IC thruster plasma exhaust velocity vs. time.

The predicted impulse-bit delivered by the Scylla-IC thruster over the 10-μs pulse period is shown in Figure 15. The total impulse-bit provided by the plasma during the pulse is approximately 5.5×10^{-6} N-s, which is not impressive for a high power propulsion system. Assuming a pulse repetition rate of 1,000 Hz, the thruster would only provide an average thrust of around 5.5×10^{-3} N, roughly equivalent to a small electrostatic ion engine. The poor theta-pinch thruster performance is a result of the low initial plasma density and high compression temperatures used in the Scylla-IC theta-pinch, which was originally intended as a fusion research device. As shown in the next chapter, increasing the plasma density and decreasing the compression temperatures should provide a more useful operating regime for deep space exploration.

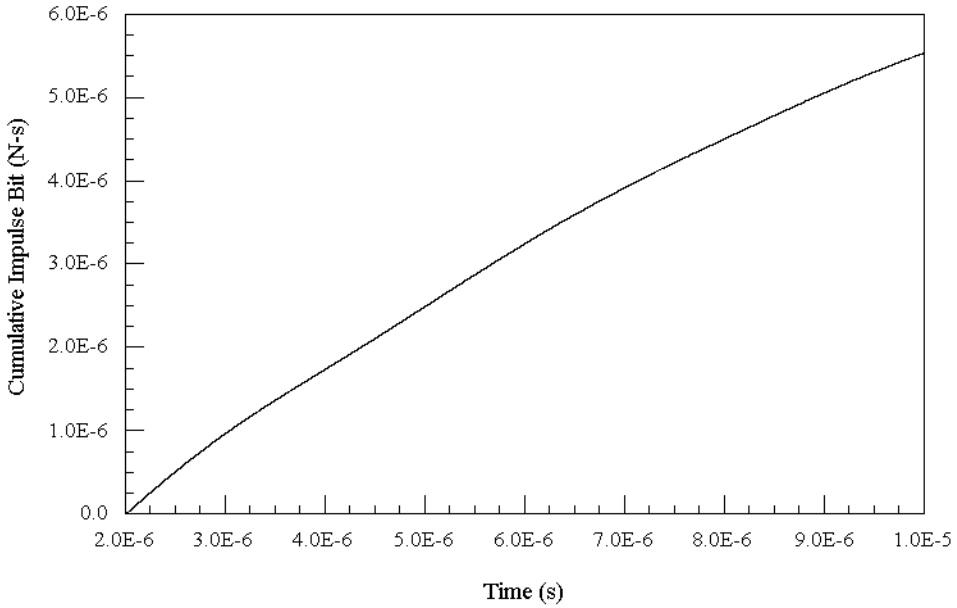

Figure 15. Scylla-IC thruster average impulse-bit vs. time.

Not only is the impulse bit too low to be of interest for propulsion, the predicted thrust efficiency for the hypothetical Scylla-IC thruster would also be extremely poor. The total mass expelled by the thruster during the discharge is approximately 7.5×10^{-11} kg, which is roughly 24% of the initial mass injected into the chamber at the start of the pulse. The total discharge energy delivered by the power bank is estimated using Equation 26 to be around 52 Joules, which is delivered over a 10-μs period for a total discharge power of 5.2-MW. As noted, the average predicted exhaust velocity for the hypothetical Scylla-IC thruster is 6.4×10^{4} m/s. Combining these values in Equation 42, the calculated thrust efficiency is only about 0.34%, indicating that only a negligible amount of the energy supplied by the capacitor bank shows up in the directed kinetic energy of the plasma exhaust. This energy has to appear somewhere, and a significant portion of the discharge energy will wind up as thermal energy in the discharge chamber walls and surrounding coil structure. Clearly, the amount of energy coupled into the directed plasma exhaust must be significantly increased for a theta-pinch device to be useful as a propulsion system.

Summary. In summary, the analytic model presented in this chapter provides a reasonable estimate of the plasma densities and temperatures to be expected in a pulsed theta-pinch thruster. The preliminary results presented in this chapter and in Chapter 2 indicate that higher-density, lower-temperature hydrogen propellants may provide better performance than the low density, high temperature deuterium plasmas used in fusion-related theta-pinch devices. In the next chapter, the analytic model is used to evaluate various theta-pinch thrusters under a variety of operating conditions as a preliminary step toward identifying an optimum thruster design.

4.0 THRUSTER PERFORMANCE MODELING

The analytic model described in Chapter 3 provides reasonably accurate number density and temperature histories for collisional theta-pinch discharges, and can be used with a fair level of confidence to predict the performance of theta-pinch plasma thrusters. As shown in Chapter 3, low density, high temperature theta-pinches can provide high plasma exhaust velocities, but cannot produce total impulse and efficiency values of interest for propulsion. In an effort to improve performance, the code was used to evaluate engine operation for a variety of initial chamber pressures, chamber sizes, and discharge times.

4.1 Change in Pressure.

The hypothetical Scylla-IC thruster described in Section 3.4 was operated with deuterium propellant at an initial pressure of 0.1-Torr, an initial preionization temperature of 1-eV, and a total discharge time of 10-μs. The discharge chamber radius was 0.019 m, the chamber length was 1 meter, and the driving magnetic field reached a peak of about 3-T in 2-μs, as shown in Figure 9 of Section 3.2. To determine the effect of initial pressure variations on thruster performance, the same chamber dimensions, preionization temperature, and driving field were used, but the initial chamber pressures were varied from 100 mTorr (1.3×10^{-4} atm) to 10 Torr (1.3×10^{-2} atm). In addition, the propellant species was changed from deuterium to hydrogen to increase the exhaust velocity for a given plasma temperature.

The predicted values of the minimum compressed plasma radius, maximum plasma number density, and maximum plasma temperature reached at compression as a function of the initial hydrogen propellant pressure are shown in Figures 16 through 18, respectively.

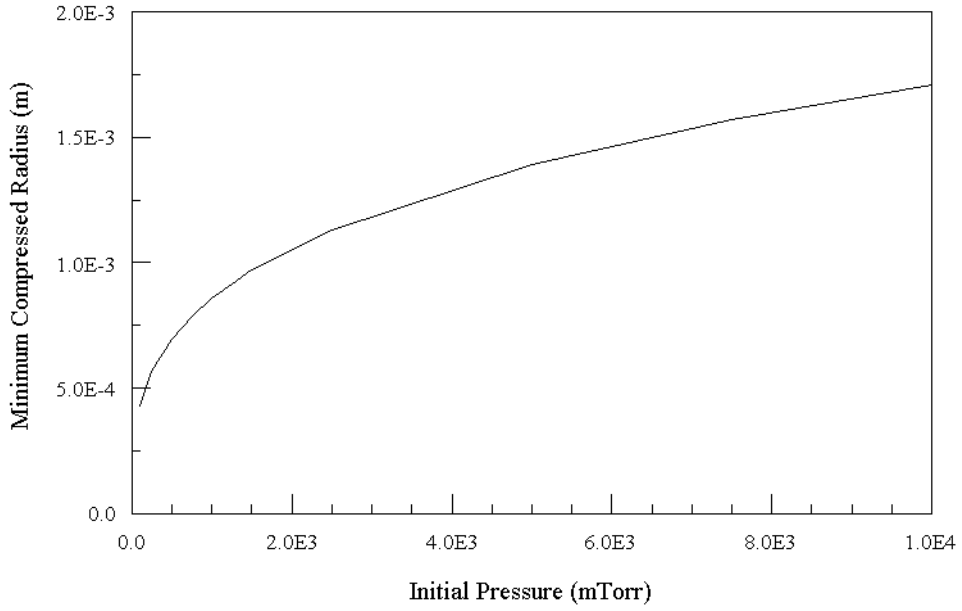

Figure 16. Compressed plasma radius vs. initial pressure for Scylla-IC thruster.

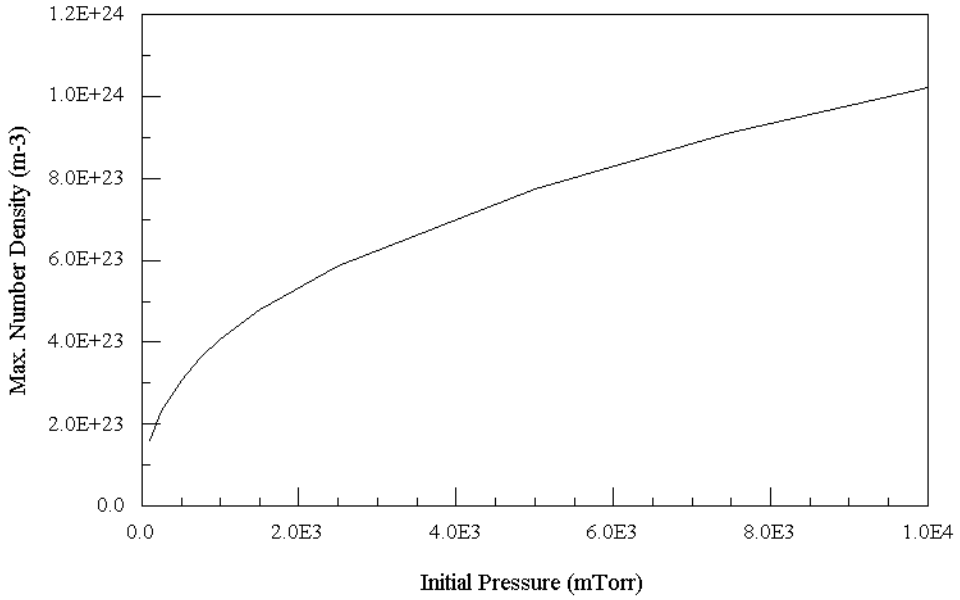

Figure 17. Maximum number density vs. initial pressure for Scylla-IC thruster.

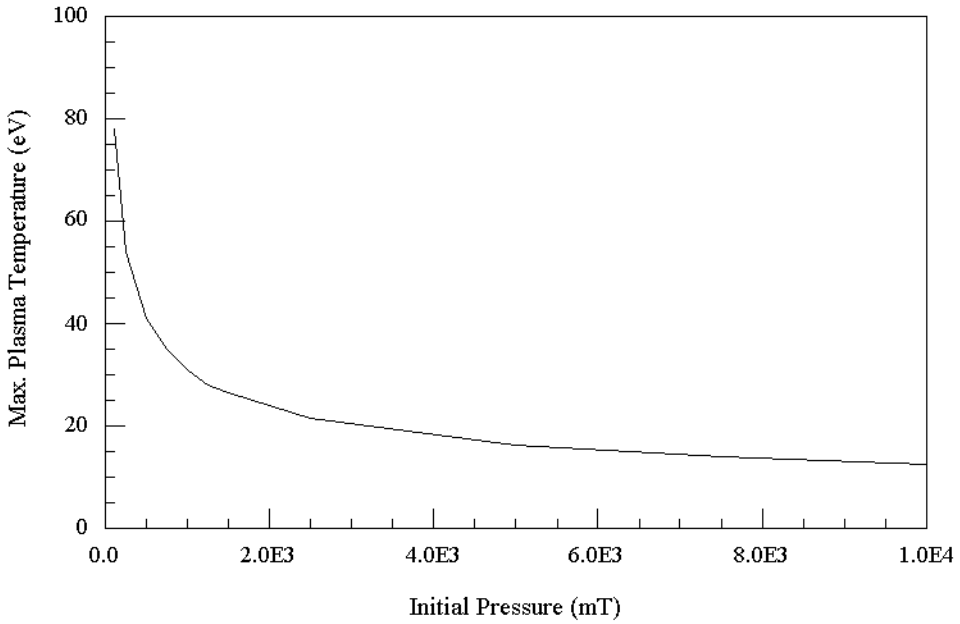

Figure 18. Maximum plasma temperature vs. initial pressure for Scylla-IC thruster.

The shape of the curve relating the minimum compression radius to the initial plasma pressure follows from the adiabatic approximation used in the model (Equation 29). The peak plasma pressure reached during compression is equal to the maximum pressure exerted by the driving magnetic field, which is the same in each case. The compressed plasma radius is then related to the initial pressure through Equation 29, which reproduces the curve shown in Figure 16 for constant values of the maximum compression pressure and initial plasma radius.

As shown in Figure 17, the maximum number density reached at compression increases with initial pressure, which is not surprising since there is more plasma in the chamber to compress. The decrease in plasma temperature with increasing initial pressure depicted in Figure 18 is also expected, since a higher number density at maximum compression requires a lower temperature to satisfy the ideal gas approximation used in the model (Equation 9).

The impact of higher number densities and lower temperatures on the performance of the hypothetical Scylla-IC thruster are shown in Figures 19 through 21. Figure 19 displays the thruster specific impulse as a function of initial pressure. The specific impulse achieved by the thruster is reduced from approximately 11,000 s at an initial pressure of 100-mTorr (0.1-Torr) to around 4,500 s at 10^4-mTorr (10-Torr), which is a consequence of the lower compression temperatures associated with operating the thruster at higher initial chamber pressures.

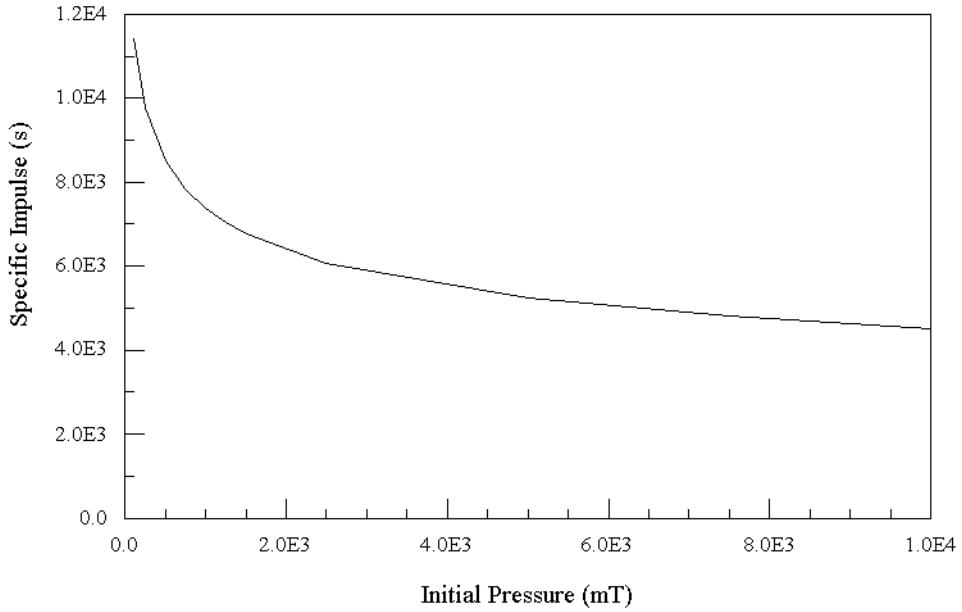

Figure 19. Average specific impulse vs. initial pressure for Scylla-IC thruster.

Figure 20 shows the impulse bit delivered by the thruster over a 10-μs pulse as a function of initial chamber pressure, and Figure 21 shows the predicted thruster efficiency over the same pressure range. The impulse bit delivered by the plasma exhaust increases from 6.8×10^{-6} N-s at an initial chamber pressure of 100-mTorr to around 1.2×10^{-4} N-s for an initial chamber pressure of 10^4-mTorr. While this is certainly an improvement, the impulse is still too low to be practical for space flight. The efficiency of the thruster goes from a low of 0.4% to a high of only 1.2%, which again is not very impressive for a high power plasma thruster. Assuming a pulse repetition rate of 1000-Hz, the average thrust delivered by the hypothetical Scylla-IC thruster operated at the highest evaluated chamber pressure is only 0.12-N, comparable to electrostatic ion engines that operate at higher specific impulse and efficiency. Clearly the asymmetric Scylla-IC design will not

make a useful thruster; the next section considers changes in geometry that may improve thruster performance.

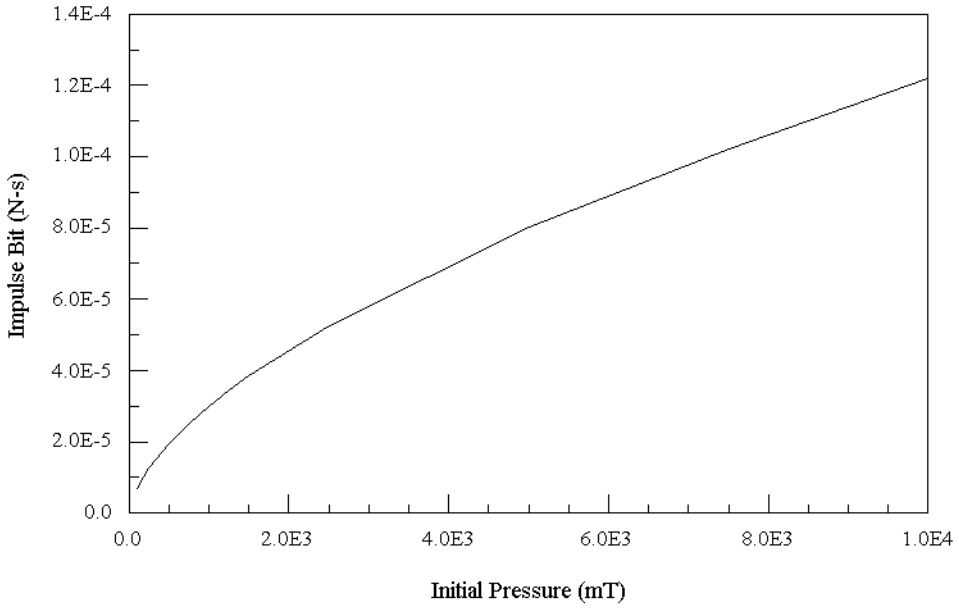

Figure 20. Impulse-bit vs. initial pressure for Scylla-IC thruster.

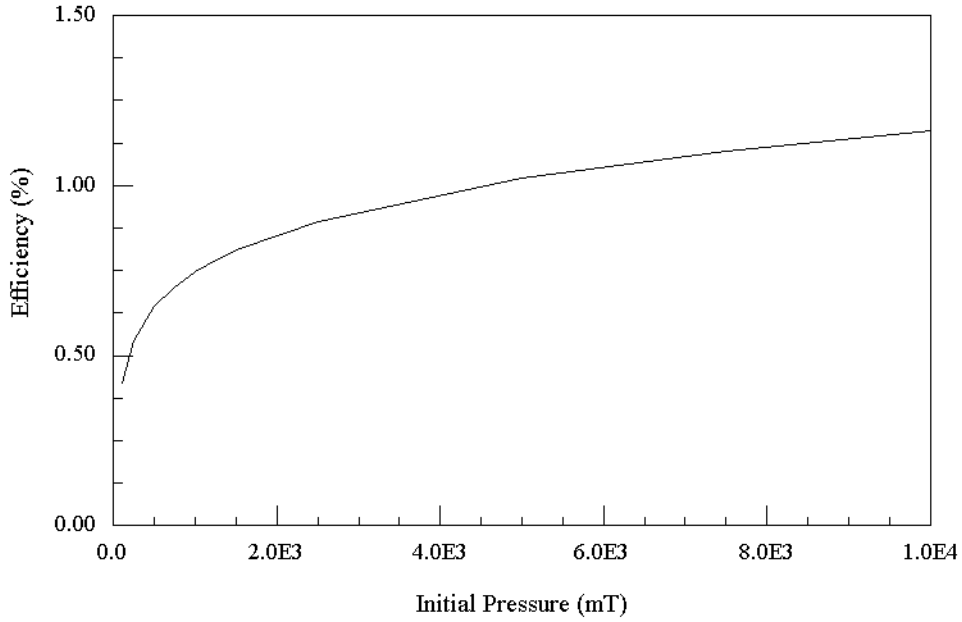

Figure 21. Efficiency vs. initial pressure for Scylla-IC thruster.

4.2 Change in Scale.

The previous section indicates that increasing the initial chamber pressure will improve the impulse bit and efficiency delivered by a theta-pinch thruster, at the expense of the average specific impulse. To explore this trend, the analytic model was used to examine the performance of theta-pinch thrusters with larger discharge chambers and longer pulse periods. The size of the discharge chamber was dramatically increased from the 0.019-m radius, 1-m long Scylla-IC theta-pinch design to a 1-meter radius, 10-meter long cylindrical chamber. The pulse period was lengthened from 10-μs to 100-μs, and the form of the driving magnetic field was changed from the Scylla-IC field shown in Figure 9 to the more rectangular pulse shape shown in Figure 22. Two axial magnetic field strengths were evaluated, corresponding to peak field values of 1-T and 2-T, respectively. The peak field strength in each case was decreased by 10% over the pulse period to mimic realistic rectangular current waveforms. Hydrogen propellant was again assumed, with an initial preionization temperature of 1.0-eV. Based on the Scylla-IC results, the presumed initial chamber pressures ranged from a low of 500-mTorr (6.6×10^{-4} atm) to a high of 100-Torr (10^5-mTorr, or 0.13 atm).

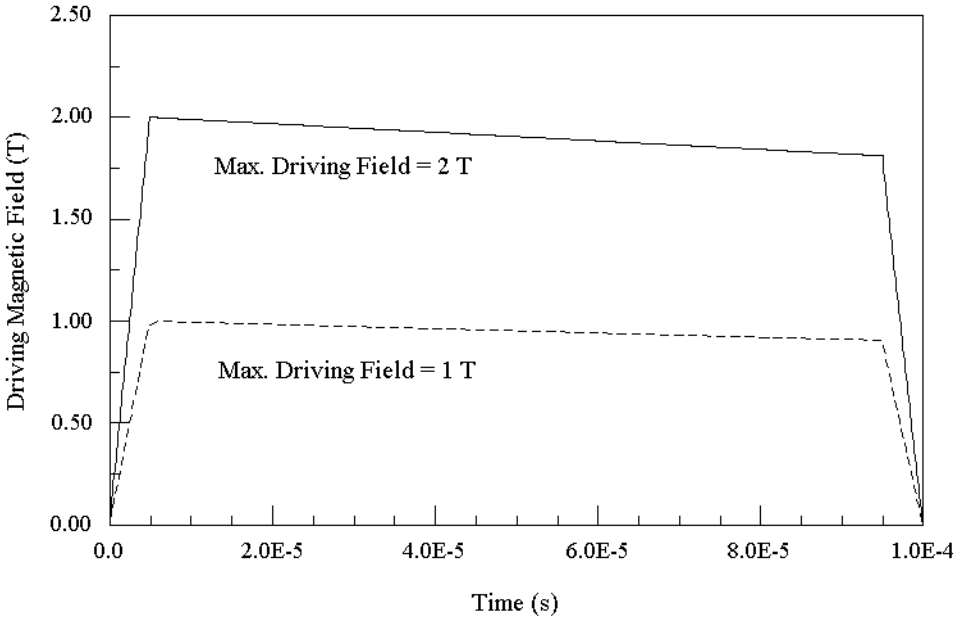

Figure 22. Driving magnetic fields for modified thruster geometry, 10^{-4} s.

Figure 23 on the following page shows the predicted compression temperatures as a function of initial chamber pressure for each driving magnetic field. For an axial magnetic field strength of 1-T, the maximum plasma temperature reached during compression ranges from 16-eV for an initial chamber pressure of 500-mTorr to a low of around 2-eV for a 100-Torr initial chamber pressure. The 2-T magnetic field is able to compress the plasma to higher temperatures, producing compressed temperature values of 28-eV to 3.5-eV over the same pressure range. Specific impulse values corresponding to these compression temperatures are shown in Figure 24 as a function of initial chamber

pressure. For low chamber pressures, the average specific impulse produced by the 1-T driving field is around 5,600 s, decreasing to 1,900 s as the initial chamber pressure is increased. For the 2-T magnetic field, the specific impulses range from a high of 7,000 s at an initial chamber pressure of 500-mTorr to a low of 2,500 s at an initial pressure of 100-Torr.

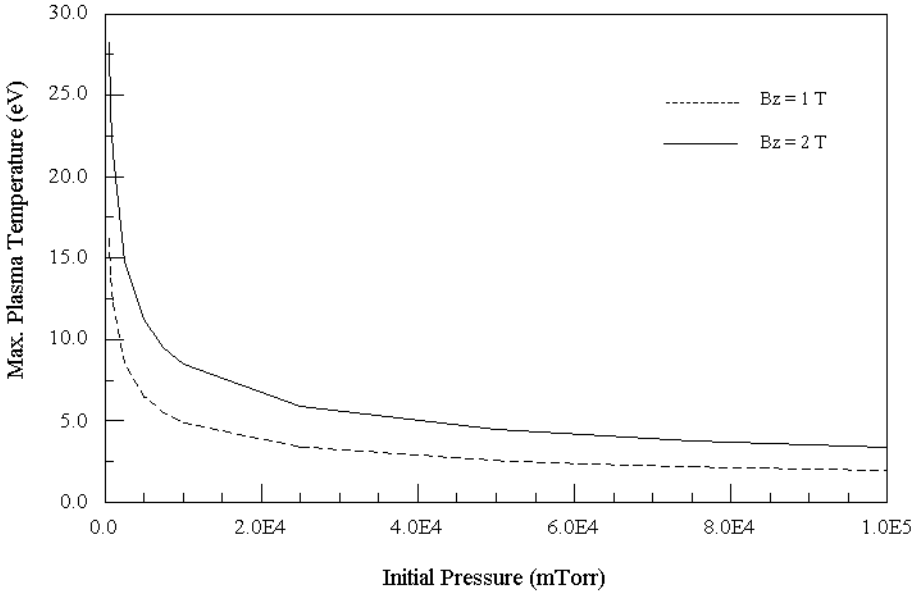

Figure 23. Maximum plasma temperature vs. initial chamber pressure.

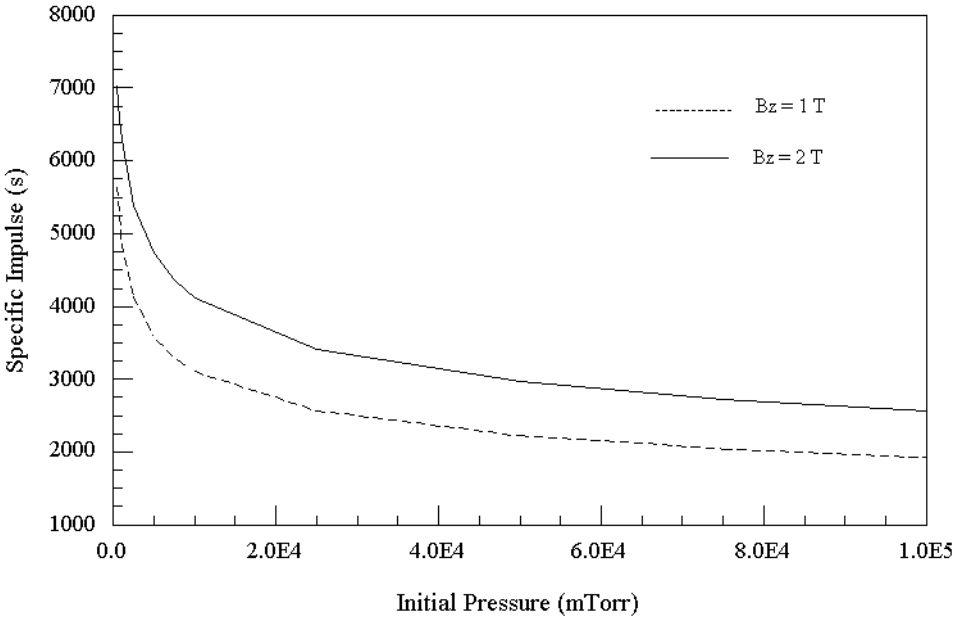

Figure 24. Average specific impulse vs. initial chamber pressure.

The impulse-bit delivered by the modified theta-pinch thruster is shown in Figure 25 for the different driving fields as a function of the initial chamber pressure. For the 1-T magnetic field, the impulse-bit delivered by the thruster ranges from 0.3 N-s for the lowest initial chamber pressure to slightly over 7 N-s for higher initial chamber pressures. For the 2-T field, the impulse-bit ranges from a low of around 0.4 N-s to a high of 12 N-s over the same pressure range.

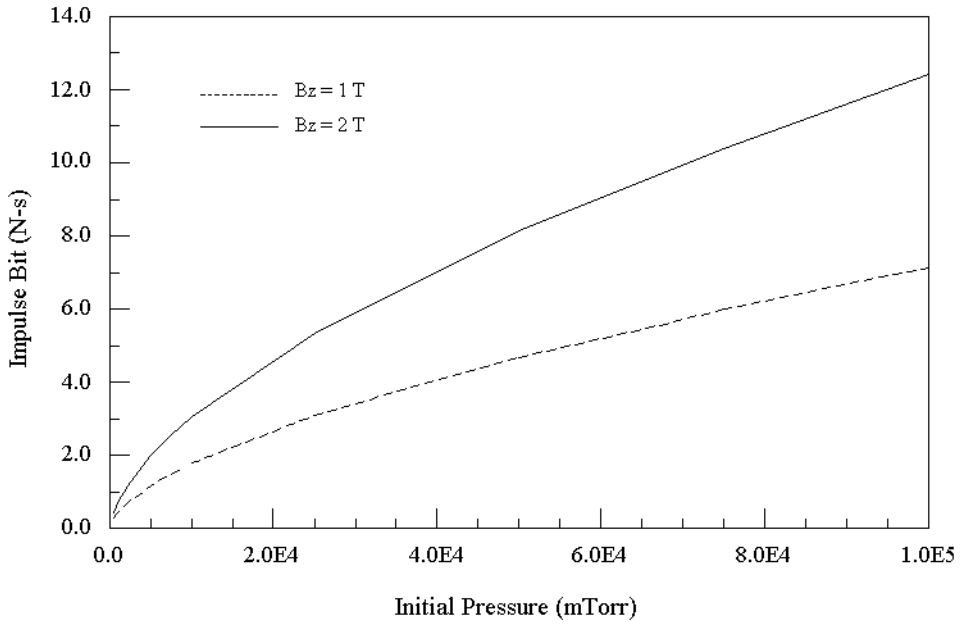

Figure 25. Impulse-bit vs. initial chamber pressure.

For a pulse repetition rate of 100-Hz, the thruster operated with a pulsed 2-T driving field and an initial chamber pressure of 100-Torr could provide an average thrust of nearly 1,200 N at a specific impulse of around 2,500 s, a unique combination that cannot be produced with current chemical or electric propulsion systems. Reducing the initial chamber pressure allows the thruster to operate at a higher specific impulse, but reduces the average thrust. For example, with an initial chamber pressure of 10-Torr the same thruster could produce an average thrust of approximately 300 N at a specific impulse of around 4,100 s. Further reductions in the initial chamber pressure would further increase the average specific impulse, but the delivered thrust becomes comparable to or less than the thrust provided by current electric propulsion systems. At an initial chamber pressure of 1-Torr, the thruster operated at 100-Hz with a 2-T axial field would produce an average thrust of 70-N at a specific impulse of 6,300 s, a propulsion regime that can be achieved with present high-power magnetoplasmadynamic thrusters operated with lithium or hydrogen propellants.[20]

Although the average thrust and specific impulse produced by the pulsed theta-pinch thruster at higher initial chamber pressures is of potential interest for deep space mission applications, the predicted efficiency of the engine is still quite poor. Figure 26 shows the efficiency of the 1-m radius, 10-m long thruster operated with 1-T and 2-T driving

magnetic fields as a function of initial chamber pressure. For the 1-T field, the efficiency ranges from 1.4% at 500-mTorr, peaks at 2.6% for an initial chamber pressure of 10-Torr, and then declines to less than 1% at the higher chamber pressures. For the 2-T case, the efficiency increases from just under 1% for a low 500-mTorr chamber pressure to around 2.7% at 50-Torr, and then decreases as the chamber pressure is increased further.

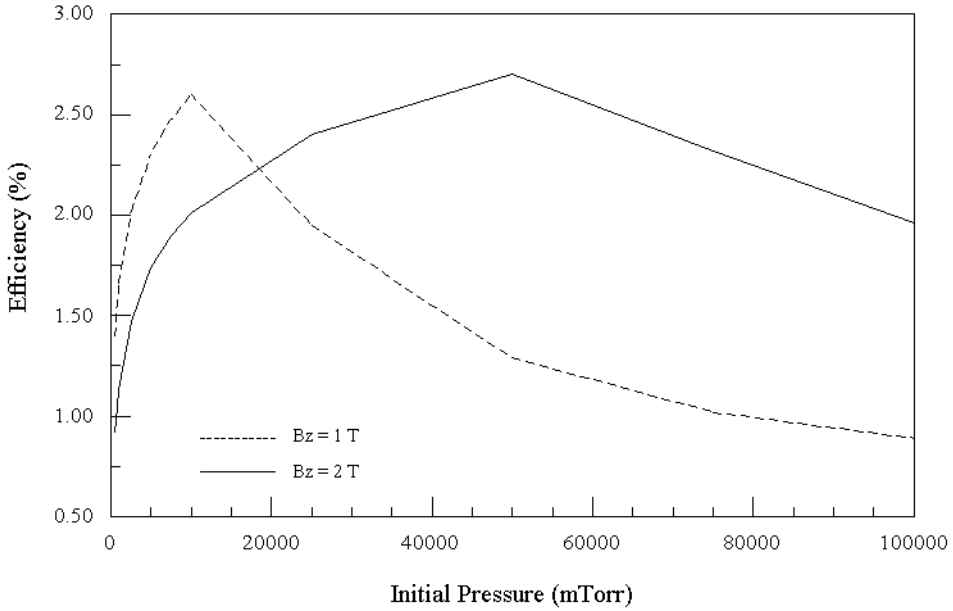

Figure 26. Thruster efficiency vs. initial chamber pressure.

The decrease in efficiency with increasing chamber pressures is ultimately due to the limited compression time provided by the discharge coil. As the initial chamber pressure is increased, the amount of propellant mass injected into the chamber increases but the compressed plasma temperature and exhaust velocity decrease. The total amount of mass expelled along the axial field lines also increases as the initial chamber pressure is increased, but the relative fraction of mass expelled vs. mass injected into the chamber actually decreases at higher pressures due to the lower exhaust velocity, as depicted in Figure 27. For the thruster operated with a 2-T magnetic field, roughly 30% of the injected mass is expelled from the chamber at low initial pressures, while only 11% of the injected mass is expelled for high initial chamber pressures. For the 1-T driving field, the fraction of mass used ranges from 23% at low pressure to around 9% at high pressure. The mass that remains in the thrust chamber at the end of the pulse period will expand radially as the energy in the discharge coil diminishes, and will presumably return to the lower initial preionization temperature since the compression process is adiabatic. While this recovery may be beneficial in terms of minimizing the addition of preionization energy, the reduced fraction of expelled mass that occurs at the higher chamber pressures limits the plasma kinetic energy delivered during a pulse. In contrast, the total discharge energy delivered during the pulse depends on the total mass injected into the chamber, which is linearly proportional to the initial chamber pressure, and on the square of the ratio of final to initial plasma temperature. Thus the growth in kinetic energy of the

plasma with increasing chamber pressure is eventually overshadowed by the increase in the discharge energy, and the thrust efficiency, not large to begin with, decreases.

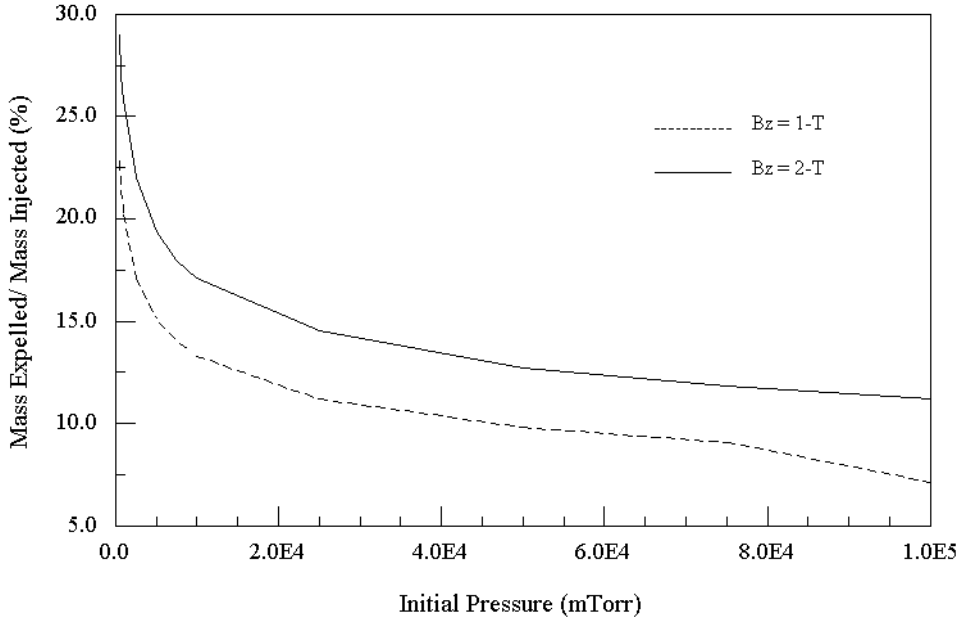

Figure 27. Fraction of propellant mass expelled vs. initial chamber pressure.

The modified theta-pinch thruster thus appears to offer a useful combination of thrust and specific impulse, but the efficiency at this point is too low for the device to be practical. For the 1-m radius thruster operating with a 2-T field, the "optimum" efficiency of 2.7% occurs for an initial chamber pressure of 50-Torr. Using Figure 23, the compressed plasma temperature corresponding to this initial chamber pressure is approximately 4.5-eV. The initial preionization temperature is assumed to be 1-eV, yielding an initial plasma energy of 2.1×10^5 J (Equation 34). The total bank energy, calculated using Equation 26, is 4.2×10^6 J; for a 100-Hz repetition rate, the average power delivered by the bank is around 4.2×10^8 Watts (420-MW). If the thruster operates at 2.7% efficiency, then roughly 1.1×10^7 Watts appears in the plasma exhaust and nearly 4.1×10^8 Watts will appear somewhere in the system as heat that will have to be dissipated. Some of this waste power can be recovered to charge the capacitor banks and perform spacecraft housekeeping duties, but a significant portion will have to be radiated into space to keep the engine walls from melting. Improvements in theta-pinch thruster performance will thus require a significant increase in thrust efficiency. One possible technique for increasing the efficiency is to increase the amount of propellant mass expelled during the pulse; since the total mass injected into the chamber will be compressed and heated, increasing the amount of mass exhausted from the thruster would improve the total impulse without significantly increasing the discharge energy. The amount of mass expelled increases linearly with the pulse duration, so if the pulse could be lengthened, the amount of mass exhausted from the thruster would be increased and the efficiency improved. This option is considered in the next section.

4.3 Change in Duration.

To investigate potential improvements in thruster performance with longer pulse periods, the analytic model was used to simulate a 1-m radius, 10-m long thruster operated with hydrogen propellant at a preionization temperature of 1-eV and a pulse duration of 10^{-3} s. Driving fields of 1-T and 2-T were again assumed, with the magnetic field distributions shown in Figure 28.

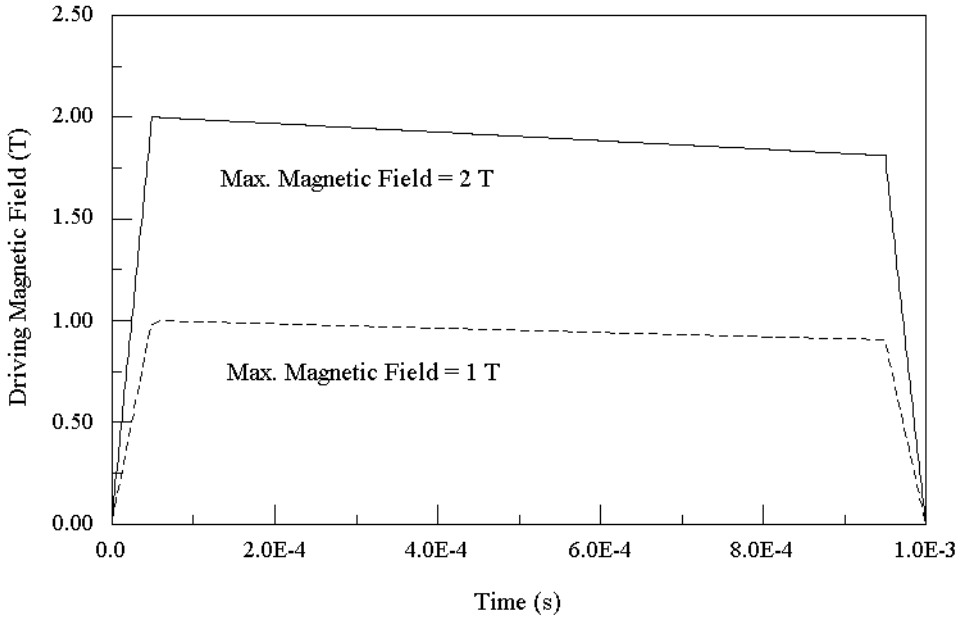

Figure 28. Driving magnetic fields for modified thruster geometry, 10^{-3} s.

The maximum plasma compression temperatures are plotted in Figure 29 as a function of the initial chamber pressure for each magnetic field strength. For the extended duration simulations, the initial chamber pressure was varied from a low of 500-mTorr (6.6×10^{-4} atm) to a high of 500-Torr (0.67 atm). The maximum compression temperatures are identical to the compression temperatures reached during the shorter 10^{-4} s discharge period (Figure 23), which is expected since the driving fields reach the same peak values in each case. For the 1-T magnetic field, the compression temperature at the lowest initial chamber pressure peaks at around 16-eV, decreasing to about 6.7-eV at the highest simulated chamber pressure. For the 2-T driving field, the compression temperature reaches 28-eV at the lower chamber pressure and decreases to 2.6-eV at the higher initial chamber pressure.

The average specific impulse for each case is shown in Figure 30. The specific impulse values achieved with the longer pulse duration are slightly higher than the average specific impulses provided by the shorter discharge times (Figure 24). This is primarily due to the form of the driving field used in each case. As noted in Section 4.2, the maximum driving field is reduced by 10% over the duration of the pulse to mimic a realistic rectangular current pulse. As a result, the magnetic field value used in the simulation drops off more quickly for shorter pulse periods. For example, the 1-T field shown in Figure 22 changes from a peak value of 1-T at 5×10^{-6} s to 0.9-T at 9.5×10^{-5} s, a drop of 10% in 9×10^{-6} seconds. In contrast, the field shown in Figure 28 drops from a

peak value of 1-T at 5×10^{-5} s to 0.9-T at 9.5×10^{-4} s, decreasing by 10% in 9×10^{-4} seconds. The confining magnetic field therefore remains higher for a longer period of time in the longer pulse simulations, and the corresponding plasma temperature remains higher for a longer period as well. Because the specific impulse is related to the plasma temperature, the average specific impulse achieved with a longer confinement period is slightly higher than the specific impulse achieved with shorter duration pulses. This result is simply an artifice of the shapes assumed for the driving magnetic fields; if the fields were constant for each pulse duration period, the specific impulse values shown in Figures 24 and 30 would be identical.

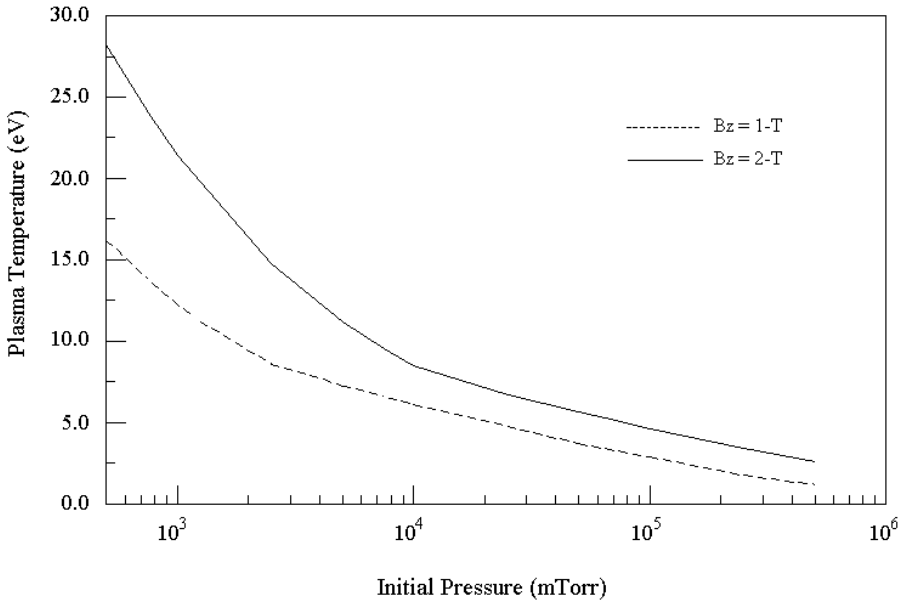

Figure 29. Maximum plasma temperature vs. initial chamber pressure.

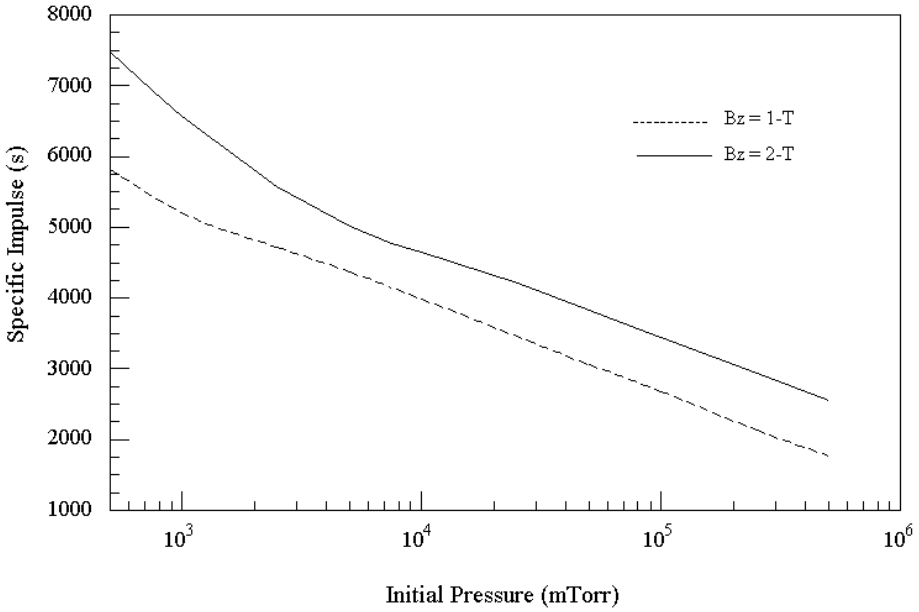

Figure 30. Average specific impulse vs. initial chamber pressure.

Figure 31 shows the impulse-bit delivered by the thruster using the longer pulse. The predicted impulse-bits are substantially higher than the impulse-bits provided by the shorter duration discharges, increasing from slightly under 1 N-s to over 190 N-s for the 1-T driving field, and from 1 N-s to around 330 N-s for the 2-T driving field over the range of simulated chamber pressures.

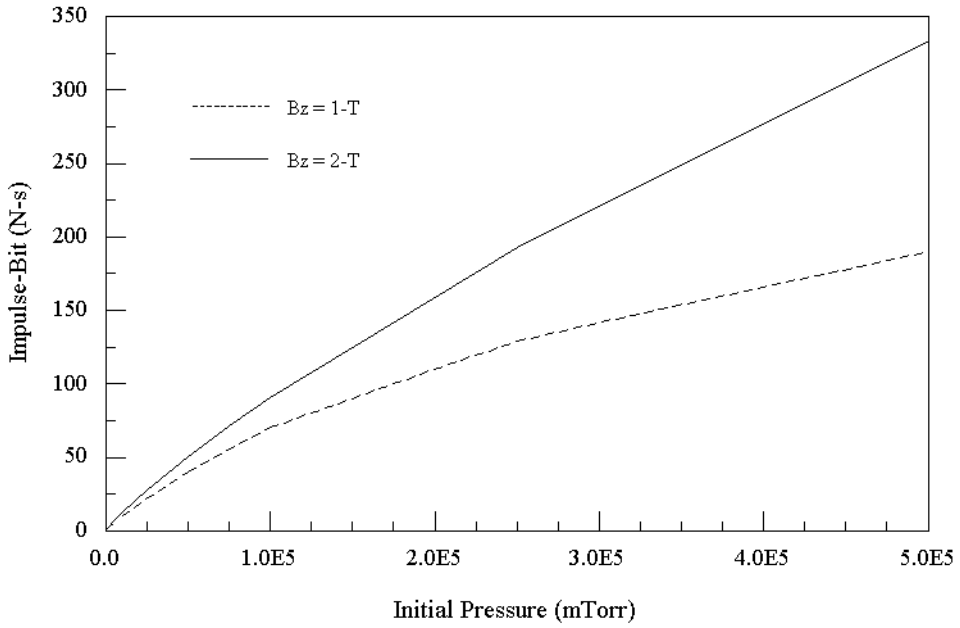

Figure 31. Impulse-bit vs. initial chamber pressure, 10^{-3} s pulse.

The pulsed thruster efficiency corresponding to the longer duration discharge is shown in Figure 32 as a function of initial chamber pressure.

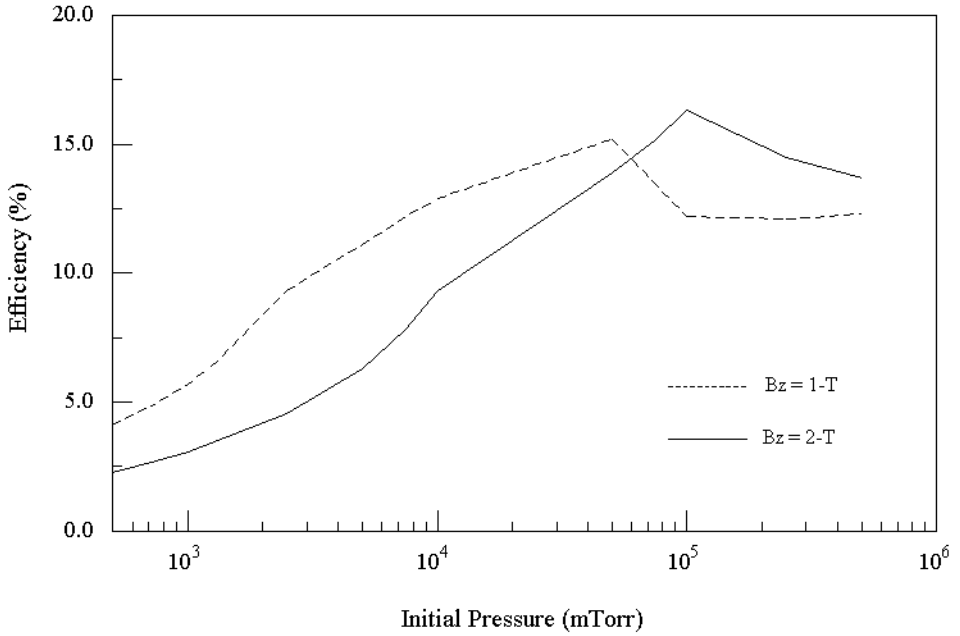

Figure 32. Efficiency vs. initial chamber pressure, 10^{-3} s pulse.

The predicted efficiencies are substantially improved when the thruster is operated with a longer discharge period. For the 1-T driving field, a peak efficiency of about 15% occurs for an initial chamber pressure of around 50-Torr. The thruster efficiency when operated with a 2-T driving field reaches 16% at an initial chamber pressure of around 100-Torr. The higher efficiencies are a consequence of better propellant mass utilization provided by the longer pulse duration. The fraction of propellant mass expelled compared to propellant mass injected remains fairly constant at around 60% over the full range of simulated chamber pressures for both the 1-T and 2-T driving fields, compared to the decreasing mass fractions observed with the short-duration pulses modeled in the previous section. While the predicted efficiencies are still lower than desired, they are within a factor of 2 of current high power magnetoplasmadynamic thrusters that operate at similar specific impulse but substantially lower thrust.[20] By tailoring the magnetic field and optimizing the initial chamber pressure, there is some hope that the pulsed theta-pinch thruster efficiencies can be further improved.

The impulse-bit delivered by the theta-pinch engine is significantly higher than the corresponding impulse delivered by current plasma propulsion devices, such that even modest pulse repetition rates will provide large average thrust values. For example, a 1-m radius, 10-m long theta-pinch thruster operated with hydrogen at a chamber pressure of 100-Torr produces an impulse-bit of around 90 N-s per pulse at an efficiency of 16%. Assuming a pulse repletion rate of 100-Hz, the average thrust produced by the engine would be around 9,000 N, with a predicted specific impulse of around 3,500 seconds. The discharge energy per pulse is predicted to be approximately 9×10^6 J, for an average engine power of 9×10^8 Watts. Operating the engine at a lower pulse rep-rate of 10-Hz reduces the average thrust to around 900-N and the average on-board power to 90-MW. These requirements are currently beyond our in-space power capabilities, but may not be unreasonable given the 20 to 40 year time frame envisioned by the NIAC charter.

4.4 Summary.

The analytic theta-pinch model was used to evaluate theta-pinch thruster performance for various chamber sizes, chamber pressures, and discharge periods. The trends in performance indicate that fairly long discharge times, on the order of 10^{-3} seconds, and fairly large discharge chambers, around 1-m in radius and 10-m long, are required for useful thruster operation. Depending on initial chamber pressures, the specific impulse of the thruster operated with a 2-T axial magnetic field varies from 7,500 s at 500-mTorr to 2,500 s at 500-Torr. The impulse-bit provided by the engine ranges from 1 N-s to 330 N-s over the same pressure range. The peak thruster efficiency is around 16%, achieved for an initial chamber pressure of 100-torr. The impulse-bit and specific impulse at this operating point are 90 N-s and 3,500 s, respectively and the discharge energy per pulse is around 9×10^6 J. For a pulse repetition rate of 10-Hz, the engine will deliver an average thrust of 900-N at 3,500 s specific impulse. Operation at this rep-rate requires an on-board power capability of around 90-MW, and the low 16% thrust efficiency will require substantial power recovery and engine cooling capabilities. Nevertheless, the combination of thrust and specific impulse provided by the theta-pinch thruster makes it a unique concept among space propulsion systems, and further development should lead to an efficient design capable of performing the bold new exploration missions envisioned by NASA and the NASA Institute for Advanced Concepts.

5.0 PRELIMINARY 2-D THRUSTER SIMULATION

In an effort to better predict the plasma properties within the theta-pinch thruster, the development of a 2-D time-dependent numerical simulation was initiated during the latter stages of the Phase I research effort. The preliminary version of the 2-D simulation uses the single-fluid, single-temperature Navier-Stokes equations for a compressible fluid, modified to incorporate magnetohydrodynamic effects. The model assumes rotational symmetry about the thruster centerline, with azimuthal derivatives set to zero. The adiabatic compression model discussed in Chapter 4 (*Analytic Theta-Pinch Model*) is used to simulate plasma compression and heating during the initial current rise in the single-turn coil. Plasma density, pressure, and temperature conditions at maximum compression are then used as initial conditions for the 2-D time dependent model. Density, energy, axial velocity, and radial velocity equations are solved using a MacCormack predictor-corrector scheme, and the equations are closed using an ideal gas equation of state. The preliminary 2-D model includes an average thermal conductivity term, but neglects the generation of internal electric and magnetic fields and plasma radiation losses. These approximations are more fully discussed in Section 5.1, which includes a parametric analysis of various plasma flow properties. Section 5.2 gives an overview of the governing equations used in the preliminary model, and the source code for the simulation is listed in Appendix C (PINCH2D.F). Section 5.3 compares preliminary 2-D code results with experimental data for the Scylla-IC theta-pinch. Section 5.4 describes future code modifications, and the chapter concludes with a brief summary of results in Section 5.5.

5.1 Approximations and Parameters.

The initial 2-D model uses single-fluid, single-temperature approximations to describe a charged plasma that is in reality composed of ions, electrons, and neutrals, each of which may have different species temperatures and flow velocities. To determine whether the simple model can provide sufficiently accurate results, an order of magnitude analysis was performed to evaluate which parameters will dominate the plasma flow physics in a pulsed theta-pinch discharge.

- Energy Equilibration.

  The first parameter of interest is the ion-electron equilibration time, t_{eq}^{ie}, which is the time it takes for ions and electrons to come into thermal equilibrium. The expression for the ion-electron equilibration time is:[52]

$$t_{eq}^{ie} = \frac{(2p)^{1/2} 6pe_0^2 m_e^{1/2} (kT_e)^{3/2}}{n_e e^4 \ln\Lambda} \tag{43}$$

  where m_e is the electron rest mass (9.1095×10^{-31} kg), ε_0 is the permittivity of free space (8.8542×10^{-12} F/m), k is Boltzmann's constant (1.3807×10^{-23} J/K), n_e is the

electron number density measured in m^{-3}, e is the electron charge (1.602×10^{-19} C), and $\ln\Lambda$ is the Coulomb logarithm, expressed as:

$$\ln\Lambda = \ln\left\{\frac{12p}{n_e^{1/2}}\left(\frac{e_0 kT}{e^2}\right)^{3/2}\right\} \tag{44}$$

The analytic models presented in Chapters 2 through 4 indicate typical plasma temperatures and number densities for a theta-pinch thruster operated with hydrogen propellant at a specific impulse of 5000 s are on the order of 5-eV and 5×10^{21} m^{-3}, respectively. For these values the Coulomb logarithm is $\ln\Lambda \approx 8$, and the ion-electron equilibration time is $t_{eq}^{ie} \approx 9\times10^{-8}$ seconds. The electrons and ions rapidly share their energy through collisions, hence the single-temperature approximation is probably not a bad assumption for the preliminary modeling effort. At the upper specific impulse range of 10000 s, the plasma density is lower ($n_e \approx 5\times10^{21}$ m^{-3}) and the temperature is higher ($T_e \approx$ 20-eV), which yields an energy equilibration time of around 5×10^{-6} seconds. This is approximately the same time required for radial plasma compression, but is shorter than the expected residence time of the plasma in a long discharge chamber. The plasma ions and electrons should therefore have sufficient time to achieve thermal equilibrium prior to exhaust from the discharge chamber. Although the single-temperature approximation is not as well justified in this case, it is still sufficiently accurate to get a general prediction of the plasma ion energy in the preliminary 2-D model.

- Radiated Energy Losses.

Radiated energy losses constitute a potential source of energy loss for high temperature plasmas, hence preliminary estimates were obtained for hydrogen plasma bremsstrahlung and synchrotron radiation. The power lost by bremsstrahlung radiation, P_{ff}, is:[53]

$$P_{ff} = \frac{32pe^6 n_e n_i Z^2}{3(4pe_0)^3 c^3 m_e h}\left(\frac{2pkT_e}{3m_e}\right)^{1/2} g_{ff} \tag{45}$$

where n_e and n_i are the electron and ion number densities (assumed to be equal), Z is the charge state of the ion (equal to unity for hydrogen), c is the speed of light (3×10^8 m/s), h is Planck's constant (6.626×10^{-34} J-s), and g_{ff} is the Gaunt factor, which is equal to 1.11 for a hydrogen plasma. As previously noted, for a thruster specific impulse of 5,000 s, the plasma temperature is about 5-eV and the number density is around 5×10^{21} m^{-3}. Substituting these values into Equation 45 yields an energy loss rate due to bremsstrahlung radiation of 9.5×10^5 J/s. Given theta-pinch pulse durations of several tens of microseconds, this energy loss is not expected to be important. However, for confinement times of several hundred microseconds, this radiated energy may constitute a significant loss term that should be taken into account. For the plasma conditions associated with higher specific impulse

values (Te ≈ 20-eV, $n_e \approx 5\times10^{20}$ m^{-3}), the bremsstrahlung radiation loss is around 2×10^4 J/s, which is lower due to the lower plasma number densities associated with higher specific impulse operation.

The mean free path for plasma absorption of all but the lowest energy bremsstrahlung photons is:

$$l_{ff} = 2.05\times10^{2}\,\frac{T_e^{1/2} n^{3}}{Z^{3} n_i^{2}} \tag{46}$$

where ν is the frequency of the radiated photon. For the plasma temperatures and densities outlined above, the mean free path for photon absorption is several orders of magnitude larger than the dimensions of the plasma, hence the photons will be lost from the plasma and absorbed in the walls of the discharge chamber. Although the energy loss from bremsstrahlung radiation may not be significant in terms of cooling the plasma, the repetitively pulsed nature of the thruster will result in substantial heating as the chamber walls absorb the bremsstrahlung photons. Bremsstrahlung radiation losses should therefore be included in future numerical simulations to better predict the thermal heat loading and required cooling of discharge chamber materials.

Synchrotron radiation losses can be estimated using:[55]

$$P_{sy} = \frac{e^2 w_{ce}^2 n_e}{3\pi e_0 c}\left(\frac{kT_e}{mc^2}\right)\left[1+\frac{5}{2}\frac{kT_e}{mc^2}+\ldots\right] \tag{47}$$

where ω_{ce} is the electron cyclotron frequency due to the motion of electrons around magnetic field lines:

$$w_{ce} = \frac{eB}{m_e} \tag{48}$$

As discussed in Chapter 2, the maximum axial magnetic field strength is assumed to be 2-T for the theta-pinch thruster; this allows a mirror ratio of around 5 for a 10-T superconducting magnet located at the upstream end of the discharge chamber. The maximum electron cyclotron frequency is thus around 3.5×10^{11} s^{-1}. For plasma conditions corresponding to a thruster specific impulse of 5,000 s, the synchrotron radiation loss is about 6×10^3 J/s, significantly lower than the bremsstrahlung radiation losses expected under the same operating conditions. For plasma conditions corresponding to a specific impulse of 10,000 s, the synchrotron radiation loss is around 2.5×10^3 J/s, again considerable smaller than the corresponding bremsstrahlung radiation losses. Plasma synchrotron losses can thus reasonably be neglected in the theta-pinch modeling effort.

- Magnetic Field Diffusion.

  The initial 2-D model assumes an impenetrable boundary layer between the axial magnetic field driving the compression and the radially compressed plasma. To evaluate this approximation, the characteristic time, τ_B, required for the magnetic field to diffuse into the plasma is calculated using:[56]

$$t_B \approx \frac{m_0 L^2}{h} \tag{49}$$

  where η is the plasma resistivity and L is a characteristic length scale of the plasma. The plasma resistivity in the radial direction is given by:[57]

$$h_\perp = 1.04 \times 10^{-4} \frac{Z \ln \Lambda}{T^{3/2}(eV)} \tag{50}$$

  where the plasma temperature has been expressed in units of electron-Volts. For a plasma temperature of around 5-eV, the resistivity is approximately 7.5×10^{-5} Ω-m. Assuming a plasma radius of around 0.1-m, the characteristic magnetic field diffusion time is around 2×10^{-4} seconds, which is sufficiently long compared to the plasma compression and exhaust time that magnetic diffusion can probably be neglected in the preliminary modeling effort. For the higher plasma temperatures corresponding to high specific impulse operation (T≈20-eV), the plasma resistivity is around 1.3×10^{-5} Ω-m, and the characteristic diffusion time is on the order of 10^{-3} seconds, which is again long enough to be neglected in a first approximation of magnetic field-plasma diffusion effects.

- Plasma Viscosity.

  The preliminary numerical model assumes negligible plasma viscosity, the accuracy of which can be evaluated by examining the Hartmann number, Ha. The Hartmann number expresses the relative importance of electromagnetic force and joule heating effects compared to viscosity effects. The Hartmann number is given by:[58]

$$Ha = BL\left(\frac{s}{h_{vis}}\right)^{1/2} \tag{51}$$

  where σ is the plasma conductivity (the inverse of the plasma resistivity) and η_{vis} is the plasma viscosity. A Hartmann number much larger than unity indicates that viscous effects can be safely ignored in a first approximation. The plasma viscosity can be calculated using:[59]

$$h_{vis} = 4.66 \times 10^{-16} \left(\frac{M^{1/2} T_i^{5/2}}{Z^4 \ln \Lambda} \right) \tag{52}$$

where M is the ion mass expressed in atomic mass units (equal to unity for hydrogen) and Z is again the ion charge (again equal to unity for hydrogen). For the plasma conditions corresponding to a thruster specific impulse of 5,000 s, the plasma ion viscosity is around 4.6×10^{-5} kg/m-s. The corresponding value of the Hartmann number is Ha $\approx 2.6 \times 10^4$ L, which is significantly larger than unity for any characteristic plasma length of interest. Viscous heating can thus be neglected in the preliminary version of the 2-D theta-pinch thruster model.

- Reynolds Number.

  A final non-dimensional parameter of interest for categorizing the plasma flow is the Reynolds number, Re. The Reynolds number indicates the relative importance of inertia to viscous forces. If Re >> 1, inertia forces dominate the flow; if Re << 1, then the viscous force acting on the flow must be taken into account. The Reynolds number is given by:[60]

$$\mathrm{Re} = \frac{VL}{n} \tag{53}$$

  where ν is the kinematic viscosity ($\nu = \eta_{vis}/\rho$), V is the flow velocity, L is a characteristic scale length, and ρ is the plasma mass density. For the plasma conditions corresponding to a thruster specific impulse of 5,000 s, the kinematic viscosity is around 5.5 m^2/s. The Reynolds number for this flow is Re $\approx 9 \times 10^3$ L, which is considerably larger than unity for lengths of interest in the theta-pinch thruster. As such, viscosity drag on the plasma flow can be ignored in the initial 2-D theta-pinch model.

5.2 Governing Equations for the 2-D Model.

Based on the analysis of parameters in the previous section, a reduced set of Navier-Stokes equations were assembled for the preliminary version of the 2-D theta-pinch simulation. The principle equations used to model the flow of the single-fluid, single-temperature plasma, presented in vector and component form, are:[61]

- Continuity:

$$\frac{\partial r}{\partial t} + \nabla \cdot (r \vec{V}) = 0 \tag{54}$$

$$\frac{\partial r}{\partial t} + \frac{\partial (r V_r)}{\partial r} + \frac{\partial (r V_z)}{\partial z} + \frac{r V_r}{r} = 0 \tag{55}$$

  where subscripts r and z refer to radial and axial directions, respectively.

- Momentum:

$$\frac{\partial(r\vec{V})}{\partial t} + (\nabla \cdot r\vec{V})\vec{V} + (r\vec{V} \cdot \nabla)\vec{V} = -\nabla P + (\vec{j} \times \vec{B}) + y_{vis} \tag{56}$$

The generation of internal electric and magnetic fields are neglected in the preliminary version of the 2-D model, hence the term $(\vec{j} \times \vec{B})$ is set to zero in the momentum equation. This is equivalent to assuming that no magnetic fields are trapped within the plasma during compression, and, as discussed in the previous section, there is complete exclusion of the applied magnetic field from the plasma interior during the discharge. Based on the above analysis, the model also assumes negligible viscosity, $\psi_{vis} = 0$. The resulting momentum components become:

Radial momentum:

$$\frac{\partial(rV_r)}{\partial t} + \frac{\partial(rV_r^2 + P)}{\partial r} + \frac{\partial(rV_rV_z)}{\partial z} + \frac{rV_rV_z}{r} = 0 \tag{57}$$

Axial momentum:

$$\frac{\partial(rV_z)}{\partial t} + \frac{\partial(rV_rV_z)}{\partial r} + \frac{\partial(rV_z^2 + P)}{\partial z} + \frac{rV_rV_z}{r} = 0 \tag{58}$$

- Energy:

The present form of the energy equation is expressed in terms of the plasma pressure:

$$\frac{\partial(rP)}{\partial t} + \frac{\partial(rPV_r)}{\partial r} + \frac{\partial(rPV_z)}{\partial z} + \frac{2}{3}rP(\nabla \cdot \vec{V}) - \frac{2}{3}(\nabla \cdot \vec{q}) = 0 \tag{59}$$

where $\vec{q} = -k_T \nabla T$, and k_T is the plasma thermal conductivity. The 2-D model currently assumes an average value for k_T throughout the plasma simulation region, calculated using:[62]

$$k_T = 4.4 \times 10^{-10} \frac{T(K)^{5/2}}{\ln \Lambda} \tag{60}$$

- Equation of State:

The above set of equations are closed with the ideal gas equation of state:

$$P = rRT = \sum nkT \tag{61}$$

where R is the gas constant, k is Boltzmann's constant, n is the plasma number density, and the summation is taken over all species present within the plasma. For the single fluid model, the pressure is taken to be P = 2nkT, where the factor of 2 is required to correctly account for electron and ions in a fully ionized plasma.

Predictor-Corrector Scheme. The continuity, momentum, and energy equations are in conservative form, and can be succinctly expressed as:

$$\frac{\P Q}{\P t}+\frac{\P F}{\P r}+\frac{\P G}{\P z}-S=0 \tag{62}$$

where (63):

$$Q=\begin{Bmatrix} r \\ rV_r \\ rV_z \\ rP \end{Bmatrix}, \qquad F=\begin{Bmatrix} rV_r \\ rV_r^2+P \\ rV_rV_z \\ rPV_r \end{Bmatrix}, \qquad G=\begin{Bmatrix} rV_z \\ rV_rV_z \\ rV_z^2+P \\ rPV_z \end{Bmatrix}, \qquad S=\begin{Bmatrix} -\dfrac{rV_r}{r} \\ -\dfrac{rV_r^2}{r} \\ -\dfrac{rV_rV_z}{r} \\ -\dfrac{2}{3}r\left(P\nabla\cdot\vec{V}+\nabla\cdot\vec{q}\right) \end{Bmatrix}$$

An explicit MacCormack predictor-corrector scheme is used to solve the component equations at each time step:[63]

- Predictor Stage:

$$q_{i,j}^{*}=q_{i,j}^{n}-\frac{\Delta t}{\Delta r}\left[F_{i+1,j}^{n}-F_{i,j}^{n}\right]-\frac{\Delta t}{\Delta z}\left[G_{i,j+1}^{n}-G_{i,j}^{n}\right]+\Delta tS_{i,j}^{n} \tag{64}$$

- Corrector Stage:

$$q_{i,j}^{n+1}=0.5\cdot\left(q_{i,j}^{n}+q_{i,j}^{*}\right)-0.5\cdot\frac{\Delta t}{\Delta r}\left[F_{i,j}^{*}-F_{i-1,j}^{*}\right]-0.5\cdot\left[G_{i,j}^{*}-G_{i,j-1}^{*}\right]+0.5\cdot\Delta tS_{i,j}^{*} \tag{65}$$

At each time step, the density, radial velocity, axial velocity, and pressure are each first predicted and then corrected according to the above prescription. The temperature at each time step is obtained from the plasma density and pressure values using the ideal gas equation of state. The equations are solved on a fixed grid consisting of 50 radial mesh points and 200 axial mesh points. The axial grid increment, Δz, is calculated by dividing the length of the simulation region (input in meters) by the number of axial grid points (200). The radial grid increment, Δr, is determined by dividing the plasma radius at compression by the number of radial grid points (50). As noted, the plasma radius at maximum compression is determined by the adiabatic portion of the simulation. The average plasma column pressure is compared to the confining magnetic field pressure at each time step, and the average plasma column radius is adjusted to match the magnetic

field pressure. Because the number of radial grid points remains constant, the time varying change in plasma column radius is modeled by changing Δr at each time step. The plasma density and pressure within the chamber is then corrected at each time step to reflect the increase or decrease in the plasma column radius.

5.3 Comparison with Experiment.

The 2-D model was compared with experimental data obtained for the Scylla-1C theta-pinch discussed in Chapter 3 (*Analytic Thruster Model*). Unlike most analytic theta-pinch models presented in the literature, the 2-D code does not include any empirical end loss or sheath terms to force a match between data and theory.

Figure 33 compares experimental plasma number density values reported for the Scylla I-C theta-pinch with predictions from the 2-D model. The number density values are not quite as accurate as the predictions made with the analytic code (Figure 10). The peak number density at compression is slightly under-predicted by the 2-D model, although it still agrees reasonably well with the experimental data. The predicted decrease in number density with time generally follows the experimental trend from roughly 2-μs until about 8-μs, at which point the simulated number density in the 2-D code plummets to roughly background values. This rapid decrease is not observed in the experimental data, and may be a result of the limited axial simulation region and corresponding inaccuracies in the 2-D plasma density boundary conditions. Future improvements to the code will extend the simulation region to include a section of the plasma exhaust plume, and an examination of boundary condition perturbations on the upstream number density distribution will be performed to eliminate artificial boundary effects during the later stages of the simulation.

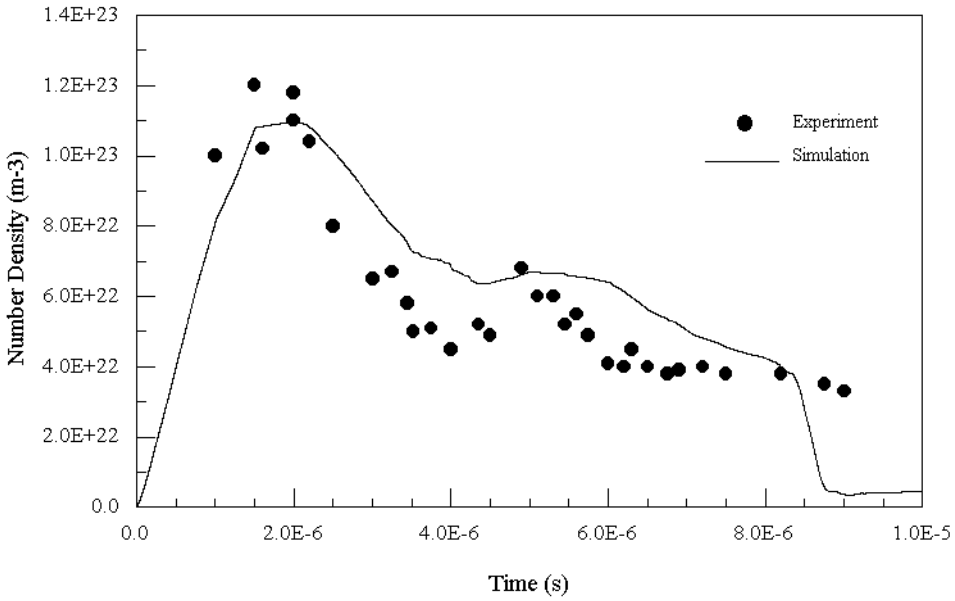

Figure 33. 2-D code predictions of Scylla-IC plasma number density vs. time.

Although the number densities are only roughly accurate, the 2-D code does a better job predicting the average plasma temperature, as shown in Figure 34. Unlike the simple analytic model outlined in Chapter 2, the 2-D simulation accurately predicts the observed plasma temperatures over the full simulation period. The small temperature spike observed at around 9-μs is probably a result of the rapidly decreasing number density in the numerical model rather than an actual temperature spike in the plasma, but even at this level the predicted temperatures fall within the range of experimental plasma temperatures. Of particular interest, the 2-D model does not have the dip in temperature between 3 and 4 μs that was observed in the prior analytic model (Figure 11), indicating that the full set of 2-D equations is required to accurately simulate plasma temperatures following compression.

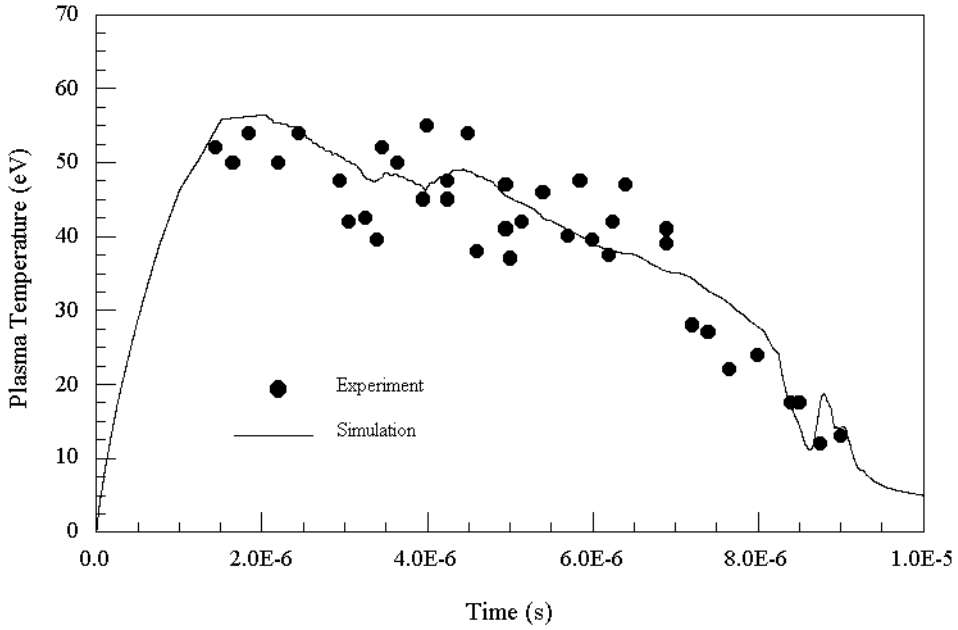

Figure 34. 2-D code predictions of Scylla-IC plasma temperature vs. time.

5.4 Model Improvements.

Although the preliminary version of the 2-D model outlined above does not perfectly reproduce the observed Scylla-IC experimental values, it does faithfully follow the general trends observed in the experimental data. It is anticipated that additional modifications to the code will lead to more accurate predictions of plasma compression and axial flow, providing a useful tool for future thruster design and development efforts. In particular, the following improvements should be incorporated into future versions of the 2-D simulation:

- Extension of the simulation region to include a portion of the thruster plume region. This is required to ensure a more accurate representation of the plasma boundary conditions, as well as to investigate potential plume divergence losses as the plasma expands away from the discharge chamber.

- Two-temperature plasma model to allow separate electron and ion energies. This is required to more accurately evaluate plasma thermal conductivity, resistivity, and viscosity effects.

- Magnetic field diffusion into the plasma and the generation of internal magnetic and electric fields. The diffusion of fields into the plasma and the trapping and generation of internal magnetic fields may lead to a decrease in the magnetic confinement pressure and the generation of joule heating within the plasma.

- More accurate treatment of the radial boundary conditions through the use of adaptive grids. As the plasma escapes axially along the field lines, the number density at the downstream end of the discharge chamber will decrease more rapidly than the density at the upstream end of the chamber. Because the magnetic pressure exerted by the discharge coil is constant along the length of the chamber, the plasma near the exit plane will pinch, creating a magnetic nozzle that will propagate upstream as more plasma is lost. This effect should be included to more accurately predict plasma exhaust velocities and impulse values.

Once more accurate predictions of the plasma properties are obtained, thruster performance can be accurately determined using the following set of equations:

- Exhaust Velocity:

  The mass-averaged plasma exhaust velocity is calculated at the exit plane of the thruster using:

$$v_{ex} = \frac{\sum_i v_{i,jc}^n r_{i,jc}^n}{\sum_i r_{i,jc}^n} \tag{66}$$

  where n is the time step index, jc is the axial grid coordinate at the exit plane of the thruster, and the summation over radial index, i, is performed from the thruster centerline to the inner chamber radius.

- Mass Flow Rate:

  The propellant mass lost from the chamber as a function of time is determined by first comparing the chamber mass density at each time step with the chamber mass density at the prior time step. The difference in average chamber mass density, $\bar{r}$, multiplied by the chamber volume determines the amount of mass, Δm, lost during a given time step:

$$\Delta m^n = \left(\bar{r}^{(n)} - \bar{r}^{(n-1)}\right) \times \left(pR^2 L\right) \tag{67}$$

where *n* again represents the time-step index. The mass flow rate, which is the amount of mass lost per unit time, is given by the change in mass, Δm, divided by the time step, Δt:

$$\dot{m}^n = \frac{\Delta m^n}{\Delta t} \tag{68}$$

- Instantaneous Thrust:

  The instantaneous thrust, F, is determined at each time step by multiplying the mass flow rate by the exhaust velocity, V_e:

$$F^n = (\dot{m} V_e)^n \tag{69}$$

- Impulse Bit:

  The impulse bit, I_{bit}, is the momentum transferred to the thruster by the pulsed plasma exhaust, measured in units of N-s. The impulse bit is determined by numerically integrating the instantaneous thrust, F, over the pulse period, τ :

$$I_{bit} = \sum_{n=1}^{N\max} F^n \Delta t \tag{70}$$

  where the time index n runs from *n* = 1 (t = 0) to *n* = Nmax (t = τ). The average thrust produced by the thruster is determined by multiplying the impulse bit by a given pulse repetition frequency, f (Hz).

- Thruster Efficiency:

  As discussed in Chapter 3, the efficiency of a pulsed thruster can be expressed as:

$$h = \frac{\frac{1}{2}\Delta M V_e^2}{E_{bank}} \tag{71}$$

  where η is the efficiency, I_{bit} is the impulse bit delivered by the thruster during each pulse, ΔM is the total mass of propellant exhausted during each pulse, and E_{bank} is the capacitor bank energy used to heat and expel the plasma. The bank energy can be estimated using:

$$E_{bank} = E_{plasma}\left(\frac{T_{mas}/T_0}{R_{coil}/R_0}\right)^2 \tag{72}$$

where E_{plasma} is the initial plasma energy (including preionization energy), T_{max} is the maximum plasma temperature achieved during compression, T_0 is the initial plasma temperature, R_{coil} is the single-turn coil radius, and R_0 is the initial plasma radius prior to compression.

5.5 Summary.

A preliminary 2-D code was developed during the Phase I research effort as a first-step toward more accurate predictions of plasma compression, heating and exhaust in a theta-pinch thruster. The current version of the 2-D code is based on a set of single-fluid, single-temperature approximations to the governing Navier-Stokes equations, which are solved on a fixed rectangular mesh that bounds the compressed plasma column. The code accurately predicts plasma temperatures, and reproduces trends in plasma number density for the Scylla-IC collisional theta-pinch. Planned improvements to the code include the incorporation of adaptive grids to more accurately represent the radial boundary between the compressed plasma and the confining magnetic field, an extension of the simulation region to include a portion of the plasma plume to better evaluate number density distributions and potential plume divergence losses, and separate electron and ion energy equations to more accurately predict thermal conductivity, resistivity, and viscosity effects. In addition, equations to evaluate the plasma velocity at the thruster exit plane and the impulse-bit delivered to the thruster by the plasma discharge will be incorporated into the code to provide thruster performance predictions. The result of the advanced modeling effort will be the development of a robust 2-D code suitable for high power theta-pinch thruster design and performance prediction.

6.0 CONCLUSIONS AND RECOMMENDATIONS

The pulsed theta-pinch thruster concept presented in this Phase I report appears to offer a unique combination of thrust and specific impulse that can enable or enhance future deep space missions. Numerical models of thruster performance indicate that a 1-m radius, 10-m long thruster operated with hydrogen propellant could provide impulse-bits ranging from 1 N-s to 330 N-s with specific impulse values of 7,500 s to 2,500 s, respectively. A pulsed magnetic field strength of 2-T is required to compress and heat the preionized hydrogen over a 10^{-3} s discharge period, with about 60% of the heated plasma exiting the chamber each period to produce thrust. The predicted thruster efficiency is fairly low, peaking at around 16% for an initial hydrogen chamber pressure of 100-Torr. The specific impulse and impulse-bit at this operating condition are 3,500 s and 90 N-s, respectively, and the required discharge energy is approximately 9×10^6 J. For a pulse repetition rate of 10-Hz, the engine would produce an average thrust of 900 N at 3500 s specific impulse and 16% efficiency. The average power needed to sustain this rep-rate is approximately 90-MW_e, a requirement that is beyond current in-space power capabilities but one that could be met within the 40-year development goal envisioned by the NASA Institute for Advanced Concepts.

The 6-month research program identified several issues that must be resolved to advance the theta-pinch thruster from concept to reality. These include:

- Propellant injection and preionization techniques. To provide uniform radial compression, the propellant has to be smoothly injected over the full length of the discharge chamber with a frequency corresponding to the thruster repetition rate. Once the propellant is injected the outer gas layers must be partially ionized to allow uniform radial compression by the pulsed axial magnetic field. Potential preionization techniques include RF-heating by external coils strategically located along the length of the thruster, short precursor current pulses sent through the single-turn coil prior to the main bank discharge, or preionized gas injection by external plasma sources. Of these methods, the precursor current seems the least complex, but other techniques may be more efficient and should be evaluated.

- Plasma detachment from axial magnetic field lines. The pulsed magnetic field produced by the single-turn discharge coil resembles the field produced by a solenoid, with magnetic field lines curving back and reconnecting along the outside of the chamber. It is anticipated that the preionized plasma will exclude most of the axial magnetic field during radial compression and exhaust, allowing the plasma to flow freely out of the chamber. However, some plasma in a sheath region may mix with the magnetic field and not separate cleanly during the exhaust. This will reduce the impulse-bit and could cause material erosion as the ionized plasma flows back toward the discharge coil. The extent to which the plasma remains attached to field lines during the discharge, and methods to mitigate this potential issue, such as collisional detachment by downstream neutral gas injection, need to be investigated.

- Plasma stability during confinement and exhaust. Prior theta-pinch experiments indicate loss of radial confinement due to radial bouncing of the high temperature, shock-driven plasma. The theta-pinch thruster does not employ rapid shock heating, but other potential instabilities such as Rayleigh-Taylor or resistive drift instabilities may occur over the relatively long confinement times required by the thruster. Instability growth rates should be modeled and checked experimentally to determine potential upper limits on the plasma compression period.

- Improvements in thrust efficiency. The theta-pinch engine operates at an average power of a few hundred megawatts, and a more efficient coupling of the discharge energy to the directed energy of the plasma propellant must be achieved to minimize chamber heating, component wear, and radiator mass. It is anticipated that a combination of numerical modeling and experimental validation will lead to significant improvements in thruster performance.

- Energy storage and power delivery systems. High-energy capacitors are fairly massive, and alternative energy storage and delivery options, such as all solid-state systems or direct-drive nuclear generators, should be evaluated in an effort to minimize mass and improve component reliability.

Based on the above requirements, a research program that combines advanced numerical models with scaled theta-pinch discharge experiments would appear to be a reasonable next step in thruster development. It is recommended that subsequent research efforts incorporate the following elements:

- Transient 2-D or 3-D MHD numerical models. The main MHD model should predict plasma parameters in the thrust chamber and exhaust plume to allow comparison with future experiments. Additional modeling efforts should be undertaken to predict plasma stability over the anticipated discharge period, and both efforts should be tied to a circuit design code that can provide realistic discharge current profiles for the single-turn coil and associated magnetic field.

- Scaled theta-pinch thruster design. Based on the code predictions, a small-scale theta-pinch thruster should be designed and fabricated to provide pulsed plasma discharge conditions dynamically similar to those of a full-scale multi-megawatt thruster.

- Experimental verification of numerical model predictions. Single-shot thruster experiments should be performed to validate the numerical model predictions. The scaled thruster should be operated at conditions dynamically similar to a full-scale theta-pinch thruster, and plasma parameters such as temperature, pressure, number density, and exhaust velocity should be measured in the chamber and exhaust plume to provide detailed comparisons with model predictions.

- Optimized thruster design. Once the numerical simulations have been verified, the codes can be used to more confidently design a full-scale theta-pinch thruster for future fabrication and testing.

If successful, the research program outlined above will lead to the design of an efficient, high-power plasma engine capable of performing the bold new exploration missions envisioned by the NASA Human Exploration and Development of Space strategic enterprise program.

ACKNOWLEDGEMENTS

This research was supported under a Phase I grant through the NASA Institute for Advanced Concepts (NIAC), Grant No. 07600-022, during the period 1 June 1999 through 30 November 1999. The Horizon Technologies Development Group expresses its sincere thanks to Dr. Robert Cassanova, Director of the NASA Institute for Advanced Concepts, and the staff of the University Space Research Association for their support during this research project.

APPENDIX A: SCALING.F

Theta-Pinch Thruster Scaling Analysis

```
C     SCALING ANALYSIS FOR THETA-PINCH THRUSTER

      OPEN(1,FILE='PINCHDAT.DAT',FORM='FORMATTED',STATUS='NEW')

500   WRITE(6,*) 'ENTER DESIRED SPECIFIC IMPULSE (s): '
      READ*, SPECIMP
      WRITE(6,*) 'ENTER CHAMBER RADIUS (M): '
      READ*,A0
      WRITE(6,*) 'ENTER INITIAL NUMBER DENSITY (#/M^3): '
      READ*,DNUM
      WRITE(6,*) 'ENTER PLASMA AMU: (eg: H=1)  '
      READ*,AMU
      WRITE(6,*) 'ENTER INITIAL TEMPERATURE (eV): '
      READ*,T0
      TK0=T0*11605.  !CONVERT TO DEGREES-K
      WRITE(6,*) 'ENTER MIRROR FIELD STRENGTH (T): '
      READ*, BM

      PI=3.1412
      VAL=1.6726E-27

C     CALCULATE REQUIRED EXHAUST VELOCITY
      VEX=9.8*SPECIMP

C     CALCULATE REQUIRED MASS FLOW RATE:
      FLOWRATE=DNUM*PI*(A0**2)*VAL*AMU*0.5*VEX

C     CALCULATE REQUIRED PLASMA TEMPERATURE (eV):
      TF=0.4*(AMU)*(VEX/1.4e4)**2
      TKF=TF*11605.  !CONVERT TO DEGREES-K

C     CALCULATE RATIO OF FINAL TO INITIAL PLASMA RADIUS:
      X=(T0/TF)**0.75

C     CALCULATE INITIAL PRESSURE:
      P0=DNUM*(1.3807E-23)*TK0

C     CALCULATE PLASMA PRESSURE AT MAX COMPRESSION:
      PF=P0*(X**(-10/3.))

C     CALCULATE REQUIRED CENTRAL CELL FIELD (T):
      B0=SQRT(2.*PF*1.26E-6)
```

```
C       CALCULATE MIRROR RATIO:
        RM=BM/B0

        IF(RM.LT.1.) THEN
        WRITE(6,*) 'MIRROR RATIO IS LESS THAN UNITY; START AGAIN'
        GO TO 500
        END IF

C       CALCULATE LOSS PROBABILITY THROUGH MIRROR
        PM=1.-SQRT((RM-1)/RM)

C       CALCULATE THRUST:
        THRUST=DNUM*PI*(A0**2)*VAL*AMU*0.5*(VEX**2)

C       WRITE DATA TO SCREEN:
        WRITE(6,*) '  EXHAUST VELOCITY (M/S):       ',VEX
        WRITE(6,*) '                         THRUST   (N):      ',THRUST
        WRITE(6,*) ' '
        WRITE(6,*) '   MINIMUM REQUIRED B-FIELD (T):      ',B0
        WRITE(6,*) '   MIRROR PARTICLE LOSS FRACT. :      ',PM
        WRITE(6,*) 'COMPRESSED PLASMA RADIUS (M):     ',X*A0
        WRITE(6,*) '          COMPRESSION RATIO (R0/RF):     ',1./X
        WRITE(6,*) '       INITIAL PLASMA PRESSURE (Pa):    ',P0
        WRITE(6,*) '         FINAL PLASMA PRESSURE (Pa):    ',PF
        WRITE(6,*) '                FINAL PLASMA TEMP. (eV):    ',TF
        WRITE(6,*)' '

C       WRITE DATA TO FILE:
        WRITE(1,101) SPECIMP
        WRITE(1,102) VEX
        WRITE(1,103) THRUST
        WRITE(1,104) FLOWRATE
        WRITE(1,105) A0
        WRITE(1,106) DNUM
        WRITE(1,107) AMU
        WRITE(1,108) T0
        WRITE(1,109) TF
        WRITE(1,110) P0
        WRITE(1,111) PF
        WRITE(1,112) BM
        WRITE(1,113) B0
        WRITE(1,114) RM
        WRITE(1,115) PM
        WRITE(1,116) X*A0
        WRITE(1,117) 1./X
        WRITE(1,120)
```

```
101     FORMAT( '  SPECIFIC IMPULSE (s): ',1PE12.6)
102     FORMAT( '  EXHAUST VELOCITY (m/s): ',1PE12.6)
103     FORMAT( '  CONTINUOUS THRUST (N): ',1PE12.6)
104     FORMAT( '  MASS FLOW RATE (kg/s): ',1PE12.6)
105     FORMAT( '  CHAMBER RADIUS (m): ',1PE12.6)
106     FORMAT( '  INITIAL NUMBER DENSITY: ',1PE12.6, 'PER M^3')
107     FORMAT( '  PLASMA SPECIES AMU: ',1PE12.6)
108     FORMAT( '  INITAL TEMPERATURE (eV): ',1PE12.6)
109     FORMAT( '  FINAL TEMPERATURE (eV): ',1PE12.6)
110     FORMAT( '  INITIAL PRESSURE (Pa): ',1PE12.6)
111     FORMAT( '  FINAL PRESSURE (Pa): ',1PE12.6)
112     FORMAT( '  MAGNET MIRROR STRENGTH (T): ',1PE12.6)
113     FORMAT( '  CENTRAL MIRROR STRENGTH (T): ',1PE12.6)
114     FORMAT( '  MIRROR RATIO VALUE: ',1PE12.6)
115     FORMAT( '  LOSS CONE FRACTION: ',1PE12.6)
116     FORMAT( '  COMPRESSED PLASMA RADIUS (m): '1PE12.6)
117     FORMAT('   COMPRESSION RATIO (R0/RF): ',1PE12.6)
120     FORMAT('  ')

        WRITE(6,*) 'RUN AGAIN? (1=Y/0=N): '
        READ*,IRUN
        IF(IRUN.EQ.1) GO TO 500

        CLOSE(1)

        STOP
        END
```

APPENDIX B: PINCH.F

Analytic Theta-Pinch Model

```
C     THETA-PINCH ANALYSIS CODE
C     SINGLE FLUID, SINGLE TEMPRATURE, COLUMN AVERAGED VALUES

      DIMENSION BVAC(50001)

      ICHECK=0          !B-FIELD CHECK
      XPAR=2.5          !END LOSS PARAMETER
      ITER=50000        !TOTAL ITERATIONS
      SHEATH=0.2        !SHEATH PARAMETER

C     INPUT PARAMETER FILE:

5000  WRITE(6,*) ' ENTER CHAMBER GEOMETRY (1=THRUSTER, 2=PINCH): '
       READ*, IGEO      !GEOMETRY FLAG
      WRITE(6,*) ' ENTER CHAMBER RADIUS (METERS): '
       READ*, CHRAD     !CHAMBER RADIUS
      WRITE(6,*) ' ENTER CHAMBER LENGTH (METERS): '
       READ*, CHLEN     !CHAMBER LENGTH
      WRITE(6,*) ' ENTER INITIAL CHAMBER PRESSURE (milliTORR): '
       READ*, PGAS      !INITIAL PRESSURE
      WRITE(6,*) ' ENTER PREIONIZED GAS TEMPERATURE (eV): '
       READ(6,*) TGAS   !INITIAL TEMPERATURE
      WRITE(6,*) ' ENTER PROPELLANT AMU (H = 1): '
       READ*, AMU       !PROPELLANT AMU
3000  WRITE(6,*) ' DRIVING MAGNETIC FIELD: '
      WRITE(6,*) '             SCYLLA-IC (1): '
      WRITE(6,*) '      USER-DEFINED (2): '
       READ*,IMAG
      WRITE(6,*) ' ENTER PLASMA BETA VALUE: '
       READ*, FRAC              !FRACTIONAL DECREASE IN B PRESSURE
      IF(IMAG.EQ.1) THEN
       TOTIME=1.E-5
       WRITE(6,*) ' TOTAL RUN TIME = 1.E-5 SEC FOR SCYLLA-IC FIELD'
       WRITE(6,*) ' '
      ELSE
       WRITE(6,*) 'ENTER MAX B-FIELD (T): '
       READ*,BMAX
       WRITE(6,*) ' ENTER TOTAL RUN TIME (SEC): '
       READ*, TOTIME
       WRITE(6,*) ' '
      END IF
```

```
C       DRIVING MAGNETIC FIELD:
        IF(IMAG.EQ.1) THEN
          ITER=50000
C       SCYLLA I-C:
          IF(ICHECK.EQ.1) THEN
          WRITE(6,*) ' OPENING B-FIELD DATA FILE...'
C       OPEN AND USE STORED DATA FILE
          OPEN(1,FILE='B_SCYLLA.TXT',FORM='FORMATTED',STATUS='OLD')
          DO 5 I=1,ITER
            READ(1,*) TIME,BVAL
            BVAC(I)=BVAL
5         CONTINUE
          CLOSE(1)
        ELSE  !CALCULATE SCYLLA-IC FIELD
C         NOTE: CALCULATED IN kG; CONVERT TO TESLA AT END
          BMAX=0.0
          BVAL=0.0
          WRITE(6,*) 'CALCULATING MAGNETIC FIELD...'
          DO 10 I=1,1300
          BVAC(I)=(I-1.)*(7.5/1299.)
10        CONTINUE
          BEND=BVAC(1300)
          DO 20 I=1300,2550
          BVAC(I)=BEND+(I-1300.)*(14.-7.5)/1250.
20        CONTINUE
          BEND=BVAC(2550)
          DO 30 I=2550,3800
          BVAC(I)=BEND+(I-2550.)*(20-14.)/1250.
30        CONTINUE
          BEND=BVAC(3800)
          DO 40 I=3800,5050
          BVAC(I)=BEND+(I-3800.)*(25-20.)/1250.
40        CONTINUE
          BEND=BVAC(5050)
          DO 50 I=5050,6300
          BVAC(I)=BEND+(I-5050.)*(28.-25.)/1250.
50        CONTINUE
          BEND=BVAC(6300)
          DO 60 I=6300,7550
          BVAC(I)=BEND+(I-6300.)*(31.5-28.)/1250.
60        CONTINUE
          BEND=BVAC(7550)
          DO 70 I=7550,8800
          BVAC(I)=BEND+(I-7550.)*(32.8-31.5)/1250.
70        CONTINUE
          BEND=BVAC(7550)
```

```
      DO 80 I=7550,10050
      BVAC(I)=BEND+(I-7550.)*(33-32.8)/1250.
80    CONTINUE
      BEND=BVAC(10050)
      DO 90 I=10050,11300
      BVAC(I)=BEND+(I-10050.)*(32.2-33.)/1250.
90    CONTINUE
      BEND=BVAC(11300)
      DO 100 I=11300,12550
      BVAC(I)=BEND+(I-11300.)*(30.-32.2)/1250.
100   CONTINUE
      BEND=BVAC(12550)
      DO 110 I=12550,13800
      BVAC(I)=BEND+(I-12550.)*(27.5-30.)/1250.
110   CONTINUE
      BEND=BVAC(13800)
      DO 120 I=13800,15050
      BVAC(I)=BEND+(I-13800.)*(25.-27.5)/1250.
120   CONTINUE
      BEND=BVAC(15050)
      DO 130 I=15050,16300
      BVAC(I)=BEND+(I-15050.)*(22.5-25.)/1250.
130   CONTINUE
      BEND=BVAC(16300)
      DO 140 I=16300,17550
      BVAC(I)=BEND+(I-16300.)*(21.3-22.5)/1250.
140   CONTINUE
      BEND=BVAC(17550)
      DO 150 I=17550,18800
      BVAC(I)=BEND+(I-17550.)*(21.-21.3)/1250.
150   CONTINUE
      BEND=BVAC(18800)
      DO 160 I=18800,20050
      BVAC(I)=BEND
160   CONTINUE
      BEND=BEND
      DO 170 I=20050,21300
      BVAC(I)=BEND+(I-20050.)*(22.-21)/1250.
170   CONTINUE
      BEND=BVAC(21300)
      DO 180 I=21300,22550
      BVAC(I)=BEND+(I-21300.)*(23.-22)/1250.
180   CONTINUE
      BEND=BVAC(22550)
      DO 190 I=22550,23800
      BVAC(I)=BEND+(I-22550.)*(24-23.)/1250.
```

```
190     CONTINUE
        BEND=BVAC(23800)
        DO 200 I=23800,25050
        BVAC(I)=BEND+(I-23800.)*(25.-24.)/1250.
200     CONTINUE
        BEND=BVAC(25050)
        DO 210 I=25050,26300
        BVAC(I)=BEND+(I-25050.)*(25.3-25.)/1250.
210     CONTINUE
        BEND=BVAC(26300)
        DO 220 I=26300,27550
        BVAC(I)=BEND+(I-26300.)*(25.5-25.3)/1250.
220     CONTINUE
        BEND=BVAC(27550)
        DO 230 I=27550,28800
        BVAC(I)=BEND+(I-27550.)*(25.3-25.5)/1250.
230     CONTINUE
        BEND=BVAC(28800)
        DO 240 I=28800,30050
        BVAC(I)=BEND+(I-28800.)*(24.9-25.3)/1250.
240     CONTINUE
        BEND=BVAC(30050)
        DO 250 I=30050,31300
        BVAC(I)=BEND+(I-30050.)*(24.-24.9)/1250.
250     CONTINUE
        BEND=BVAC(31300)
        DO 260 I=31300,32550
        BVAC(I)=BEND+(I-31300.)*(23.-24.)/1250.
260     CONTINUE
        BEND=BVAC(32550)
        DO 270 I=32550,33800
        BVAC(I)=BEND+(I-32550.)*(22.-23.)/1250.
270     CONTINUE
        BEND=BVAC(33800)
        DO 280 I=33800,35050
        BVAC(I)=BEND+(I-33800.)*(21.5-22.)/1250.
280     CONTINUE
        BEND=BVAC(35050)
        DO 290 I=35050,36300
        BVAC(I)=BEND+(I-35050.)*(21.0-21.5)/1250.
290     CONTINUE
        BEND=BVAC(36300)
        DO 300 I=36300,37550
        BVAC(I)=BEND+(I-36300.)*(20.3-21.)/1250.
300     CONTINUE
        BEND=BVAC(37550)
```

```
      DO 310 I=37550,38800
      BVAC(I)=BEND+(I-37550.)*(20-20.3)/1250.
310   CONTINUE
      BEND=BVAC(38800)
      DO 320 I=38800,40050
      BVAC(I)=BEND+(I-38800.)*(20.3-20.)/1250.
320   CONTINUE
      BEND=BVAC(40050)
      DO 330 I=40050,41300
      BVAC(I)=BEND+(I-40050)*(21.-20.3)/1250.
330   CONTINUE
      BEND=BVAC(41300)
      DO 340 I=41300,42550
      BVAC(I)=BEND+(I-41300.)*(21.7-21.)/1250.
340   CONTINUE
      BEND=BVAC(42550)
      DO 350 I=42550,43800
      BVAC(I)=BEND+(I-42550.)*(21.8-21.7)/1250.
350   CONTINUE
      BEND=BVAC(43800)
      DO 360 I=43800,45050
      BVAC(I)=BEND+(I-43800.)*(21.3-21.8)/1250.
360   CONTINUE
      BEND=BVAC(45050)
      DO 370 I=45050,46300
      BVAC(I)=BEND+(I-45050.)*(20.5-21.3)/1250.
370   CONTINUE
      BEND=BVAC(46300)
      DO 380 I=46300,47550
      BVAC(I)=BEND+(I-46300.)*(20.-20.5)/1250.
380   CONTINUE
      BEND=BVAC(47550)
      DO 390 I=47550,48800
      BVAC(I)=BEND+(I-47550.)*(19.5-20.)/1250.
390   CONTINUE
      BEND=BVAC(48800)
      DO 400 I=48800,50001
      BVAC(I)=BEND-(I-48800.)/1250.
400   CONTINUE
C     CONVERT VALUES TO TESLA:
      DO 410 I=1,ITER
      BVAC(I)=BVAC(I)/10.
410   CONTINUE
      WRITE(6,*) 'B-FIELD CALCULATIONS COMPLETE, STORING DATA...'
      OPEN(1,FILE='B_SCYLLA.TXT',FORM='FORMATTED',STATUS='NEW')
      DO 420 I=1,ITER
```

```
          WRITE(1,*) DT*(I-1), BVAC(I)
420       CONTINUE
          CLOSE(1)
         END IF
         ICHECK=1
        END IF

        IF(IMAG.EQ.2) THEN
         ITER=10000
C       INITIALIZE MAGNETIC FIELD ARRAY:
         DO 500 I=1,ITER
          BVAC(I)=0.0
500       CONTINUE
C       CALCULATE FIELD WITH QUICK RAMP, 10% DROOP:
         WRITE(6,*) 'CALCULATING MAGNETIC FIELD...'
C       RAMP UP, SLOPE BMAX WITH 10% DROOP, RAMP DOWN:
         IUP=500   !RAMP UP AND DOWN IN FIRST 5% OF TIME STEPS
         ICON=10001-IUP    !APPROX FLAT B-FIELD WITH 10% DROOP
         DO 510 I=1,10001
         IF(I.LE.IUP) BVAC(I)=(BMAX/IUP)*I
         IF((I.GT.IUP).AND.(I.LE.ICON)) THEN
          BVAC(I)=BMAX*(1.-0.1*(I-IUP)/ICON)
         END IF
         IF(I.GT.ICON) THEN
          BVAC(I)=BVAC(ICON)-(BVAC(ICON)/IUP)*(I-ICON+1.)
         END IF
         IF(BVAC(I).LT.0.) BVAC(I)=0.0
510       CONTINUE
        END IF

        WRITE(6,*) 'FINISHED FIELD CALCULATIONS...'

C       SET TIME STEP:
        DT=TOTIME/ITER

C       ACCOUNT FOR BETA < 1 IN PLASMA:
        IF(INT(FRAC).NE.1) THEN
         DO 520 I=1,ITER
          BVAC(I)=BVAC(I)*FRAC
520       CONTINUE
        END IF

C       SET CONSTANTS:
         PI=3.14159                    !PI
         XMU=PI*4.E-7                  !PERMEABILITY
         BK=1.3807E-23                 !BOLTMANN'S CONSTANT
```

```
      XMASS=AMU*1.6726E-27          !ION MASS
      IF(INT(AMU).LE.2) XION=13.6   !IONIZATION POTENTIAL

C     CONVERT PRESSURE FROM mTORR TO Pa:
      P0=PGAS*133.3/1000.
      PAV=P0
C     CONVERT TEMPERATURE FROM eV TO KELVIN:
      TEV=TGAS
      T0=TGAS*1.1605E4
      TAV=T0
      TMAX=0.
      RNEW=CHRAD
      BFLUX=0.0
      BPLASMA=0.0

C     INITIAL NUMBER DENSITY:
      DAV=P0/(BK*T0)
      DAV0=DAV
C     INITIAL COLUMN NUMBER:
      AVNUM=DAV*PI*(CHRAD**2)*CHLEN
      AVNUM0=AVNUM
      OLDNUM=AVNUM

C     CALCULATE INITIAL PROPELLANT IONIZATION FRACTION: (SAHA)
      A=0.
      B=0.
      EXPVAL=27.-(0.43*XION/TEV)
      A=3.*(TEV**1.5)*(10.**(EXPVAL))
      B=SQRT(A+4.*DAV0)
      C=SQRT(A)/2.
      FRACION=(C*B-(A/2.))/DAV0
      IF(FRACION.GT.1.) FRACION=1.0
      WRITE(6,*) ' '
      WRITE(6,*) '   INITIAL IONIZATION FRACTION = ', FRACION

      WRITE(6,*)
      WRITE(6,*) '   ***  WRITE ALL DATA TO FILES? (1=Y, 0=N): '
      READ*,IWRITE

      IF(IWRITE.EQ.1)THEN
C       OPEN DATA FILES:
C       NOTE: REQUIRES THESE DUMMY FILES TO EXIST IN FOLDER:
        OPEN(3,FILE='DATA1.TXT',FORM='FORMATTED',STATUS='OLD')
        WRITE(3,900)
        OPEN(4,FILE='DATA2.TXT',FORM='FORMATTED',STATUS='OLD')
        WRITE(4,910)
```

```
      END IF

C     ************************************************
C     COMPRESSION PHASE:
C     PLASMA COMPRESSES AS APPLIED FIELD INCREASES
C     ************************************************

      DO 550 I=1,ITER

      ICOMP=I
      TIME=I*DT

      IF(I.GT.1) THEN
        BMAX=BVAC(I-1)                          !MAX B-FIELD
        IF(BVAC(I-1).GE.BVAC(I)) GO TO 1500     !JUMP OUT OF LOOP
      END IF

C     NEW PLASMA PRESSURE:
        PAV=(BVAC(I)**2)/(2.*XMU)
        PRAT=PAV/P0

C     NEW PLASMA RADIUS:
        RNEW=CHRAD/(PRAT**0.3)
        RMIN=RNEW

C     NEW AVERAGE NUMBER DENSITY:
C     (ASSUMES COLUMN NUMBER CONSTANT DURING COMPRESSION)
        DAV=AVNUM0/(PI*(RNEW**2)*CHLEN)
        DMAX=DAV

C     NEW PLASMA TEMPERATURE:
        TAV=PAV/(2.*DAV*BK)
        TMAX=TAV

C     WRITE TO DATA FILE:
       IF(IWRITE.EQ.1) THEN
         WRITE(3,920) TIME,RNEW,PAV,AVNUM,DAV,TAV/1.1605E4
       END IF

550   CONTINUE

C     CALCULATE AVERAGE IONIZATION FRACTION AT COMPRESSION:
1500    A=0.
        B=0.
        EXPVAL=27.-(0.43*XION*1.1605E4/TAV)
        A=3.*((TAV/1.1605E4)**1.5)*(10.**(EXPVAL))
```

```
        B=SQRT(A+4.*DAV)
        C=SQRT(A)/2.
        FRACMAX=(C*B-(A/2.))/DAV
        IF(FRACMAX.GT.1.) FRACMAX=1.0
        WRITE(6,*) ' '
        WRITE(6,*) ' IONIZATION FRACTION AT COMPRESSION: ',FRACMAX
C       ENERGY CONTAINED IN IONIZATION AND DISSOCIATION:
        ENVALUE=AVNUM0*(4.47+FRACMAX*13.6)*1.6E-19  !JOULES

C       **********************************
C       EXHAUST PHASE:
C       PLASMA LOST FROM THETA-PINCH
C       **********************************

C       INITIALIZE VALUES:

        ISUM=0
        VSUM=0.0
        TMAX=0.0
        BFLUX=0.0
        TOTIMP=0.0
        AVIMP=0.0
        TOTMASS=0.0
        RMAX=RNEW
        K=0

        DO 600 I=ICOMP,ITER-1

        K=K+1
        TIME=I*DT               !TIME VALUE
        OLDNUM=AVNUM            !PREVIOUS COLUMN PARTICLE NUMBER
        OLDTEMP=TAV             !PREVIOUS TEMPERATURE VALUE
        OLDDEN=DAV              !PREVIOUS DENSITY VALUE
        OLDRAD=RNEW             !PREVIOUS RADIUS VALUE

C       CALCULATE THERMAL VELOCITY AT MAX TEMPERATURE:
        IF(TAV.GT.TMAX) TMAX=TAV
        VMAX=SQRT(3.*BK*TMAX/XMASS)

C       CONFINEMENT TIME:
        IF(IGEO.EQ.1) THEN      !THRUSTER
         TCON=XPAR*CHLEN/VMAX
        ELSE                    !THETA-PINCH
         TCON=XPAR*(CHLEN/2.)/VMAX
        END IF
         IF(TCON.LT.TOTIME) TCON=TOTIME
```

```
C       COULOMB LOGARITHM
          CLOG=23.-LOG(1217*SQRT(DAV/(TAV**3)))
          IF(CLOG.LT.5.) CLOG=5

C       THERMAL CONDUCTIVITY
          TK=(4.4E-10)*(TAV**2.5)/CLOG

C       THERMAL CONDUCTION TIME
          TCTIME=SHEATH/TK

C       CHANGE IN COLUMN PARTICLE NUMBER THIS TIME STEP:
        AVNUM=OLDNUM*(1.-DT/TCON)
        IF(AVNUM.LE.0.) THEN
          WRITE(6,*) 'AVERAGE COLUMN NUMBER IS LESS THAN ZERO...'
          WRITE(6,*) 'TIME = ',TIME
          WRITE(6,*) 'RE-RUN PROGRAM? (1/Y,0/N): '
          READ*,IRUN
          IF(IRUN.EQ.1) THEN
            GO TO 5000
          ELSE
            GO TO 2000
          END IF
        END IF

C       PLASMA RESISTIVITY:
          RESIST=8.24E-11*CLOG/(TAV**1.5)

C       PLASMA COLUMN CROSS SECTIONAL AREA:
          AREA=PI*(RNEW**2)*CHLEN

C       INDUCED MAGNETIC FLUX:
          TERM1=8.*PI*RESIST*BVAC(I)/XMU
          TERM2=1.-BFLUX/(BVAC(I)*AREA)
          BFLUX=BFLUX+(TERM1*TERM2)*DT

C       INDUCED MAGNETIC FIELD IN PLASMA:
          BPLASMA=BFLUX/AREA

C       NEW PLASMA PRESSURE:
          XTIME=(K-1.)*DT
          PAV=((BVAC(I)**2)-(BPLASMA**2))*(1.-(XTIME/TOTIME))/(2.*XMU)

C       NEW NUMBER DENSITY:
          DAV=AVNUM/(PI*(RNEW**2)*CHLEN)
```

```
C       NEW TEMPERATURE:
          TAV=PAV/(2.*DAV*BK)

C       PLASMA RADIATION LOSSES
C       ESTIMATE TOTAL ENERGY IN PLASMA:
          EZERO=1.5*BK*TAV*DAV*PI*(RNEW**2)*CHLEN
C       ESTIMATE RADIATIVE TEMPERATURE LOSS:
         IF(TAV.GT.0.) THEN
           PLOST=(1.59E-40)*(DAV**2)*SQRT(TAV)
         ELSE
          PLOST=0.0
         END IF
         ELOST=PLOST*DT*PI*(RNEW**2)*CHLEN
C       ADJUSTED ENERGY VALUE:
          ELEFT=EZERO-ELOST
C       ADJUSTED PLASMA TEMPERATURE:
          TADJ=ELEFT/(1.5*BK*DAV*PI*(RNEW**2)*CHLEN)
          TAV=TADJ

C       NEW RADIUS VALUE:
          X1=1.5*BK*DAV*(TAV-OLDTEMP)/DT
          X2=4.*BK*TAV*(DAV-OLDDEN)/DT
         IF(TCTIME.EQ.0.) THEN
          X3=0.0
         ELSE
          X3=2.*1.5*BK*DAV*TAV/TCTIME
         END IF
          X4=4.*BK*DAV*TAV
          X5=PAV
          XTERM=(X1+X2+X3)/(X4+X5)
          XOLD=OLDRAD**2
          XVAL=XOLD*(1.-XTERM*DT)
         IF(XVAL.GT.0.) THEN
          RNEW=SQRT(XVAL)
          IF(RNEW.LT.RMAX) RNEW=RMAX
         ELSE
          RNEW=RMAX
         END IF

C       NUMBER OF PARTICLES LOST IN EXHAUST:
          DELNUM=OLDNUM-AVNUM

C       AVERAGE MASS LOST THIS TIME STEP:
          DELMASS=DELNUM*XMASS

C       TOTAL MASS EXPELLED DURING PULSE:
```

```
        TOTMASS=TOTMASS+DELMASS

C       AVERAGE MASS LOSS RATE THIS TIME STEP:
        DELMDOT=DELMASS/DT

C       RMS PARTICLE VELOCITY:
        IF(TAV.GT.0.) THEN
         VEL=SQRT(3.*BK*TAV/XMASS)
        ELSE
         VEL=0.0
        END IF

C       SUM FOR AVERAGE VELOCITY VALUE OVER IMPULSE:
         VSUM=VSUM+VEL
         ISUM=ISUM+1

C       INSTANTANEOUS THRUST THIS TIME STEP:
         THRUST=(DELMDOT*VEL)

C       INSTANTANEOUS IMPULSE-BIT THIS TIME STEP:
         AVIMP=(THRUST*DT)

C       TOTAL IMPULSE (N-s):
         TOTIMP=TOTIMP+AVIMP

        IF(IWRITE.EQ.1) THEN
C        WRITE TO DATA FILE:
         WRITE(3,920) TIME,RNEW,PAV,AVNUM,DAV,TAV/1.1605E4
         WRITE(4,920) TIME,VEL,THRUST,AVIMP,TOTIMP
        END IF

600     CONTINUE

C       WRITE FINAL DATA VALUES TO SCREEN:
         DMASS=AVNUM0*XMASS       !INITIAL MASS IN CHAMBER
         PMASS=TOTMASS/DMASS      !FRACTION OF MASS EXPELLED
         AVGV=VSUM/ISUM           !AVERAGE PLASMA VELOCITY
         SPECIMP=AVGV/9.8                 !AVERAGE SPECIFIC IMPULSE
         EPLASMA=AVNUM0*TEV*1.6E-19       !INITIAL PLASMA ENERGY
         EBANK=EPLASMA*((TMAX/T0)**2)     !CAP BANK ENERGY
         IF(EBANK.LT.ENVALUE) EBANK=ENVALUE
         ETOTAL=EPLASMA+EBANK             !TOTAL ENERGY
         EFF=(TOTIMP*AVGV)/(2.*ETOTAL)    !THRUSTER EFFICIENCY
         WRITE(6,*) 'MAX B FIELD (T):            ',BMAX
         WRITE(6,*) 'INITIAL PARTICLE NUMBER:            ',AVNUM0
         WRITE(6,*) 'PREIONIZATION FRACTION:             ',FRACION
```

```
      WRITE(6,*) 'RADIUS AT COMPRESSION (m):          ',RMIN
      WRITE(6,*) 'MAXIMUM PLASMA TEMP (eV):           ',TMAX/11605.
      WRITE(6,*) 'MAX NUM DENSITY AT COMP:            ',DMAX
      WRITE(6,*) 'AVERAGE VELOCITY (M/S):             ',AVGV
      WRITE(6,*) 'AVERAGE SPECIFIC IMPULSE (S):       ',AVGV/9.8
      WRITE(6,*) 'AVERAGE IMPULSE BIT (N-S):          ',TOTIMP
      WRITE(6,*) 'PROPELLANT MASS BIT (KG):           ',TOTMASS
      WRITE(6,*) 'FRACTION OF MASS EXPELLED (%):      ',PMASS*100.
      WRITE(6,*) 'INITIAL PLASMA ENERGY (J):          ',EPLASMA
      WRITE(6,*) 'TOTAL IONIZATION ENERGY (J):        ',ENVALUE
      WRITE(6,*) 'REQUIRED BANK ENERGY (J):           ',EBANK
      WRITE(6,*) 'TOTAL DISCHARGE ENERGY (J):         ',ETOTAL
      WRITE(6,*) 'EST. THRUSTER EFFICIENCY (%):       ',EFF*100.
      WRITE(6,*) ' '

C     CHECK ON FINAL DATA WRITE:
      WRITE(6,*) ' WRITE FINAL DATA TO FILE (1/Y,0/N): '
      READ*,IFINAL
      IF(IFINAL.EQ.1) THEN
C       WRITE FINAL VALUES TO TO DATA FILE:
C       NOTE: REQUIRES DUMMY 'THRUSTER.TXT' FILE IN FOLDER:
        OPEN(10,FILE='THRUSTER.TXT',FORM='FORMATTED',STATUS='OLD')
        WRITE(10,960) DT,TOTIME,TCON
        WRITE(10,962) BMAX
        WRITE(10,950) CHRAD,CHLEN
        WRITE(10,951) PGAS,TGAS
        WRITE(10,965) AVNUM0,DAV0
        WRITE(10,966) FRACION,FRACMAX
        WRITE(10,952) XPAR,SHEATH
        WRITE(10,953) RMIN,DMAX,TMAX/11605.
        WRITE(10,954) AVGV, SPECIMP,TOTIMP
        WRITE(10,955) DMASS,TOTMASS,PMASS*100.
        WRITE(10,956) ENVALUE,EPLASMA,EBANK
        WRITE(10,957) ETOTAL,EFF*100.
        WRITE(10,980)
      END IF

960   FORMAT(' TIME STEP: '1PE12.6,' TOTAL TIME: ', 1PE12.6,
     &    ' CONFINEMENT TIME: ',1PE12.6)
962   FORMAT(' MAXIMUM MAGNETIC FIELD STRENGTH (T): ',1PE12.6)
900   FORMAT('  TIME, RADIUS, PRESSURE, NUMBER, DENSITY,'
     &    ' TEMPERATURE:')
910   FORMAT('  TIME, VELOCITY, THRUST, AV.IMP., IMPULSE BIT')
920   FORMAT(1PE12.6,2X,1PE12.6,2X,1PE12.6,2X,1PE12.6,2X,1PE12.6,
     &    2X,1PE12.6)
950   FORMAT(' CHAMBER RADIUS (m), LENGTH (m): ',1PE12.6,2X,
```

```
     &       1PE12.6)
951  FORMAT(' INITIAL PRESSURE (mT): ',1PE12.6,
     &       2X,'INITIAL TEMPERATURE (eV):', 1PE12.6)
952  FORMAT(' END LOSS AND SHEATH PARAMETERS: ',1PE12.6,2X,
     &       1PE12.6)
953  FORMAT(' COMP. RADIUS (m): ',1PE12.6,
     &      ' MAX NUM DENSITY (M-3): ',1PE12.6,
     &      ' MAX TEMP (eV):  ',1PE12.6)
954  FORMAT(' AVG VELOCITY (m/s):  ',1PE12.6,2X,
     &       ' Isp (s): ',1PE12.6,2X,
     &       ' IMPULSE-BIT (N-s): ',1PE12.6)
955  FORMAT(' MASS: INJECTED (kg): ',1PE12.6,2X,
     &       ' EXPELLED (kg): ',1PE12.6, 2X,
     &       ' PERCENT USED: ',1PE12.6)
956  FORMAT(' ENERGY :  IONIZATION (J): ',1PE12.6,2X,
     &       ' HEATING (J): ',1PE12.6,2X,
     &       ' BANK (J): ',1PE12.6)
957  FORMAT(' TOTAL PULSE ENERGY (J): ',1PE12.6,
     &       ' THRUSTER EFFICIENCY (%): ',1PE12.6)
965  FORMAT(' PARTICLE NUMBER: ',1PE12.6,
     &       ' INITIAL NUMBER DENSITY: ',1PE12.6)
966  FORMAT(' INITIAL PROPELLANT IONIZATION FRACTION: ',
     &        1PE12.6,'  FINAL PLASMA ION FRACTION: ',1PE12.6)
980  FORMAT('  ')

2000 WRITE(6,*) 'PROGRAM COMPLETE'
       WRITE(6,*) ' '
     WRITE(6,*) 'RUN AGAIN? (1=Y,0=N): '
      READ*,IRUN
     IF(IRUN.EQ.1) GO TO 5000

     IF(IWRITE.EQ.1) THEN
      CLOSE(2)
      CLOSE(3)
     END IF
     CLOSE(10)

     STOP
     END
```

APPENDIX C: PINCH2D.F CODE

2-D Numerical Theta Pinch Simulation

```
C     PROGRAM PINCH2D.F:  2-D THETA PINCH THRUSTER SIMULATION

      DIMENSION RHO(201,51),P(201,51),T(201,51),VR(201,51),
     &          VZ(201,51),BVAC(50001),RHO1(201,51),VR1(201,51),
     &          VZ1(201,51),P1(201,51),QVAL(201,51),QVAL1(201,51)

C     ********************************************
C     THETA PINCH THRUSTER INPUT PARAMETERS
C     ********************************************

C     INPUT DATA:
      WRITE(6,*) 'ENTER TOTAL RUN TIME (s): '
        READ*,TOTIME
      WRITE(6,*) 'ENTER CHAMBER RADIUS (m): '
        READ*, RCHMBR          !chamber radius
      WRITE(6,*) 'ENTER CHAMBER LENGTH (m): '
        READ*, ZCHMBR          !chamber length
      WRITE(6,*) 'ENTER INITIAL GAS PRESSURE (mT): '
        READ*, P0              !initial gas pressure
      WRITE(6,*) 'ENTER INITIAL GAS TEMPERATURE (eV): '
        READ*, T0              !initial gas temperature
      WRITE(6,*) 'ENTER PROPELLANT AMU (H=1): '
        READ*, AMU                    !propellant atomic mass
      WRITE(6,*) 'B-FIELD FROM STORED DATA FILE? (1=Y/0=N): '
        READ*,IMAG
      IF(IMAG.EQ.1) THEN
        WRITE(6,*) 'THRUSTER (1) OR THETA-PINCH (2)? '
        READ*,IGEO
      END IF
        IF(IGEO.EQ.0) IGEO=1
        WRITE(6,*) 'BETA VALUE (KINETIC/MAGNETIC): '
        READ*,BETA

      IF(IMAG.EQ.0) THEN
       OPEN(1,FILE='BVAC.TXT',FORM='FORMATTED',STATUS='NEW')
       WRITE(6,*) 'ENTER MAXIMUM CHAMBER B-FIELD (T): '
       READ*, BMAX
       BMAX=BMAX*BETA
C     TIME STEP:
        DT=TOTIME/50000.
```

```
C       VACUUM MAGNETIC FIELD VALUES:
C       RAMP UP IN FIRST 1%, BMAX WITH 10% DROOP, RAMP DOWN:
         IUP=500   !RAMP UP AND DOWN IN FIRST 1% OF TIME STEPS
         ICON=50001-IUP    !CONSTANT FIELD WITH 10% DROOP
         DO 5 I=1,50001
          IF(I.LE.IUP) BVAC(I)=(BMAX/IUP)*I
          IF((I.GT.IUP).AND.(I.LE.ICON)) THEN
            BVAC(I)=BMAX*(1.-0.1*(I-IUP)/ICON)
          END IF
          IF(I.GT.ICON) THEN
           BVAC(I)=BVAC(ICON)-(BVAC(ICON)/IUP)*(I-ICON+1.)
          END IF
         IF(BVAC(I).LT.0.) BVAC(I)=0.0
          BVAL=BVAC(I)
          WRITE(1,*) I*DT,BVAL
5        CONTINUE
         CLOSE (1)
        ELSE
         OPEN(1,FILE='BVAC.TXT',FORM='FORMATTED',STATUS='OLD')
         READ(1,*) DT,TOTIME
         DO 7 I=1,50001
          READ(1,*) J,TVAL,BVAL
          BVAC(I)=BETA*BVAL
7        CONTINUE
        END IF

C       OPEN DATA FILES:
        OPEN(2,FILE='DENSITY.TXT',FORM='FORMATTED',STATUS='NEW')
        OPEN(3,FILE='VELOCITY.TXT',FORM='FORMATTED',STATUS='NEW')
        OPEN(4,FILE='P_AND_T.TXT',FORM='FORMATTED',STATUS='NEW')
        OPEN(5,FILE='CLDEN.TXT',FORM='FORMATTED',STATUS='NEW')
        OPEN(20,FILE='INFO.TXT',FORM='FORMATTED',STATUS='NEW')
        OPEN(21,FILE='DATA1.TXT',FORM='FORMATTED',STATUS='NEW')
        OPEN(22,FILE='DATA2.TXT',FORM='FORMATTED',STATUS='NEW')

C       MAX SIMULATION DISTANCE:
         ZMAX=(ZCHMBR/IGEO)*1.5

C       SET SOME CONSTANTS:
        PI=3.141592654                  !PI
        XMU=4.*PI*1.E-7                 !PERMEABILITY OF FREE SPACE
        BOLTZCON=1.3807E-23             !BOLTZMANN'S CONSTANT
        XMASS=AMU*1.6726E-27            !ION MASS
        P0=P0*133.3/1000.               !CONVERT TO PASCALS
        T0=T0*1.1605E4                  !CONVERT TO DEGREES-K
        D0=(P0*XMASS)/(BOLTZCON*T0) !INITIAL GAS DENSITY
```

```
      PMIN=P0/1.E3                    !MINIMUM GAS PRESSURE
      TMIN=500.                       !MINIMUM GAS TEMPERATURE
      DMIN=(PMIN*XMASS)/(2.*BOLTZCON*TMIN)  !MIN DENSITY
      AVNUM=D0*PI*(RCHMBR**2)*ZCHMBR/(IGEO*XMASS)

C     SET GRID INDICES:
      DR=RCHMBR/50.          !RADIAL INCREMENT
      DZ=ZMAX/200.           !AXIAL INCREMENT
      NR=50                  !RADIAL GRID BOUNDARY
      NZ=200                 !AXIAL GRID BOUNDARY
      JC=INT(ZCHMBR/(IGEO*DZ)+0.1) !CHAMBER AXIAL GRID BOUNDARY
      ICOUNT=50001           !TOTAL NUMBER OF TIME STEPS

C     INITIALIZE ARRAYS:
      DO 10 I=1,NR+1
      DO 20 J=1,NZ+1
      IF(J.LE.JC) THEN
        T(J,I)=T0
        P(J,I)=P0
        RHO(J,I)=D0
        ELSE
        T(J,I)=TMIN
        P(J,I)=PMIN
        RHO(J,I)=DMIN
      END IF
       P1(J,I)=0.0
       VR(J,I)=0.0
       VZ(J,I)=0.0
       VR1(J,I)=0.0
       VZ1(J,I)=0.0
       RHO1(J,I)=0.0
20    CONTINUE
10    CONTINUE
      VEX=0.0
      TOTIMP=0.0

C     WRITE INITIAL DATA TO FILE:
      WRITE(20,900) DT, TOTIME
      WRITE(20,910) RCHMBR, ZCHMBR
      WRITE(20,920) P0,T0,D0
      WRITE(20,930) AMU

C     ************************************
C     INITIAL PLASMA COMPRESSION PHASE
C     ************************************
```

```
      WRITE(20,940)

      ILOOP=1       !INITIALIZE LOOP COUNTER
      OLDB=0.0      !INITIALIZE B-FIELD CHECK
      LCOUNT=0

      DO 40 I=1,50001

      LCOUNT=LCOUNT+1
      TIME=DT*ILOOP

C     IF MAX COMPRESSION REACHED, JUMP OUT OF LOOP:
      IF(BVAC(I).LT.OLDB) GO TO 500

C     CALCULATE PLASMA VALUES:
       PAV=(BVAC(I)**2)/(2.*XMU)
       PRATIO=PAV/P0
       RNEW=RCHMBR/(PRATIO**0.3)  !NEW PLASMA RADIUS
       DAV=IGEO*AVNUM*XMASS/(PI*(RNEW**2)*ZCHMBR)
       TAV=(PAV*XMASS)/(2.*BOLTZCON*DAV)
       XNUMDEN=DAV/XMASS
       OLDB=BVAC(I)   !RESET B-FIELD CHECK VALUE
       ILOOP=ILOOP+1
       IF(LCOUNT.EQ.5) THEN
        LCOUNT=0
        WRITE(20,950) TIME,RNEW
        WRITE(20,960) PAV,TAV,DAV
        WRITE(21,*) TIME,RNEW,PAV,DAV
        WRITE(22,*) TIME,XNUMDEN,TAV/11605.,VEX,TOTIMP
       END IF

40    CONTINUE


C     ******************************************************
C     MAXIMUM PLASMA COMPRESSION ACHIEVED
C     RESET RADIAL COORDINATES FOR MODEL REFINEMENT
C     ******************************************************


500   RMAX=RNEW             !MAX RADIAL DISTANCE FOR SIMULATION
      DR=RMAX/50.           !NEW RADIAL INCREMENT
      ILOOP=ILOOP-1         !CORRECT TIME LOOP COUNTER

C     AVERAGE NUMBER DENSITY IN CHAMBER:
        XNUMDEN=DAV/XMASS
```

```
C       AVERAGE PLASMA THERMAL CONDUCTIVITY:
          TK=(2.E-10)*(TAV**2.5)/(SQRT(AMU)*10.) !AVG TK

C       WRITE VALUES AT MAX COMPRESSION:
         WRITE(20,950) TIME,RNEW
         WRITE(20,960) PAV,TAV,DAV
         WRITE(21,*) TIME,RNEW,PAV,DAV
         WRITE(22,*) TIME,XNUMDEN,TAV/11605.,VEX,TOTIMP
C       WRITE COMPRESSED PLASMA INFO TO DATA FILE:
         WRITE(20,970) DR,RMAX,RNEW

C       ********************************
C       START 2-D PLASMA FLOW MODEL
C       ********************************

C       INITIAL PLASMA DISTRIBUTION:
        DO 80 J=1,NZ+1
        DO 90 I=1,NR+1
         IF(J.LE.JC) THEN
          P(J,I)=PAV          !AVERAGE COMPRESSION VALUES
          RHO(J,I)=DAV        !INSIDE CHMABER AT START
         ELSE
          P(J,I)=PAV*(JC+10-J)/10.
          RHO(J,I)=DAV*(JC+10-J)/10.
         END IF
         IF(P(J,I).LT.PMIN) P(J,I)=PMIN
         IF(RHO(J,I).LT.DMIN) RHO(J,I)=DMIN
         T(J,I)=(P(J,I)*XMASS)/(2.*BOLTZCON*RHO(J,I))
         IF(T(J,I).LT.TMIN) T(J,I)=TMIN
90      CONTINUE
80      CONTINUE

        WRITE(20,990)

        K=0
        KRAD=0
        FIN=0.0
        DOLD=0.0
        DMDT=0.0
        DMASS=0.0
        DELRHO=0.0
        TOTIMP=0.0
        MCOUNT=0

C       WRITE CENTERLINE PLASMA DENSITY AT COMPRESSION:
          WRITE(5,*) TIME
```

```
          DO 100 J=1,NZ+1
          WRITE(5,*) (J-1)*DZ,RHO(J,1)
100       CONTINUE

2000   ILOOP=ILOOP+1     !CONTINUE LOOP COUNTER
       TIME=ILOOP*DT     !TIME VALUE
       K=K+1
       KRAD=KRAD+1
       MCOUNT=MCOUNT+1
       DOLD=DAV
       ROLD=RNEW

C      *****************
C      PREDICTOR STEP:
C      *****************

       CALL RHOPRED(DR,DZ,DT,NR,NZ,RHO,VR,VZ,RHO1,DAV,DMIN)

       CALL VRPRED(DR,DZ,DT,NR,NZ,RHO,VR,VZ,P,VR1,RHO1,
     &                  QVAL,QVAL1)

       CALL VZPRED(DR,DZ,DT,NR,NZ,RHO,VR,VZ,P,VZ1,RHO1,
     &                  QVAL,QVAL1)

       CALL ENPRED(DR,DZ,DT,NR,NZ,P,T,TK,VR,VZ,P1,PMIN)

C      ******************
C      CORRECTOR STEP:
C      ******************

       CALL RHOCORR(DR,DZ,DT,NR,NZ,JC,RHO,RHO1,VR1,VZ1,
     &                   DAV,DMIN)

       CALL VRCORR(DR,DZ,DT,NR,NZ,RHO,RHO1,VR,VR1,VZ1,P1,
     &                  QVAL,QVAL1)

       CALL VZCORR(DR,DZ,DT,NR,NZ,RHO,RHO1,VR1,VZ,VZ1,P1,
     &                  QVAL,QVAL1)

       CALL ENCORR(DR,DZ,DT,NR,NZ,JC,P,T,TK,P1,VR1,VZ1,
     &                  PAV,PMIN)


C      NEW RADIUS FROM PRESSURE BALANCE:
         PMAG=(BVAC(ILOOP)**2)/(2.*XMU)
         RNEW=RMAX/((PMAG/PAV)**0.3)
```

```
        DR=RNEW/50.
        XRAD=ROLD/RNEW

C       SMOOTH VALUES:
        DO 150 I=1,NR+1
        DO 160 J=2,NZ+1
         IF(P(J,I).GT.P(J-1,I)) P(J,I)=P(J-1,I)
         IF(VZ(J,I).LT.VZ(J-1,I)) VZ(J,I)=VZ(J-1,I)
         IF(RHO(J,I).GT.RHO(J-1,I)) RHO(J,I)=RHO(J-1,I)
160     CONTINUE
150     CONTINUE

C       CORRECTED TEMPERATURE:
         TSUM=0.0
         RSUM=0.0
         TSUM1=0.0
         DSUM1=0.0
         KSUM=0
        DO 170 I=1,NR+1
        DO 180 J=1,NZ+1
         T(J,I)=(P(J,I)*XMASS)/(2.*BOLTZCON*RHO(J,I))
         IF(T(J,I).LT.TMIN) T(J,I)=TMIN
         TSUM1=TSUM1+T(J,I)
         DSUM1=DSUM1+RHO(J,I)
         KSUM=KSUM+1
        IF(J.LE.JC) THEN      !AVG CHAMBER PLASMA TEMPERATURE
         TSUM=TSUM+(T(J,I)*RHO(J,I))
         RSUM=RSUM+RHO(J,I)
        END IF
180     CONTINUE
170     CONTINUE
        TAV=TSUM/RSUM
        TAV1=TSUM1/KSUM
        DAV1=DSUM1/KSUM
        XDEN1=DAV1/XMASS

C       AVERAGE COULOMB LOGARITHM:
         CLOG=23.-LOG(1217.*SQRT(XDEN1/(TAV1**3)))
         IF(CLOG.LT.5.) CLOG=5.
C       AVERAGE ION THERMAL CONDUCTIVITY COEFFICIENT:
         OLDTK=TK
         TK=(2.E-10)*(TAV1**2.5)/(SQRT(AMU)*CLOG)
         TK=(TK+OLDTK)/2.

C       AVERAGE NUMBER DENSITY IN CHAMBER:
         XNUMDEN=DAV/XMASS
```

```
C       MODIFY PRESSURE, DENSITY FOR CHANGE IN RADIUS:
        DO 190 I=1,NR+1
        DO 200 J=1,NZ+1
          P(J,I)=P(J,I)*(XRAD**2)
          RHO(J,I)=RHO(J,I)*(XRAD**2)
200     CONTINUE
190     CONTINUE

C       EXHAUST VELOCITY:
        VSUM=0.0
        DSUM=0.0
        DO 210 I=1,NR+1
          VSUM=VSUM+(VZ(JC,I)*RHO(J,I))
          DSUM=DSUM+RHO(J,I)
210     CONTINUE
        VEX=VSUM/DSUM

C       CHANGE IN MASS DENSITY WITHIN THRUSTER:
          DELRHO=ABS(DOLD-DAV)

C       MASS LOST FROM CHAMBER:
          DMASS=DELRHO*PI*(RNEW**2)*ZCHMBR

C       MASS FLOW RATE FROM THRUSTER:
          DMDT=DMASS/DT

C       INSTANTANEOUS THRUST:
          FIN=DMDT*VEX

C       TOTAL IMPULSE BIT:
          TOTIMP=TOTIMP+FIN*DT

        IF(MCOUNT.EQ.10) THEN
C        WRITE DATA TO INFO FILE:
          WRITE(20,1000) TIME
          WRITE(20,1010) DR,RNEW
          WRITE(20,1050) PAV,TAV,DAV
          WRITE(20,1150) VEX,FIN,TOTIMP
C       WRITE DATA TO DATA FILE FOR LINE PLOTS:
          WRITE(21,*) TIME,RNEW,PAV,DAV
          WRITE(22,*) TIME,XNUMDEN,TAV/11605.,VEX,TOTIMP
C       WRITE DATA TO SCREEN:
          WRITE(6,*) TIME,PAV,TAV/11605.,XNUMDEN,VEX
C       RESET COUNTER:
          MCOUNT=0
```

```
      END IF

      IF((K.EQ.10000).OR.(K.EQ.50000)) THEN
       DO 220 I=1,NR+1
       DO 230 J=1,NZ+1
        WRITE(2,1100) J,I,RHO(J,I)
        WRITE(3,1200) J,I,VR(J,I),VZ(J,I)
        WRITE(4,1200) J,I,P(J,I),T(J,I)
230     CONTINUE
220     CONTINUE
      END IF

C     WRITE CENTERLINE DENSITY AT VARIOUS TIMES:
      IF(KRAD.EQ.10000) THEN
        WRITE(5,*) TIME
        DO 260 J=1,NZ+1
          WRITE(5,*) (J-1)*DZ,RHO(J,1)
260     CONTINUE
        KRAD=0
      END IF

C     CHECK TIME LOOP:
      IF(ILOOP.LT.ICOUNT) GO TO 2000

C     **********************
C     FORMAT STATEMENTS:
C     **********************

900   FORMAT(' TIME STEP (S): ',1E12.6,
     &     ' TOTAL RUN TIME (S): ',1PE12.6)
910   FORMAT(' CHAMBER RADIUS (M): ',1PE12.6,
     &     ' CHAMBER LENGTH (M): ',1PE12.6)
920   FORMAT(' INITIAL PRESSURE (Pa): ',1PE12.6,
     &     ' TEMP (K): ',1PE12.6,' DENSITY: ',1PE12.6)
930   FORMAT(' PROPELLANT AMU: ',1PE12.6)
940   FORMAT('  *** COMPRESSED PLASMA VALUES ***')
950   FORMAT(' TIME (S): ',1PE12.6,' PLASMA RADIUS (M):',
     &       1PE12.6)
960   FORMAT(' AVG. PRESSURE (Pa): ',1PE12.6,
     &     ' TEMP (K): ',1PE12.6,' DENSITY: ',1PE12.6)
970   FORMAT(' DR: ',1PE12.6,' RMAX: ',1PE12.6,' RNEW: ',1PE12.6)
980   FORMAT(' PLASMA RADIUS: ',1PE12.6,' INDEX: ',I5)
990   FORMAT(' ****2-D PLASMA FLOW MODEL****')
1000  FORMAT(' TIME: ',1PE12.6)
1010  FORMAT('      DR: ',1PE12.6,' PLASMA RADIUS: ',1PE12.6)
```

```
1050   FORMAT('      PAV: ',1PE12.6,' TAV: ',1PE12.6,'  DAV: ',
     &        1PE12.6)
1100   FORMAT(2I5,1PE15.6)
1150   FORMAT('      VEX: ',1PE12.6,' THR: ',1PE12.6,' IBIT: ',
     &        1PE12.6)
1200   FORMAT(2I5,2X,1PE12.6,2X,1PE12.6)

3000   CLOSE(2)
       CLOSE(3)
       CLOSE(4)
       CLOSE(5)
       CLOSE(20)
       CLOSE(21)

       STOP
       END PROGRAM


C      **********
C      SUBROUTINE LISTINGS:
C      **********

       SUBROUTINE RHOPRED(DR,DZ,DT,NR,NZ,RHO,VR,VZ,RHO1,DAV,
     &        DMIN)

       DIMENSION RHO(NZ+1,NR+1),RHO1(NZ+1,NR+1),VR(NZ+1,NR+1),
     &        VZ(NZ+1,NR+1)

       DTR=DT/DR
       DTZ=DT/DZ

C      DENSITY PREDICTOR STEP:
       DO 100 J=2,NZ
       DO 110 I=2,NR
       FUP=RHO(J,I+1)*VR(J,I+1)
       FDN=RHO(J,I)*VR(J,I)
       GUP=RHO(J+1,I)*VZ(J+1,I)
       GDN=RHO(J,I)*VZ(J,I)
       S=-RHO(J,I)*VR(J,I)/((I-1.)*DR)
       RHO1(J,I)=RHO(J,I)-DTR*(FUP-FDN)-DTZ*(GUP-GDN)+DT*S
110    CONTINUE
100    CONTINUE

       DO 140 I=2,NR
       DO 150 J=2,NZ
       IF(RHO1(J,I).LT.DMIN) RHO1(J,I)=DMIN
```

```
150   CONTINUE
140   CONTINUE

      DO 120 I=1,NR+1
      RHO1(1,I)=RHO1(2,I)
      RHO1(NZ+1,I)=RHO1(NZ,I)
120   CONTINUE
      DO 130 J=1,NZ+1
      RHO1(J,1)=RHO1(J,2)
      RHO1(J,NR+1)=RHO1(J,NR)
130   CONTINUE

      RETURN
      END


      SUBROUTINE VRPRED(DR,DZ,DT,NR,NZ,RHO,VR,VZ,P,VR1,RHO1,
     &      QVAL,QVAL1)

      DIMENSION RHO(NZ+1,NR+1),VR(NZ+1,NR+1),VZ(NZ+1,NR+1),
     &      VR1(NZ+1,NR+1),QVAL(NZ+1,NR+1),QVAL1(NZ+1,NR+1),
     &      RHO1(NZ+1,NR+1),P(NZ+1,NR+1)

      DTR=DT/DR
      DTZ=DT/DZ

      DO 10 I=1,NR+1
      DO 20 J=1,NZ+1
      QVAL(J,I)=0.0
      QVAL1(J,I)=0.0
20    CONTINUE
10    CONTINUE

C     RADIAL VELOCITY PREDICTOR STEP:
      DO 100 J=2,NZ
      DO 110 I=2,NR
      QVAL(J,I)=RHO(J,I)*VR(J,I)
      FUP=RHO(J,I+1)*(VR(J,I+1)**2)+P(J,I+1)
      FDN=RHO(J,I)*(VR(J,I)**2)+P(J,I)
      GUP=RHO(J+1,I)*VR(J+1,I)*VZ(J+1,I)
      GDN=RHO(J,I)*VR(J,I)*VZ(J,I)
      S=-RHO(J,I)*(VR(J,I)**2)/((I-1.)*DR)
      QVAL1(J,I)=QVAL(J,I)-DTR*(FUP-FDN)-DTZ*(GUP-GDN)+DT*S
110   CONTINUE
100   CONTINUE
```

```
      DO 120 I=1,NR+1
      QVAL1(1,I)=QVAL1(2,I)
      QVAL1(NZ+1,I)=QVAL1(NZ,I)
120   CONTINUE
      DO 130 J=1,NZ+1
      QVAL1(J,1)=0.0
      QVAL1(J,NR+1)=QVAL1(J,NR)
130   CONTINUE

      DO 140 J=1,NZ+1
      VR1(J,1)=0.0
      DO 150 I=2,NR+1
      VR1(J,I)=QVAL1(J,I)/RHO1(J,I)
150   CONTINUE
140   CONTINUE

      RETURN
      END


      SUBROUTINE VZPRED(DR,DZ,DT,NR,NZ,RHO,VR,VZ,P,VZ1,RHO1,
     &      QVAL,QVAL1)

      DIMENSION RHO(NZ+1,NR+1),VR(NZ+1,NR+1),VZ(NZ+1,NR+1),
     &      VZ1(NZ+1,NR+1),QVAL(NZ+1,NR+1),QVAL1(NZ+1,NR+1),
     &      RHO1(NZ+1,NR+1),P(NZ+1,NR+1)

      DTR=DT/DR
      DTZ=DT/DZ

      DO 10 I=1,NR+1
      DO 20 J=1,NZ+1
      QVAL(J,I)=0.0
      QVAL1(J,I)=0.0
20    CONTINUE
10    CONTINUE

C     AXIAL VELOCITY PREDICTOR STEP:
      DO 100 J=2,NZ
      DO 110 I=2,NR
      QVAL(J,I)=RHO(J,I)*VZ(J,I)
      FUP=RHO(J,I+1)*VR(J,I+1)*VZ(J,I+1)
      FDN=RHO(J,I)*VR(J,I)*VZ(J,I)
      GUP=RHO(J+1,I)*(VZ(J+1,I)**2)+P(J+1,I)
      GDN=RHO(J,I)*(VZ(J,I)**2)+P(J,I)
      S=-RHO(J,I)*VR(J,I)*VZ(J,I)/((I-1.)*DR)
```

```
      QVAL1(J,I)=QVAL(J,I)-DTR*(FUP-FDN)-DTZ*(GUP-GDN)+DT*S
110   CONTINUE
100   CONTINUE

      DO 120 I=1,NR+1
      QVAL1(1,I)=QVAL1(2,I)
      QVAL1(NZ+1,I)=QVAL1(NZ,I)
120   CONTINUE
      DO 130 J=1,NZ+1
      QVAL1(J,1)=QVAL1(J,2)
      QVAL1(J,NR+1)=QVAL1(J,NR)
130   CONTINUE

      DO 140 J=1,NZ+1
      DO 150 I=1,NR+1
      VZ1(J,I)=QVAL1(J,I)/RHO1(J,I)
      IF(VZ1(J,I).LT.0.) VZ1(J,I)=0.0
150   CONTINUE
140   CONTINUE

      RETURN
      END


      SUBROUTINE ENPRED(DR,DZ,DT,NR,NZ,P,T,TK,VR,VZ,P1,PMIN)

      DIMENSION P(NZ+1,NR+1),P1(NZ+1,NR+1),VR(NZ+1,NR+1),
     &          VZ(NZ+1,NR+1),T(NZ+1,NR+1)

      DTR=DT/DR
      DTZ=DT/DZ

      DO 100 J=2,NZ
      DO 110 I=2,NR
      FUP=P(J,I+1)*VR(J,I+1)
      FDN=P(J,I)*VR(J,I)
      GUP=P(J+1,I)*VZ(J+1,I)
      GDN=P(J,I)*VZ(J,I)
      S1=(5./3.)*P(J,I)*VR(J,I)/((I-1.)*DR)
      S2=(VR(J,I+1)-VR(J,I-1))/(2.*DR)
      S3=(VZ(J+1,I)-VZ(J-1,I))/(2.*DZ)
      S4A=(T(J,I+1)-2.*T(J,I)+T(J,I-1))/(DR**2)
      S4B=(T(J,I+1)-T(J,I-1))/(2.*(I-1.)*(DR**2))
      S4C=(T(J+1,I)-2.*T(J,I)+T(J-1,I))/(DZ**2)
      S4=-TK*(S4A+S4B+S4C)
      S=-(S1+(2./3.)*(S2+S3)-S4)
```

```
      P1(J,I)=P(J,I)-DTR*(FUP-FDN)-DTZ*(GUP-GDN)+DT*S
110   CONTINUE
100   CONTINUE

      DO 140 I=2,NR
      DO 150 J=2,NZ
      IF(P1(J,I).LT.PMIN) P1(J,I)=PMIN
150   CONTINUE
140   CONTINUE

      DO 120 I=1,NR+1
      P1(1,I)=P1(2,I)
      P1(NZ+1,I)=P1(NZ,I)
120   CONTINUE
      DO 130 J=2,NZ
      P1(J,1)=P1(J,2)
      P1(J,NR+1)=P1(J,NR)
130   CONTINUE

      RETURN
      END


      SUBROUTINE RHOCORR(DR,DZ,DT,NR,NZ,JC,RHO,RHO1,VR1,VZ1,
     &          DAV,DMIN)

      DIMENSION RHO(NZ+1,NR+1),RHO1(NZ+1,NR+1),VR1(NZ+1,NR+1),
     &         VZ1(NZ+1,NR+1)

      DTR=DT/DR
      DTZ=DT/DZ

      DO 100 J=2,NZ
      DO 110 I=2,NR
      QVAL=RHO(J,I)+RHO1(J,I)
      FUP=RHO1(J,I)*VR1(J,I)
      FDN=RHO1(J,I-1)*VR1(J,I-1)
      GUP=RHO1(J,I)*VZ1(J,I)
      GDN=RHO1(J-1,I)*VZ1(J-1,I)
      S=-RHO1(J,I)*VR1(J,I)/((I-1.)*DR)
      RHO(J,I)=0.5*(QVAL-DTR*(FUP-FDN)-DTZ*(GUP-GDN)+DT*S)
110   CONTINUE
100   CONTINUE

      DO 140 I=2,NR
      DO 150 J=2,NZ
```

```
      IF(RHO(J,I).LT.DMIN) RHO(J,I)=DMIN
150   CONTINUE
140   CONTINUE

      DO 120 I=1,NR+1
      RHO(1,I)=RHO(2,I)
      RHO(NZ+1,I)=RHO(NZ,I)
120   CONTINUE
      DO 130 J=1,NZ+1
      RHO(J,1)=RHO(J,2)
      RHO(J,NR+1)=RHO(J,NR)
130   CONTINUE

C     AVERAGE CHAMBER DENSITY:
      DAV=0.0
      DSUM=0.0
      KSUM=0.0
      DO 160 J=1,JC
      DO 170 I=1,NR+1
      DSUM=DSUM+RHO(J,I)
      KSUM=KSUM+1
170   CONTINUE
160   CONTINUE
      DAV=DSUM/KSUM

      RETURN
      END


      SUBROUTINE VRCORR(DR,DZ,DT,NR,NZ,RHO,RHO1,VR,VR1,VZ1,P1,
     &          QVAL,QVAL1)

      DIMENSION RHO(NZ+1,NR+1),RHO1(NZ+1,NR+1),VR(NZ+1,NR+1),
     &     VR1(NZ+1,NR+1),VZ1(NZ+1,NR+1),P1(NZ+1,NR+1),
     &     QVAL(NZ+1,NR+1),QVAL1(NZ+1,NR+1)

      DTR=DT/DR
      DTZ=DT/DZ

      DO 10 I=1,NR+1
      DO 20 J=1,NZ+1
      QVAL(J,I)=RHO(J,I)*VR(J,I)
      QVAL1(J,I)=RHO1(J,I)*VR1(J,I)
20    CONTINUE
10    CONTINUE
```

```
      DO 100 J=2,NZ
      DO 110 I=2,NR
      QTERM=QVAL(J,I)+QVAL1(J,I)
      FUP=RHO1(J,I)*(VR1(J,I)**2)+P1(J,I)
      FDN=RHO1(J,I-1)*(VR1(J,I-1)**2)+P1(J,I-1)
      GUP=RHO1(J,I)*VR1(J,I)*VZ1(J,I)
      GDN=RHO1(J-1,I)*VR1(J-1,I)*VZ1(J-1,I)
      S=-RHO1(J,I)*(VR1(J,I)**2)/((I-1.)*DR)
      QVAL(J,I)=0.5*(QTERM-DTR*(FUP-FDN)-DTZ*(GUP-GDN)+DT*S)
110   CONTINUE
100   CONTINUE

      DO 120 I=1,NR+1
      QVAL(1,I)=QVAL(2,I)
      QVAL(NZ+1,I)=QVAL(NZ,I)
120   CONTINUE
      DO 130 J=1,NZ+1
      QVAL(J,1)=0.0
      QVAL(J,NR+1)=QVAL(J,NR)
130   CONTINUE

      DO 140 J=1,NZ+1
      VR(J,1)=0.0
      DO 150 I=1,NR+1
      VR(J,I)=QVAL(J,I)/RHO(J,I)
150   CONTINUE
140   CONTINUE

    RETURN
    END


      SUBROUTINE VZCORR(DR,DZ,DT,NR,NZ,RHO,RHO1,VR1,VZ,VZ1,P1,
     &          QVAL,QVAL1)

      DIMENSION RHO(NZ+1,NR+1),RHO1(NZ+1,NR+1),VR1(NZ+1,NR+1),
     &      VZ(NZ+1,NR+1),VZ1(NZ+1,NR+1),P1(NZ+1,NR+1),
     &      QVAL(NZ+1,NR+1),QVAL1(NZ+1,NR+1)

      DTR=DT/DR
      DTZ=DT/DZ

      DO 10 J=1,NZ+1
      DO 20 I=1,NR+1
      QVAL(J,I)=RHO(J,I)*VZ(J,I)
      QVAL1(J,I)=RHO1(J,I)*VZ1(J,I)
```

```
20      CONTINUE
10      CONTINUE

        DO 100 J=2,NZ
        DO 110 I=2,NR
        QTERM=QVAL(J,I)+QVAL1(J,I)
        FUP=RHO1(J,I)*VR1(J,I)*VZ1(J,I)
        FDN=RHO1(J,I-1)*VR1(J,I-1)*VZ1(J,I-1)
        GUP=RHO1(J,I)*(VZ1(J,I)**2)+P1(J,I)
        GDN=RHO1(J-1,I)*(VZ1(J-1,I)**2)+P1(J-1,I)
        S=-RHO1(J,I)*VR1(J,I)*VZ1(J,I)/((I-1.)*DR)
        QVAL(J,I)=0.5*(QTERM-DTR*(FUP-FDN)-DTZ*(GUP-GDN)+DT*S)
110     CONTINUE
100     CONTINUE

        DO 120 I=1,NR+1
        QVAL(1,I)=QVAL(2,I)
        QVAL(NZ+1,I)=QVAL(NZ,I)
120     CONTINUE
        DO 130 J=1,NZ+1
        QVAL(J,1)=QVAL(J,2)
        QVAL(J,NR+1)=QVAL(J,NR)
130     CONTINUE

        DO 140 J=1,NZ+1
        DO 150 I=1,NR+1
        VZ(J,I)=QVAL(J,I)/RHO(J,I)
        IF(VZ(J,I).LT.0.) VZ(J,I)=0.0
150     CONTINUE
140     CONTINUE

        RETURN
        END


        SUBROUTINE ENCORR(DR,DZ,DT,NR,NZ,JC,P,T,TK,P1,VR1,VZ1,
     &              PAV,PMIN)

        DIMENSION P(NZ+1,NR+1),P1(NZ+1,NR+1),VR1(NZ+1,NR+1),
     &          VZ1(NZ+1,NR+1),T(NZ+1,NR+1)

        DTR=DT/DR
        DTZ=DT/DZ

        DO 100 J=2,NZ
        DO 110 I=2,NR
```

```
      QTERM=P1(J,I)+P(J,I)
      FUP=P1(J,I)*VR1(J,I)
      FDN=P1(J,I-1)*VR1(J,I-1)
      GUP=P1(J,I)*VZ1(J,I)
      GDN=P1(J-1,I)*VZ1(J-1,I)
      S1=(5./3.)*P1(J,I)*VR1(J,I)/((I-1.)*DR)
      S2=(VR1(J,I+1)-VR1(J,I-1))/(2.*DR)
      S3=(VZ1(J+1,I)-VZ1(J-1,I))/(2.*DZ)
      S4A=(T(J,I+1)-2.*T(J,I)+T(J,I-1))/(DR**2)
      S4B=(T(J,I+1)-T(J,I-1))/(2.*(I-1.)*(DR**2))
      S4C=(T(J+1,I)-2.*T(J,I)+T(J-1,I))/(DZ**2)
      S4=-TK*(S4A+S4B+S4C)
      S=-(S1+(2./3.)*(S2+S3)-S4)
      P(J,I)=0.5*(QTERM-DTR*(FUP-FDN)-DTZ*(GUP-GDN)+DT*S)
110   CONTINUE
100   CONTINUE

      DO 140 I=2,NR
      DO 150 J=2,NZ
      IF(P(J,I).LT.PMIN) P(J,I)=PMIN
150   CONTINUE
140   CONTINUE

      DO 120 I=1,NR+1
      P(1,I)=P(2,I)
      P(NZ+1,I)=P(NZ,I)
120   CONTINUE
      DO 130 J=2,NZ
      P(J,1)=P(J,2)
      P(J,NR+1)=P(J,NR)
130   CONTINUE

C     AVERAGE CHAMBER PRESSURE:
      PAV=0.0
      PSUM=0.0
      KSUM=0
      DO 160 J=1,JC
      DO 170 I=1,NR+1
      PSUM=PSUM+P(J,I)
      KSUM=KSUM+1
170   CONTINUE
160   CONTINUE
      PAV=PSUM/KSUM

      RETURN
      END
```

REFERENCES

[1.] Sutton, G. P., Rocket Propulsion Elements, 6th Ed., J. Wiley & Sons, New York, 1992

[2.] Schmidt. G., Brown, N., Hyde, E., and Turner, S., "Propulsion Research and Technology at the NASA Marshall Space Flight Center", AIAA-98-3230, presented at the 34th Joint Propulsion Conference, Cleveland, OH, July 1998.

[3.] Jahn, R. G., Physics of Electric Propulsion, McGraw-Hill, New York, 1968.

[4.] Sovey, J., Hamley, J., Haag, T., Patterson, M., Pencil, E., Peterson, T., Pinero, L., Power, J., Rawlin, V., Sarmiento, C., Anderson, J., Bond, T., Cardwell, G. I. Christensen, J., "Development of an Ion Thruster and Power Processor for New Millenium's Deep Space 1 Mission", NASA-TM-113129, Dec 1997.

[5.] Myers, R. M., "Electromagnetic Propulsion for Spacecraft", AIAA-93-1086, presented at the AIAA/AHS/ASEE Aerospace Design Conference, Irvine, CA, Feb 1993.

[6.] Curran, F., Bennet, G., Watkins, M., Byers, D., Brophy, J, and Sercel, J., "An Overview of the NASA Electric Propulsion Program", IEPC-91-002, presented at the 22nd Electric Propulsion Conference, Viareggio, Italy, Oct 1991.

[7.] Curran, F., Watkins, M., Byers, D., and Garrison, P., "The NASA Low Thrust Propulsion Program", AIAA-92-3703, presented at the 28th Joint Propulsion Conference, Nashville, TN, July 1992.

[8.] Thompson, T. L. and S. L. Rodgers (eds.), Proceedings of the High Energy Density Matter (HEDM) Contractor's Conference, USAF Phillips Laboratory Report PL-TR-94-3036, June 1994.

[9.] Carrick, P. and S. Tam, (eds.), Proceedings of the High Energy Density Matter (HEDM) Contractor's Conference, USAF Phillips Laboratory Report PL-TR-95-3039, June 1995.

[10.] Gunn, S., "Development of Nuclear Rocket Engine Technology", AIAA-89-2386, presented at the 25th Joint Propulsion Conference, Monterey, CA, July 1989.

[11.] Sievers, R., Livingston, J., and Pierce, B., "NERVA Propulsion System Design Considerations", AIAA-90-1951, presented at the 26th Joint Propulsion Conference, Orlando, FL, July 1990.

[12.] El-Genk, M. and Hoover, M. (eds), *Nuclear Thermal Propulsion Concepts*, Chapter 15 in Proceedings of the Tenth Symposium on Space Nuclear Power and Propulsion, AIP Conference Proceedings 271, American Institute of Physics Press, New York, 1993.

[13.] Deininger, W. and Nock, K., "A Review of Electric Propulsion Spacecraft System Concepts", AIAA-90-2553, presented at the 21st International Electric Propulsion Conference, Orlando, FL, July 1990.

[14.] El-Genk, M. and Hoover, M. (eds), *Nuclear Electric Propulsion Systems*, Chapter 32 in Proceedings of the Tenth Symposium on Space Nuclear Power and Propulsion, AIP Conference Proceedings 271, American Institute of Physics Press, New York, 1993.

[15.] El-Genk, M. and Hoover, M. (eds), *Nuclear Thermal Propulsion Technology*, Chapters 35 and 39 in Proceedings of the Tenth Symposium on Space Nuclear Power and Propulsion, AIP Conference Proceedings 271, American Institute of Physics Press, New York, 1993.

[16.] George, J., Hack, K., Dudzinski, L., Gefert, L, and Gilland, J., "Piloted Mars Mission Planning: NEP Technology and Power Levels", *Proceedings of the Tenth Symposium on Space Nuclear Power and Propulsion*, AIP Conference Proceedings 271, American Institute of Physics Press, New York, 1993, pp. 493-500.

[17.] Miller, T. and Bennett, G., "Nuclear Propulsion for Space Exploration", Proceedings of the Ninth Symposium on Space Nuclear Power Systems, AIP Conference Proceedings 246, American Institute of Physics Press, New York, 1992, pp. 24-29.

[18.] Sovey, J., Hamley, J., Patterson, M., Rawlin, V., and Myers, R., "The Evolutionary Development of High Specific Impulse Electric Thruster Technology", AIAA-92-1556, presented at the AIAA Space Programs and Technologies Conference, Huntsville, AL, March 1992.

[19.] Mantenieks, M. and Myers, R., "100-kW Class Applied-Field Thruster Component Wear", Proceedings of the Tenth Symposium on Space Nuclear Power and Propulsion, AIP Conference Proceedings 271, American Institute of Physics Press, New York, 1993, pp. 1317-1325.

[20.] Myers, R., Mantenieks, M., and LaPointe, M., "MPD Thruster Technology", AIAA-91-3568, presented at the AIAA/NASA/OAI Conference on Advanced SEI Technologies, Cleveland, OH, Sept 1991.

[21.] Gilland, J., "Application of a Helicon Discharge to Electric Propulsion", AIAA-98-3934, presented at the 34th Joint Propulsion Conference, Cleveland, OH, July 1998.

[22.] Sercel, J., "Electron-Cyclotron-Resonance (ECR) Plasma Thruster Research", AIAA-88-2916, presented at the 24th Joint Propulsion Conference, Boston, MA, July 1988.

[23.] Hooper, E., Stallard, B., and Makowski, M., "Whistler Wave Driven Plasma Thruster", UCRLJC110921, Lawrence Livermore National Laboratory, Oct 1992.

[24.] Wantuck, P. and Hull, D., "Experimental Measurements in a Radio-Frequency Discharge Heated Supersonic Flow: Evaluation of a Potential Electric Thruster", AIAA-91-3615, presented at the AIAA/NASA/OAI Conference on Advanced SEI Technologies, Cleveland, OH, Sept 1991.

[25.] Byers, D. and LaPointe, M., "The NASA Lewis Research Center Program in Advanced Propulsion Concepts", Proceedings of the Second Annual Workshop on Advanced Propulsion Concepts, JPL-D-8052, Jet Propulsion Laboratory, Pasadena, CA, Nov 1990, pp. 79-84.

[26.] Shulze, N., "Fusion Energy for Space Missions in the 21st Century", NASA TM-4298, Aug 1991.

[27.] Williams, C., Borowski, S., Dudzinski, L., and Juhasz, A., "A Spherical Torus Nuclear Fusion Reactor Space Propulsion Vehicle Concept for Fast Interplanetary Travel", AIAA-98-3591, presented at the 34th Joint Propulsion Conference, Cleveland, OH, July 1998.

[28.] Emrich, W., "Performance Optimization of the Gasdynamic Mirror Propulsion system", AIAA-98-3588, presented at the 34th Joint Propulsion Conference, Cleveland, OH, July 1998.

[29.] Arakawa, Y. and Kimura, I., "Prospects for Inertial-Confinement Fusion Rocket Propulsion", IAF-83-396, 14th International Symposium on Space Science and Technology, Tokyo, Japan, May 1984.

[30.] Hyde, R., "A Laser-Fusion Rocket for Interplanetary Propulsion", A87-18201-06-12, in Proceedings of the 34th International Astronautical Federation, published by AGNE Inc., 1984.

[31.] Miley, G., Nadler, J., Temple, B., Bolt, S., and Kislev, H., "Critical Technology Demonstration of Plasma Focus Type MPD Thruster", USAF Phillips Laboratory Report PL-TR-91-3111, May 1992.

[32.] Nardi, V., Powell, C., and Brzosko, J., "Evaluation of the Plasma Focus as a Thruster with Neutron-Lean Fusion Reactions", USAF Phillips Laboratory Report PL-TR-92-3008, June 1993.

[33.] Choi, C. and Cox, L., "Engineering Considerations for the Self-Energizing Magneto-plasmadynamic (MPD)-Type Fusion Plasma Thruster", USAF Phillips Laboratory Report PL-TR-94-3037, Aug 1994.

[34.] Morgan, D., "Concepts for the Design of an Antimatter Annihilation Rocket", *J. British Interplanetary Soc.*, 35, 1982, pp. 405-412.

[35]. Forward, R., "Antiproton Annihilation Propulsion", USAF Rocket Propulsion Laboratory Report AFRPL TR-85-034, Sept 1985.

[36.] Cassenti, B., "High Specific Impulse Antimatter Rockets", AIAA-91-2548, presented at the 27th Joint Propulsion Conference, Sacramento, CA, June 1991.

[37.] Gaidos, G., Lewis, R., Smith, G., Dundore, B., and Chakrabarti, S., "Antiproton-Catalyzed Microfission Fusion Propulsion Systems for Exploration of the Outer Solar System and Beyond", AIAA-98-3589, presented at the 34th Joint Propulsion Conference, Cleveland, OH, July 1998.

[38.] LaPointe, M., "Antiproton Powered Propulsion with Magnetically Confined Plasma Engines", *J. Propulsion and Power*, 7 (5) 1991, pp. 749-759.

[39.] Bodin, H. A. B., Green, T. S., Newton, A. A. , Niblett, G. B. F., and Reynolds, J. A., "Plasma Containment and Stability in a Megajoule Theta-Pinch Experiment", Plasma Physics and Nuclear Controlled Fusion Research, Vol. 1, International Atomic Energy Agency, Vienna, 1966, pp. 193-222.

[40.] Quinn, W. E., Little, E. M., Ribe, F. L., and Sawyer, G. A., "Stability and End Loss of a 3.5-MJ Theta-Pinch (Scylla-IV)", Plasma Physics and Nuclear Controlled Fusion Research, Vol. 1, International Atomic Energy Agency, Vienna, 1966, pp. 237-248.

[41.] Bodin, H. A. B., McCartan, J., Newton, A. A., and Wolf, G. H., "Diffusion and Stability of High-β Plasma in an 8-meter Theta-Pinch", Plasma Physics and Nuclear Controlled Fusion Research, Vol. II, International Atomic Energy Agency, Vienna, 1969, pp. 533-551.

[42.] Hamm, J. J., Knoepfel, H., Krogler, H., Linhart, J. G., and Verbeek, R., "Very-High Density Theta-Pinch", Plasma Physics and Nuclear Controlled Fusion Research, Vol. II, International Atomic Energy Agency, Vienna, 1969, pp. 629-638.

[43.] Rose, D. J. and Clark, M. C. Jr., Plasma and Controlled Fusion, MIT Press, Massachusetts Institute of Technology and J. Wiley & Sons, Inc., New York, 1961, p.382.

[44.] Sutton, G. P., Rocket Propulsion Elements, 6th ed., J. Wiley & Sons, New York, 1992.

[45.] Miyamoto, K., Plasma Physics for Nuclear Fusion, MIT Press, Cambridge, 1989, pp. 150-152.

[46.] Miyamoto, K., Plasma Physics for Nuclear Fusion, MIT Press, Cambridge, 1989, pp. 148-149.

[47.] Glasstone, S. and Lovberg, R. H., Controlled Thermonuclear Reactions, D. van Nostrand Company, Inc., Princeton, NJ, 1960, pp. 366-400.

[48.] Kolb, A. C., referenced in Rose, D. J. and Clark, M. C. Jr., Plasma and Controlled Fusion, MIT Press, Massachusetts Institute of Technology and J. Wiley & Sons, Inc., New York, 1961, pp. 382-386.

[49.] Stover, E., "Computer Simulation of Plasma Behavior in Open-Ended Linear Theta Machines", U. S. Department of Energy Report DOE/ET/53018-6, April 1981.

[50.] Stover, E., Klevans, E., and York, T., "Computer Modeling of Linear Theta-Pinch Machines", *Phys Fluids*, 21 (11), Nov 1978, pp. 2090-2102.

[51.] McKenna, K. F. and York, T. M., "End Loss From a Collision Dominated Theta-Pinch Plasma", *Phys Fluids*, 20 (9), Sep 1977, pp. 1556-1565.

[52.] Gross, R. A., Fusion Energy, J, Wiley & Sons, New York, 1984, p. 54.

[53.] Gross, R. A., Fusion Energy, J, Wiley & Sons, New York, 1984, pp.66-67.

[54.] Gross, R. A., Fusion Energy, J, Wiley & Sons, New York, 1984, p. 67.

[55.] Gross, R. A., Fusion Energy, J, Wiley & Sons, New York, 1984, pp. 67-68.

[56.] Chen, F. A., Plasma Physics and Controlled Fusion, Plenum Press, N.Y., 1984, pp. 205-206.

[57.] Chen, F. A., Plasma Physics and Controlled Fusion, Plenum Press, N.Y., 1984, pp. 181-183.

[58.] Gross, R. A., Fusion Energy, J, Wiley & Sons, New York, 1984, p. 76.

[59.] Cambel, A. B., Plasma Physics and Magnetofluidmechanics, McGraw-Hill Book Co., 1963, pp. 184-186.

[60.] Gross, R. A., Fusion Energy, J, Wiley & Sons, New York, 1984, p. 77.

[61.] Sutton, G. W. and Sherman, A., Engineering Magnetohydrodynamics, McGraw-Hill Book Co., New York, 1965.

[62.] Cambel, A. B., Plasma Physics and Magnetofluidmechanics, McGraw-Hill Book Co., 1963, pp. 182-184.

[63.] Fletcher, C. A. J., Computational Techniques for Fluid Dynamics, Vol. II, Springer-Verlag, New York, 1988, pp. 404-407.